Prepared for:

Rijkswaterstaat, Rijksinstituut voor Kust en Zee

# On the use of a horizontal k-ε model for shallow-water flow

June 2000

Z2747.50

WL | delft hydraulics

# On the use of a horizontal k-ε model for shallow-water flow

M. Bijvelds and E.D. de Goede

June 2000

WL | delft hydraulics

WL | delft hydraulics

CLIENT: Rijkswaterstaat, Rijksinstituut voor Kust en Zee (RIKZ)

TITLE: On the use of a horizontal k-ε model for shallow-water flow


ABSTRACT:

In three-dimensional shallow water modelling the horizontal eddy-viscosity may be assumed to be a superposition of two eddy-viscosities, representing the 2D large-scale and 3D small-scale turbulence, respectively. Usually, the eddy-viscosity corresponding to the 2D large-scale turbulence is assumed to be a both in space and time constant value, whereas the 3D eddy-viscosity is computed by the well-known $k$-$\varepsilon$ turbulence closure model. In TRIWAQ the horizontal eddy-viscosity is defined as a constant, which can be specified by the user.

For applications such as the simulation of flows near barriers, groynes and sluices the approach with a constant horizontal eddy-viscosity is considered to be unsuitable. Therefore, in this project a horizontal turbulence model for the computation of the 2D eddy-viscosity in TRIWAQ has been implemented. In particular, the two-length-scale model developed in (Bijvelds, 1997) has been employed, in which a depth-averaged (2D) and a 3D k-ε model are used for the computation of the horizontal eddy-viscosity and the vertical eddy-viscosity, respectively.

In this report the implementation of the horizontal $k$-$\varepsilon$ model in TRIWAQ is examined for three applications, namely the yacht harbour "t Steel", a shallow-water mixing layer model and a 3D MOHA (Monding Haringvliet) model. After several changes in the implementation a robust implementation for the accurate computation of the horizontal viscosity has been developed.


REFERENCES: Contract number RKZ-745, part of NAUTILUS 10.3 project

| VER. | ORIGINATOR | | DATE | REMARKS | REVIEW | | APPROVED BY | |
|---|---|---|---|---|---|---|---|---|
| 0.1 | | | 26-4-00 | draft version | | | | |
| 1.0 | | | 11-5-00 | first final version | | | | |
| 1.1 | | | 26-5-00 | second final version | | | | |
| 1.2 | M. Bijvelds, E. de Goede | ME | 21-6-00 | third final version | G.S. Stelling | | T. Schilperoort | |
| | | | | | | | | |
| | | | | | | | | |

| | | | | | | | | |
|---|---|---|---|---|---|---|---|---|
| PROJECT IDENTIFICATION: | | Z2747.50 | | | | | | |
| KEYWORDS: | | 2D large scale turbulence, horizontal k-ε model, TRIWAQ, 3D MOHA model | | | | | | |
| CONTENTS: | TEXT PAGES | 36 | TABLE | 3 | FIGURES | 36 | APPENDICES | 1 |
| STATUS: | ☐ PRELIMINARY | | ☐ DRAFT | | ☒ FINAL | | | |

# Contents


**1 Introduction ..... 1–1**

**2 A two-length scale k-ε turbulence model ..... 2–1**

2.1 Horizontal turbulence modelling ..... 2–1

2.2 Standard 3D k-ε turbulence model ..... 2–3

2.3 Depth-averaged *k-ε* turbulence model ..... 2–5

2.3.1 Boundary conditions ..... 2–6
2.3.2 Initial conditions ..... 2–6

**3 Numerical aspects ..... 3–1**

3.1 Grid staggering ..... 3–1

3.2 Space discretization ..... 3–2

3.2.1 Horizontal k-ε turbulence model ..... 3–2
3.2.2 Horizontal eddy-viscosity terms in momentum equations ..... 3–3
3.2.3 Time integration of Reynolds stresses ..... 3–4

3.3 Time integration of horizontal k-ε turbulence model ..... 3–4

3.4 Boundary conditions ..... 3–7

**4 Test models ..... 4–1**

4.1 Yacht harbour "t Steel" ..... 4–1

4.1.1 Model characteristics ..... 4–3
4.1.2 Model results ..... 4–4

4.2 Shallow-water mixing layer model ..... 4–5

4.3 MOHA (MOnding HAringvliet) model ..... 4–8

**5 Conclusions ..... 5–1**

**6 References ..... 6–1**

# Appendices

## A Further research

A.1 MOHA model with Smagorinsky implementation ..... A–2

A.2 Sensitivity analysis for the horizontal k-ε model ..... A–3

A.3 MOHA model with first-order upwind advection ..... A–5

# List of Figures

**Yacht harbour "t Steel":**

4.1.1 Bathymetry of yacht harbour "t Steel"
4.1.2 Computational grid of "t Steel" model
4.1.3 Shallow-water mixing layer in yacht harbour "t Steel" (measurements)
4.1.4 Velocity field at the mixing layer between river and harbour entrance at the surface and bottom layer (computed)
4.1.5 Velocity field at harbour entrance (computed versus measured)
4.1.6 Velocity field primarly gyre at harbour entrance (computed versus measured)
4.1.7 Velocity field secondary gyre in harbour (computed versus measured)
4.1.8 Contours of tracer concentration
4.1.9 Contours of horizontal TKE, dissipation and viscosity
4.1.10 Contours of horizontal TKE, dissipation and viscosity computed in (Bijvelds, 1997)

***Shallow-water mixing layer model:***

4.2.1 Contours of horizontal TKE, dissipation and viscosity after 1 minute
4.2.2 Contours of tracer concentration after 1 minute
4.2.3 Contours of horizontal TKE, dissipation and viscosity after 50 minutes
4.2.4 Contours of tracer concentration after 50 minutes
4.2.5 Contours of Reynolds stress after 50 minutes

**Monding Haringvliet (MOHA) model:**

4.3.1 Bathymetry of MOHA model
4.3.2 Time series of velocities near Haringvliet sluices
4.3.3 Time series of salinity at stations MTP 1-3 and PUT-4
4.3.4 Time series of salinity at stations Paal 2 W and Paal 2 O

**MOHA model with Smagorinsky:**

A.1.1 Time series of velocities near Haringvliet sluices
A.1.2 Time series of salinity at stations MTP 1-3 and PUT-4
A.1.3 Time series of salinity at stations Paal 2 W and Paal 2 O
A.1.4 Contours of horizontal viscosity at 11 March 1997
A.1.5 Contours of salinity at 11 March 1997 00:00 hr
A.1.6 Contours of salinity at 11 March 1997 12:00 hr
A.1.7 Contours of salinity at 12 March 1997 00:00 hr

**Sensitivity analysis for 2D MOHA model:**

A.2.1 Computational grid of reduced MOHA model
A.2.2 Contours of horizontal TKE, dissipation and viscosity for reference run
A.2.3 Contours of horizontal TKE, dissipation and viscosity for adapted closed boundary implementation
A.2.4 Contours of horizontal TKE, dissipation and viscosity for different values of $c_{\varepsilon 2}$
A.2.5 Contours of horizontal TKE, dissipation and viscosity for different grid resolution

**3D MOHA model with first-order upwind advection:**

A.3.1 Contours of horizontal TKE, dissipation and viscosity at 11 March 1997 0:00 hr
A.3.2 Contours of horizontal TKE, dissipation and viscosity at 11 March 1997 3:00 hr
A.3.3 Contours of horizontal TKE, dissipation and viscosity at 11 March 1997 6:00 hr
A.3.4 Contours of horizontal TKE, dissipation and viscosity at 11 March 1997 9:00 hr
A.3.5 Contours of horizontal TKE, dissipation and viscosity at 11 March 1997 12:00 hr
A.3.6 Contours of horizontal viscosity at 11 March 1997
A.3.7 Contours of salinity at 11 March 1997 00:00 hr
A.3.8 Contours of salinity at 11 March 1997 12:00 hr
A.3.9 Contours of salinity at 12 March 1997 00:00 hr

# 1 Introduction

In the three-dimensional shallow-water model TRIWAQ it is assumed that the horizontal length scales of the flow are much larger than the vertical length scales. Under such conditions the Reynolds-averaged Navier-Stokes equations are reduced to the shallow-water equations. To close the set of equations a turbulence model is used, which expresses the turbulent stresses in the time-mean flow properties. In engineering applications, this is often done by means of the Boussinesq hypothesis (or eddy-viscosity concept), in which the turbulent stresses are related to the gradient of the momentum.

In shallow-water flows turbulence is often anisotropic, which means that turbulent structures with *two different length scales* exist. One length scale is associated with large horizontal turbulence structures (*quasi two-dimensional turbulence*) that are generated in regions of horizontal shear. The other length scale is associated with small scale turbulence *(3D turbulence*), which is smaller than the water depth. 3D turbulence is generated near the bottom and the free surface. In the present version of TRIWAQ the horizontal eddy-viscosity is based on the horizontal length scale and the vertical eddy-viscosity is based on the vertical length scale. The eddy-viscosity corresponding to the horizontal length scale is assumed to be constant (both in space and time), whereas the vertical eddy-viscosity is computed by a turbulence closure model, for example the standard $k$-$\varepsilon$ model (Launder and Spalding, 1974). The $k$-$\varepsilon$ model is based on two transport equations for the turbulent kinetic energy and the energy dissipation, respectively. The $k$-$\varepsilon$ model has been implemented in TRIWAQ (Zijlema, 1998) and in Delft3D-FLOW (Delft Hydraulics, 1999).

In estuaries and coastal seas the large scale flow patterns are usually determined by tidal forcing, the baroclinic pressure gradient, bottom friction or by advection, whereas the horizontal viscosity has little effect. This is different for small scale exchange flows generated by lateral shear like in mixing layers, separation flows, wakes and jets. Mixing layers develop at harbour entrances, along groyne fields and flood planes. The horizontal exchange of momentum and matter is then dependent on the horizontal eddy-viscosity of the mixing layer, which should take into account the history of the flow. For such applications a constant value for the horizontal eddy-viscosity is considered to be unsuitable. Therefore, RIKZ commissioned WL | Delft Hydraulics, in co-operation with Delft University of Technology and EDS, to implement in this project a more sophisticated formulation for the horizontal eddy-viscosity in TRIWAQ. In particular, the two-length-scale model, in which both 2D and 3D $k$-$\varepsilon$ models occur, developed in (Bijvelds, 1997) will be employed. We remark that such a two-length-scale model does not bridge the gap between the horizontal turbulent eddies and the grid size. For that purpose a subgrid scale model should be implemented. The two-length-scale model requires a sufficiently fine horizontal grid to resolve the horizontal velocity gradients of the mean flow, which generate the quasi two-dimensional turbulence.

In (Bijvelds and De Goede, 1999) a literature study on horizontal $k$-$\varepsilon$ modelling was carried out. Next, a conceptual model and an algorithmic implementation of the horizontal $k$-$\varepsilon$ model for TRIWAQ was presented (De Goede and Bijvelds, 1999). This model is almost identical to the one described in (Bijvelds, 1997). A slightly more implicit time integration method is proposed.

In this report the implementation of the horizontal $k$-$\varepsilon$ model in TRIWAQ as described in (De Goede and Bijvelds, 1999) will be examined for three applications, namely yacht harbour "t Steel" (Bijvelds, 1997), a shallow-water mixing layer model (Tukker, 1997) and a MOHA (Monding Haringvliet) model (Soerdjbali, 1999). These test models have been specified by RIKZ. The first two models have also been simulated with a physical scale model at the Hydromechanics Laboratory if the Civil Engineering Faculty of the Delft University of Technology. For all three models measurements are available. The measurements will to used to validate the implementation of the horizontal $k$-$\varepsilon$ model in TRIWAQ.

Chapter 2 contains the conceptual description of the horizontal $k$-$\varepsilon$ model, whereas in Chapter 3 the algorithmic implementation is discussed. In Chapter 4 the numerical results for the three above-mentioned test models are described. Finally, Chapter 5 contains the conclusions.

This project is carried out by order of RIKZ as part of the NAUTILUS 10.3 project (contract number RKZ-745). At RIKZ this project is supported by M. Zijlema.

# 2 A two-length scale k-ε turbulence model

## 2.1 Horizontal turbulence modelling

Many shallow-water models use a horizontal eddy-viscosity $\nu_t^h$ that is constant in time (and often also constant in space), see e.g. (Delft Hydraulics, 1981), (Zijlema, 1998) and (Delft Hydraulics, 1999). This means that the value of $\nu_t^h$ does not depend on local flow characteristics. The horizontal eddy-viscosity is mainly applied for model calibration and sometimes for improving the stability of the computations. For large-scale tidal or density driven applications such an approximation has proven to be sufficiently accurate. However, for small-scale phenomena such as horizontal mixing layers, separation, wakes and jets, a more sophisticated approach for the computation of the horizontal eddy-viscosity $\nu_t^h$ should be applied.

Usually, in shallow-water modelling the Reynolds stress tensor $\tau_{ij}$ in the momentum equations follows the Boussinesq hypothesis. In Cartesian co-ordinates the Reynolds-averaged shallow-water equations can be written as

$$\frac{\partial u_i}{\partial t} + u_j \frac{\partial u_i}{\partial x_j} + \frac{1}{\rho}\frac{\partial p}{\partial x_i} - \frac{1}{\rho}\frac{\partial \tau_{ij}}{\partial x_j} = f_i, \qquad i = 1,\ldots,2 \tag{2.1}$$

Owing to the hydrostatic pressure assumption we have for the vertical direction

$$\frac{1}{\rho}\frac{\partial p}{\partial x_3} = -g \tag{2.2}$$

In Eq. (2.1) the Reynolds stress tensor $\tau_{ij}$ is defined by

$$\tau_{ij} = -2\rho \nu_j S_{ij} \quad i,j = 1,\ldots,3 \tag{2.3a}$$

with

$$S_{ij} = \frac{1}{2}\left(\frac{\partial u_i}{\partial x_j} + \frac{\partial u_j}{\partial x_i}\right) \tag{2.3b}$$

and $\nu_j$ defined by

$$\nu_1 = \nu_2 = \nu_t^h \quad and \quad \nu_3 = \nu_t^v \tag{2.3c}$$

representing the horizontal eddy-viscosity and vertical eddy-viscosity, respectively. In Eq. (2.3) $S_{ij}$ denotes the Cartesian deformation tensor of the flow field. We remark that, in agreement with the boundary layer approximation, the three-dimensional Reynolds stress

tensor and deformation tensor has been simplified by neglecting the vertical accelerations (shallow-water), see also (Uittenbogaard, 1992) and (Zijlema, 1998). It is assumed that two different length scales exist. Reynolds stresses which transfer momentum in the vertical direction are modelled by using a vertical eddy-viscosity $\nu_t^v$ and the Reynolds stresses which transfer momentum in the horizontal direction are modelled by the horizontal eddy-viscosity $\nu_t^h$.

From Eqs. (2.3a-c) it can be verified that the Reynolds stress tensor in horizontal direction, in which the terms in vertical direction are neglected, reads

$$\tau_{11} = -\rho \nu_t^h \left( \frac{\partial u_1}{\partial x_1} \right), \tau_{22} = -\rho \nu_t^h \left( \frac{\partial u_2}{\partial x_2} \right), \tau_{12} = \tau_{21} = -\rho \nu_t^h \left( \frac{\partial u_1}{\partial x_2} + \frac{\partial u_2}{\partial x_1} \right) \quad (2.4)$$

Thus, the turbulent momentum fluxes in horizontal direction for the horizontal velocities $u_1$ and $u_2$ may be written in the form

$$\frac{1}{\rho} F_x = \left( \frac{\partial \tau_{11}}{\partial x_1} \right) + \left( \frac{\partial \tau_{12}}{\partial x_2} \right) \quad and \quad \frac{1}{\rho} F_y = \left( \frac{\partial \tau_{22}}{\partial x_2} \right) + \left( \frac{\partial \tau_{21}}{\partial x_1} \right) \quad (2.5)$$

In TRIWAQ, however, the shallow-water equations are not based on Reynolds stresses, but on the Laplace operator, yielding

$$F_x = \left[ \nu_h \right] \left( \frac{\partial^2 u_1}{\partial x_1^2} \right) \quad and \quad F_y = \left[ \nu_h \right] \left( \frac{\partial^2 u_2}{\partial x_2^2} \right) \quad (2.6)$$

with $\left[ \nu_h \right]$ a constant value for the horizontal eddy-viscosity that is specified in the TRIWAQ input file, see also Eq. (2.44) in (Zijlema, 1998). We remark that the Laplace operator is a simplification of the Reynolds stress terms.

In the present version of TRIWAQ the 3D turbulence is determined by a turbulence model (for example, the standard 3D *k-ε* model, see next section), whereas the 2D part is specified as a constant by the user via the input file. The horizontal eddy-viscosity is based on the horizontal length scale and the vertical eddy-viscosity is based on the vertical length scale.

In this project the horizontal eddy-viscosity will not be defined according to the present approach in TRIWAQ, which reads (cf. Eq. (2.3c))

$$\nu_t^h = \nu_1 = \nu_2 = \left[ \nu_h \right]$$

but according to

$$\nu_t^h = \nu_1 = \nu_2 = \left[ \nu_h \right] + \nu_t^{2D} + \nu_t^{3D} \quad (2.7a)$$

$$\nu_t^v = \nu_3 = \nu_t^{3D} \quad (2.7b)$$

The horizontal eddy-viscosity $\nu_t^h$ is defined as the superposition of three eddy-viscosities, representing the eddy-viscosity specified by the user, the quasi 2D (large scale) turbulence $\nu_t^{2D}$ and the 3D (small-scale) turbulence $\nu_t^{3D}$, respectively. In this project a method for the computation of the quasi 2D (large scale) turbulence will be implemented in TRIWAQ. We remark that these three horizontal eddy-viscosities are at different locations in the SIMONA Data Storage (SDS) file.

Summarizing, the implementation of the horizontal eddy-viscosity that will be applied in this project, makes use of a combination of Eq. (2.5) and Eq. (2.6). The constant horizontal eddy-viscosity $\left[\nu_h\right]$, which is specified by the user via the TRIWAQ input file, is used for the computation of the Laplace operator, see Eq. (2.6). Additionally, in case of a horizontal turbulence model, which also has to be specified via the TRIWAQ input file, the second and third term in the right-hand side of Eq. (2.7a) are used to compute the Reynolds stress tensor as defined in Eq. (2.5). In this way, upward compatibility with the present operational version of TRIWAQ is maintained.

In (De Goede and Bijvelds, 1999) a two-length-scale turbulence model for implementation in TRIWAQ has been described. The method consists of two distinct k-ε models that independently model the 3D and quasi-2D turbulence. The vertical eddy-viscosity $\nu_t^v$ is computed with a 3D k-ε turbulence model, in which the production of turbulent kinetic energy results from vertical shear only, generated at the bottom and/or free surface. Note that $\nu_t^v$ is used for the computation of the vertical Reynolds stresses. The quasi 2D (large-scale) part of the horizontal eddy-viscosity $\nu_t^h$ is calculated by a 2D depth-averaged k-ε model, in which the production of turbulent kinetic energy results from horizontal depth-averaged velocity gradients. This 2D part of two-length-scale turbulence model is comparable to the standard $k$-$\varepsilon$ model of (Rastogi and Rodi, 1980), but takes into account anisotropic behaviour of turbulence. The coefficients in both the 3D and 2D turbulence model are taken equal to the standard k-ε model (Launder and Spalding, 1974). Direct interaction between the two turbulence models, by means of energy transfer, is neglected (Bijvelds and De Goede, 1999). However, interaction via the mean-flow equations still occurs. In the following sections the two-length-scale turbulence model will be described in more detail.

## 2.2 Standard 3D k-ε turbulence model

For the sake of completeness we will start with a short description of the standard 3D $k$-$\varepsilon$ model. For a detailed description we refer to (Launder and Spalding, 1974). In the standard $k$-$\varepsilon$ turbulence model, both the turbulent kinetic energy $k$ and the dissipation rate $\varepsilon$ of the turbulent kinetic energy are computed by solving transport equations. The standard $k$-ε model accounts for the transport and history effects of turbulence. Next, the vertical eddy-viscosity is computed from these turbulent quantities by

$$\nu_t^{3D} = c_\mu \frac{k^2}{\varepsilon} \tag{2.8}$$

where $c_\mu$ is a calibration constant. The transport equations for $k$ and $\varepsilon$ are given by

$$\frac{\partial k}{\partial t} + u\frac{\partial k}{\partial x} + v\frac{\partial k}{\partial y} + \omega\frac{\partial k}{\partial z} = \frac{\partial}{\partial z}\left(\frac{\nu_t^{3D}}{\sigma_k}\frac{\partial k}{\partial z}\right) + P_k + B_k - \varepsilon \tag{2.9}$$

$$\frac{\partial \varepsilon}{\partial t} + u\frac{\partial \varepsilon}{\partial x} + v\frac{\partial \varepsilon}{\partial y} + \omega\frac{\partial \varepsilon}{\partial z} = \frac{\partial}{\partial z}\left(\frac{\nu_t^{3D}}{\sigma_\varepsilon}\frac{\partial \varepsilon}{\partial z}\right) + P_\varepsilon + B_\varepsilon - c_{\varepsilon 2}\frac{\varepsilon^2}{k} \tag{2.10}$$

with $u$, $v$ and $\omega$ the layer-averaged velocities. In Eqs. (2.9-10) the production terms $P_k$ and $P_\varepsilon$ are defined by

$$\begin{aligned} P_k &= \nu_t^{3D}\left[\left(\frac{\partial u}{\partial z}\right)^2 + \left(\frac{\partial v}{\partial z}\right)^2\right] \\ P_\varepsilon &= c_{\varepsilon 1}\frac{\varepsilon}{k}P_k \end{aligned} \tag{2.11}$$

Similarly, for the buoyancy fluxes we have

$$\begin{aligned} B_k &= \frac{\nu_t^{3D}}{\sigma_\rho}\frac{g}{\rho}\frac{\partial \rho}{\partial z} \\ B_\varepsilon &= c_{\varepsilon 1}\frac{\varepsilon}{k}(1 - c_{\varepsilon 3})B_k \end{aligned} \tag{2.12}$$

The coefficients $\sigma_k$, $\sigma_\varepsilon$, $c_{\varepsilon 1}$, $c_{\varepsilon 2}$ and $c_{\varepsilon 3}$ in (2.9-12) are closure constants.

In case of non-stratified flows, the 3D $k$-ε turbulence model contains five closure constants given by

$$c_\mu = 0.09,\ c_{\varepsilon 1} = 1.44,\ c_{\varepsilon 2} = 1.92,\ \sigma_k = 1.0,\ \sigma_\varepsilon = 1.3 \tag{2.13}$$

The values of these constants, as recommended by (Launder and Spalding, 1974), are consistent with benchmark experiments for equilibrium boundary layers and isotropic turbulence. In TRIWAQ these values may be changed by the user. For stratified flows, the following extra closure constants are required:

$$\sigma_p = 0.7,\ \sigma_{\varepsilon 3} = \begin{cases} 1 & \text{if } B_k < 0 \\ 0 & \text{if } B_k > 0 \end{cases} \tag{2.14}$$

Production due to horizontal shear is neglected in Eq. (2.11). This is based on the assumption that horizontal length scales are large compared to the vertical length scales. It is important to discretize accurately in the vertical direction and to resolve the boundary layer near the bed and free surface (Van Kester, 1994). The horizontal gradients of the horizontal velocity are considered to be important for small-scale phenomena that will be examined in this project (see Chapter 1). We remark that it is also possible to incorporate

the horizontal shear terms in the 3D $k$-$\varepsilon$ model. However, such a model is still based on a one-length scale concept, which can not distinguish between the length-scale for the horizontal eddy-viscosity and the length-scale for the vertical eddy-viscosity.

## 2.3 Depth-averaged $k$-$\varepsilon$ turbulence model

As described in the previous section, the 3D $k$-$\varepsilon$ model in TRIWAQ only takes into account the effects of turbulence due to vertical velocity gradients, see Eqs. (2.9-11). The effects of anisotropy in TRIWAQ are introduced by specifying a (2D) horizontal eddy-viscosity constant via the TRIWAQ input file. This horizontal eddy-viscosity, however, has an empirical character, which may vary per application. For large-scale flows the horizontal eddy-viscosity coefficient has little effect on the flow patterns, but for small-scale flows (e.g. laboratory scale) a two-length-scale turbulence model is needed.

A two-length-scale turbulence model exists of two separate turbulence models that account for the different length scales present in the flow, see (Bijvelds, 1997). The small-scale turbulence generated by bottom friction (and other vertical velocity gradients) is modelled by the 3D $k$-$\varepsilon$ model whereas the effects of the larger eddies generated in the mixing layer are embodied in a depth-averaged 2D $k$-$\varepsilon$ model. The models represent the 3D- and 2D eddy-viscosities, respectively.

In the depth-averaged $k$-$\varepsilon$ turbulence model, both the depth-averaged turbulent kinetic energy $\overline{k}$ and the dissipation rate $\overline{\varepsilon}$ of the depth-averaged turbulent kinetic energy are computed by solving transport equations. Next, the horizontal eddy-viscosity is computed from these turbulent quantities by

$$\nu_t^{2D} = c_\mu \frac{\overline{k}^2}{\overline{\varepsilon}} \tag{2.15}$$

In Cartesian co-ordinates the equations used for the depth-averaged turbulent kinetic energy $\overline{k}$ and the dissipation rate $\overline{\varepsilon}$ of the turbulent kinetic energy read, see e.g., (Rodi, 1980) and (Rastogi and Rodi, 1985)

$$\frac{\partial \overline{k}}{\partial t} + U\frac{\partial \overline{k}}{\partial x} + V\frac{\partial \overline{k}}{\partial y} = \frac{\partial}{\partial x}\left(\frac{\nu_t^{2D}}{\sigma_k}\frac{\partial \overline{k}}{\partial x}\right) + \frac{\partial}{\partial y}\left(\frac{\nu_t^{2D}}{\sigma_k}\frac{\partial \overline{k}}{\partial y}\right) + \overline{P_k} - \overline{\varepsilon} \tag{2.16}$$

$$\frac{\partial \overline{\varepsilon}}{\partial t} + U\frac{\partial \overline{\varepsilon}}{\partial x} + V\frac{\partial \overline{\varepsilon}}{\partial y} = \frac{\partial}{\partial x}\left(\frac{\nu_t^{2D}}{\sigma_\varepsilon}\frac{\partial \overline{\varepsilon}}{\partial x}\right) + \frac{\partial}{\partial y}\left(\frac{\nu_t^{2D}}{\sigma_\varepsilon}\frac{\partial \overline{\varepsilon}}{\partial y}\right) + \overline{P_\varepsilon} - c_{\varepsilon 2}\frac{\overline{\varepsilon}^2}{\overline{k}} \tag{2.17}$$

where the overbar for $k$ and $\varepsilon$ indicates a depth-averaged value.

The production terms $\overline{P_k}$ and $\overline{P_\varepsilon}$ are determined by the horizontal shear of the depth-averaged velocities, according to

$$\overline{P_k} = \nu_t^{2D}\left[\left(\left(\frac{\partial U}{\partial y}\right)+\left(\frac{\partial V}{\partial x}\right)\right)^2+2\left(\frac{\partial U}{\partial x}\right)^2+2\left(\frac{\partial V}{\partial x}\right)^2\right] \qquad (2.18)$$

$$\overline{P_\varepsilon} = c_{\varepsilon 1}\frac{\overline{\varepsilon}}{\overline{k}}\,\overline{P_k}$$

The implementation in TRIWAQ is in orthogonal curvilinear co-ordinates. In the implementation of the production terms the curvature of the grid is considered as a higher order term and may be neglected.

The production term $\overline{P_\varepsilon}$ is computed as follows:

$$\overline{P_\varepsilon} = c_{\varepsilon 1}\frac{\overline{\varepsilon}}{\overline{k}}\,\nu_t^{2D}\left[\left(\left(\frac{\partial U}{\partial y}\right)+\left(\frac{\partial V}{\partial x}\right)\right)^2+2\left(\frac{\partial U}{\partial x}\right)^2+2\left(\frac{\partial V}{\partial x}\right)^2\right] \qquad (2.18a)$$

$$= c_{\varepsilon 1}\,c_\mu\,\overline{k}\left[\left(\left(\frac{\partial U}{\partial y}\right)+\left(\frac{\partial V}{\partial x}\right)\right)^2+2\left(\frac{\partial U}{\partial x}\right)^2+2\left(\frac{\partial V}{\partial x}\right)^2\right]$$

In Eqs. (2.16-18) $U$ and $V$ represent the depth-averaged velocities. Furthermore, it is assumed that the closure constants for the depth-averaged $k$-$\varepsilon$ turbulence model are equal to the ones of the 3D $k$-$\varepsilon$ turbulence model, cf. Eq. (2.13).

### 2.3.1 Boundary conditions

For the 3D $k$-$\varepsilon$ turbulence model no boundary conditions have to be specified by the user, see (Zijlema, 1998). From numerical point of view, the boundary conditions for the turbulent quantities $k$ and $\varepsilon$ are copied from the interior, which is the so-called mirroring approach. For the horizontal $k$-$\varepsilon$ turbulence model we propose the same approach in case of outflow. However, in case of inflow a fixed value for $\overline{k}$ and $\overline{\varepsilon}$ will be prescribed, which will be discussed in the next chapter. Thus, similarly to the 3D $k$-$\varepsilon$ turbulence model, no boundary conditions for $\overline{k}$ and $\overline{\varepsilon}$ have to be specified by the user.

### 2.3.2 Initial conditions

Initial conditions for the $\overline{k}$ and $\overline{\varepsilon}$ of the horizontal turbulence model have to be specified by the user, see also Section 2.9.2.1 in the User's Guide WAQUA. The already existing section INITIAL/TURBULENCE_TRANS, which is used for the initialization of the 3D $k$-$\varepsilon$ turbulence model, will be extended for the horizontal $k$-$\varepsilon$ turbulence model. This will be done as follows:

```
INITIAL
   TURBULENCE TRANS
```

with

```
TURBULENCE TRANS
   ENERGY
   DISSIPATION
   HOR ENERGY
   HOR DISSIPation
```

**Explanation:**

**HOR_ENERGY**

- Initial values for turbulent horizontal kinetic energy (default 0.01).

```
HOR ENERGY
   GLOBAL
      (see paragraph 2.1.2.1)
   LOCAL
      (see paragraph 2.1.2.2)
```

**HOR_DISSIPATION**

- Initial values for horizontal dissipation rate (default 0.1).

```
HOR DISSIPation
   GLOBAL
      (see paragraph 2.1.2.1)
   LOCAL
      (see paragraph 2.1.2.2)
```

The default values for $\overline{k}$ and $\overline{\varepsilon}$ are 0.01 and 0.1, respectively. We remark that no initial values are required for the horizontal eddy-viscosity. The horizontal eddy-viscosity is computed from the $\overline{k}$ and $\overline{\varepsilon}$ values, see Eq. (2.15).

Summarizing, the above described approach for the initialization of the horizontal $k$-$\varepsilon$ turbulence model is similar to the approach of the 3D $k$-$\varepsilon$ turbulence model.

# 3 Numerical aspects

In this section we will describe the space and time discretization for the horizontal $k$-$\varepsilon$ turbulence model that will be implemented in TRIWAQ.

## 3.1 Grid staggering

TRIWAQ is a numerical model based on finite differences. To discretize the shallow-water equations in horizontal space, the model area is covered by a rectangular, curvilinear or spherical grid. It is assumed that the grid is orthogonal and well-structured. In case of a curvilinear grid, a file with curvilinear grid co-ordinates in the physical space, has to be provided. The numerical grid transformation is known by the mapping of the co-ordinates of the grid vertices. The geometrical quantities introduced in the transformed equations, see e.g. Eq. (3.3) in (Zijlema, 1998), have to be discretized on the computational grid.

The primitive variables water level and layer-averaged velocities ($u$, $v$, $\omega$) in the three co-ordinate directions respectively, describe the flow. To discretize the 3D shallow-water equations, the variables are arranged in a special way on the grid, viz. on the so-called Arakawa C-grid. The water level points (pressure points) are defined in the centre of a cell (control volume). The velocity components are perpendicular to the grid cell faces where they are situated. The depth points are located at the cell corners.

With respect to the grid staggering of the turbulent quantities in TRIWAQ, for the 3D $k$-$\varepsilon$ turbulence model $k$ and $\varepsilon$ are located at $\omega$-velocity points, see Section 4.6 in (Zijlema, 1998). In this way, the discretization of the production terms in Eq. (2.11) and the buoyancy terms in Eq. (2.12) can be carried out more accurately compared to the commonly applied situation in which the turbulence quantities are located at pressure points, because less averaging is required.

However, for the horizontal $k$-$\varepsilon$ turbulence model the situation is the other way around. In this case it is advantageous to locate the turbulent quantities $\overline{k}$ and $\overline{\varepsilon}$ at depth points (cell corners). The advantage of this choice is that the Reynolds shear stresses are computed more accurately, because no averaging is required. We remark that averaging for the computation of the normal Reynolds stresses increases, but these terms are considered to be of less importance.

The horizontal eddy-viscosity is computed at depth points, which is different from the approach for the vertical eddy-viscosity in TRIWAQ, which is specified at ω velocity points. We remark that in (Bijvelds, 1997) both the horizontal eddy-viscosity and the vertical eddy-viscosity are computed at depth points.

## 3.2 Space discretization

### 3.2.1 Horizontal k-ε turbulence model

In the discretization of the 3D $k$-$\varepsilon$ turbulence model a first-order upwind scheme is applied for the discretization of the horizontal advective terms to guarantee positive solutions (no negative turbulent energy) which is imperative when solving the $k$-$\varepsilon$ transport equations. However, this method suffers from cross-wind diffusion when the local velocity vector is not aligned with the horizontal grid. This numerical diffusion may cause a numerical error, as has been shown in (Bijvelds, 1997) for the circulation in a harbour model. Grid refinement or grid adaptation in order to make the grid aligned with the streamlines are expensive remedies to reduce this artificial diffusion. Therefore, (Bijvelds, 1997) employs for the advective terms the upwind scheme along streamlines rather than along grid lines. This method is called the *directional upwind method* (Van Eijkeren et al., 1993).

Depending on the local velocity vector, or more precisely, on the local CFL number in the depth point, three different points on the grid are involved in the computation of the advection terms . If we consider the situation in which the depth-averaged velocities satisfy $U > V > 0$ and the local Courant numbers in horizontal direction satisfy $CFL_x > CFL_y$, then the points with index *(i,j)*, *(i-1,j)* and *(i-1,j-1)* are used, whereas in the conventional first-order upwind method points with index *(i,j)*, *(i-1,j)* and *(i,j-1)* are employed. In this way, a more accurate solution is guaranteed. The artificial cross-wind diffusion related to first-order discretization smears out the solution in regions where the flow crosses the cells under a considerable angle, causing the turbulence to die out rapidly. Application of the integration along streamlines suppresses this numerical side-effect yielding a physically more realistic solution.

The directional upwind method makes use of an explicit time integration scheme and is considered to be optimal in the class of linear advection schemes. The method is positive as long as the stability criterion

$$CFL_x = \frac{U\,\Delta t}{\Delta x} \le 1 \quad and \quad CFL_y = \frac{V\,\Delta t}{\Delta x} \le 1 \tag{3.1}$$

is fulfilled.

In (Bijvelds, 1999) the above described directional upwind method has been applied to advective terms of both the momentum equations and the $k$-$\varepsilon$ transport equations. However, in this project we will only apply this approach for the advective terms in the horizontal $k$-$\varepsilon$ transport equations. In this way, the upward compatibility in TRIWAQ can be guaranteed. Moreover, for the momentum equations in TRIWAQ a higher-order upwind scheme is used in combination with central differences, instead of a first-order upwind approach.

The diffusion terms are discretized by using (standard) second-order central differences.

For shallow-water flows the 3D turbulence is characterised as wall turbulence. The production and dissipation close to the bottom are roughly equal and large. These terms mainly determine the solution of the 3D $k$-$\varepsilon$ equations on the entire computational region. The 2D turbulence is characterised as free turbulence. It is generated in the horizontal mixing layer and transported to other regions, where it slowly decays (Booij, 1989). In analogy to the 3D turbulence model, $\overline{k}$ and $\overline{\varepsilon}$ are discretized in a non-conservative way. Although the transport mechanism is important in this case, we propose a non-conservative discretization. A conservative discretization would require considerable averaging of horizontal velocities in the advective transport and also introduce inaccuracy.

### 3.2.2 Horizontal eddy-viscosity terms in momentum equations

As already described in Section 3.1, it is proposed to locate the turbulent quantities $\overline{k}$ and $\overline{\varepsilon}$ at depth points (cell corners). Consequently, the horizontal eddy-viscosity is computed at depth points as well. Then, the Reynolds shear stresses (cf. Eq. (2.4))

$$\tau_{12} = \tau_{21} = \rho(\nu_t^{2D} + \nu_t^{3D}) \left( \frac{\partial U}{\partial y} + \frac{\partial V}{\partial x} \right) \tag{3.2a}$$

can be computed without any averaging of horizontal eddy-viscosities, because these stresses are required at depth points. Only $\nu_t^{3D}$ need to be interpolated to depth points. On the other hand, the normal Reynolds stresses

$$\tau_{11} = \rho\,(\nu_t^{2D} + \nu_t^{3D}) \left( \frac{\partial U}{\partial x} \right) \quad \textit{and} \quad \tau_{22} = \rho\,(\nu_t^{2D} + \nu_t^{3D}) \left( \frac{\partial V}{\partial y} \right) \tag{3.2b}$$

are computed at the centre of grid cell and thus require additional averaging. In this case, the horizontal eddy-viscosities, which are known at depth points, have to be averaged to water level points. All four corner points will be involved according to

$$\left[\nu_t^{2D}\right]_{centre(m,n)} = 0.25\left(\left[\nu_t^{2D}\right]_{m,n} + \left[\nu_t^{2D}\right]_{m-1,n} + \left[\nu_t^{2D}\right]_{m,n-1} + \left[\nu_t^{2D}\right]_{m-1,n-1}\right) \tag{3.3}$$

with *(m,n)* denoting the co-ordinates on the computational grid in $x$- and $y$-direction, respectively. After computation of both the normal Reynolds stresses and the Reynolds shear stresses the turbulent momentum fluxes are computed, see Eq. (2.5). The computation of the momentum fluxes in Eq. (2.5) does not require additional averaging.

The complete Reynolds stresses have been added to the momentum equations in TRIWAQ. The implementation of the eddy-viscosity specified by the user via the TRIWAQ input file has not been changed. If a horizontal $k$-$\varepsilon$ turbulence model is selected by the user, see also Section 2.2.2, the eddy-viscosity corresponding to the above described Reynolds stresses are added to the momentum equations.

### 3.2.3 Time integration of Reynolds stresses

The time integration of the horizontal eddy-viscosity that is specified by the user and of the Reynolds stresses in case of a horizontal k-ε turbulence model is explicit in time. An implicit time integration of the Reynolds stress terms would lead to a coupled system of equations for the *U*- and *V*-component, which would require a lot of memory space and probably a large computational effect. The explicit time integration introduces a stability condition, which is of the form

$$\Delta t \le \frac{1}{2\nu_t^h}\left(\frac{1}{\Delta x^2}+\frac{1}{\Delta y^2}\right)^{-1} \tag{3.4a}$$

with $\Delta x$ and $\Delta y$ the mesh sizes in $x$- and $y$-direction, respectively.

In experiments it has been observed that very occasionally this time step restriction is violated. To enhance the robustness of the implementation, we implemented in TRIWAQ an upper bound for the horizontal eddy-viscosity of

$$\nu_t^{2D} \le \frac{1}{2\Delta t}\left(\frac{1}{\Delta x^2}+\frac{1}{\Delta y^2}\right)^{-1} \tag{3.4b}$$

We remark that the time step restriction (3.4) is only applied to the quasi 2D (large-scale) part of the horizontal eddy-viscosity. In the diagnostic file of a TRIWAQ simulation (the so-called waqpro-m file) a warning is given if in one or more points the horizontal viscosity restriction (3.4b) is applied. If this warning appears frequently, then one is advised to reduce the time step.

## 3.3 Time integration of horizontal k-ε turbulence model

The time integration consists of two stages. At both stages the same time integration method is applied for the horizontal $k$-$\varepsilon$ turbulence model. We will therefore only give a description of the first stage. An operator splitting method is applied. A stage consists of two steps. In the first step the following equation is approximated:

$$\frac{\partial \bar{k}}{\partial t}+U\frac{\partial \bar{k}}{\partial x}+V\frac{\partial \bar{k}}{\partial y}=0 \tag{3.5}$$

$$\frac{\partial \bar{\varepsilon}}{\partial t}+U\frac{\partial \bar{\varepsilon}}{\partial x}+V\frac{\partial \bar{\varepsilon}}{\partial y}=0 \tag{3.6}$$

In the second step we have the remaining terms

$$\frac{\partial \bar{k}}{\partial t}=\frac{\partial}{\partial x}\left(\frac{\nu_t^{2D}}{\sigma_k}\frac{\partial \bar{k}}{\partial x}\right)+\frac{\partial}{\partial y}\left(\frac{\nu_t^{2D}}{\sigma_k}\frac{\partial \bar{k}}{\partial y}\right)+\overline{P_k}-\bar{\varepsilon} \tag{3.7}$$

$$\frac{\partial \overline{\varepsilon}}{\partial t} = \frac{\partial}{\partial x}\left(\frac{\nu_t^{2D}}{\sigma_\varepsilon}\frac{\partial \overline{\varepsilon}}{\partial x}\right) + \frac{\partial}{\partial y}\left(\frac{\nu_t^{2D}}{\sigma_\varepsilon}\frac{\partial \overline{\varepsilon}}{\partial y}\right) + \overline{P_\varepsilon} - c_{\varepsilon 2}\frac{\overline{\varepsilon}^2}{\overline{k}} \tag{3.8}$$

The discretization of the advective terms, production term, diffusion term will be discussed for the turbulent kinetic energy $\overline{k}$ only, because for $\overline{\varepsilon}$ the same discretizations are applied. Only the discretization of the dissipation term will be treated separately.

In the first step the discretization of the horizontal advective terms leads to a system of equations of the form

$$\frac{\hat{\overline{k}}_{m,n} - \overline{k}^n_{m,n}}{\Delta t / 2} = \overline{\overline{U^n_{m,n}}}\; G_x\left(\overline{k}^n_{m,n}, \Delta x\right) + \overline{\overline{V^n_{m,n}}}\; G_y\left(\overline{k}^n_{m,n}, \Delta y\right) \tag{3.9}$$

with $G_x$ and $G_y$ representing the directional upwind discretization, $\overline{\overline{U^n_{m,n}}}$, $\overline{\overline{V^n_{m,n}}}$ averaged values in depth points and $\hat{\overline{k}}_{m,n}$ and $\overline{k}^n_{m,n}$ denoting an approximation of the numerical solution at the intermediate and old time level, respectively. Owing to the explicit time integration of the directional upwind method the computation of the turbulent quantities is straightforward.

Positivity of the numerical solution is only guaranteed for the directional upwind method if the stability criterion (3.1) is fulfilled. However, this criterion may be violated during the simulation. In the TRIWAQ implementation we therefore reject negative values at the new time level for $\overline{k}$ and $\overline{\varepsilon}$. Then, the values at the old time level are applied at the new time level as well. In the diagnostic file of a simulation (the so-called waqpro-m file) a warning is given. If this warning appears frequently, then one is advised to reduce the time step.

In the second step the time integration is of the form

$$\frac{\overline{k}^{\bullet}_{m,n} - \hat{\overline{k}}_{m,n}}{\Delta t / 2} = G_{production/dissipation/diffusion} \tag{3.10}$$

with the right hand-side in Eq. (3.10) denoting the discretization of the production, dissipation and diffusion term, respectively. Similarly to $\hat{\overline{k}}_{m,n}$, $\overline{k}^{\bullet}_{m,n}$ also denotes the numerical solution at the intermediate level.

The horizontal eddy-diffusion term is discretized as follows:

$$\left[\frac{\partial}{\partial x}\left(\frac{\nu_t^{2D}}{\sigma_k}\frac{\partial \overline{k}}{\partial x}\right)+\frac{\partial}{\partial y}\left(\frac{\nu_t^{2D}}{\sigma_k}\frac{\partial \overline{k}}{\partial y}\right)\right]_{m,n} =$$

$$\frac{1}{\sigma_k}\left\{\left[\nu_t^{2D}\right]_{m+1/2,n}\frac{\overline{k}^{*}_{m+1,n}-\overline{k}^{*}_{m,n}}{\Delta x}-\left[\nu_t^{2D}\right]_{m-1/2,n}\frac{\overline{k}^{*}_{m,n}-\overline{k}^{*}_{m-1,n}}{\Delta x}\right\}+ \qquad (3.11)$$

$$\frac{1}{\sigma_k}\left\{\left[\nu_t^{2D}\right]_{m,n+1/2}\frac{\overline{k}^{\wedge}_{m,n+1}-\overline{k}^{\wedge}_{m,n}}{\Delta y}-\left[\nu_t^{2D}\right]_{m,n-1/2}\frac{\overline{k}^{\wedge}_{m,n}-\overline{k}^{\wedge}_{m,n-1}}{\Delta y}\right\}$$

in which averaging to velocity points is required for $\left[\nu_t^{2D}\right]_{m\pm1/2,n}$, $\left[\nu_t^{2D}\right]_{m,n\pm1/2}$. From Eq. (3.11) it can be seen that an ADI time integration method is applied for the horizontal eddy-diffusion term. The derivatives in $x$-direction are treated implicitly, whereas the term in $y$-direction uses an explicit integration.

The discretization of the production term in Eq. (2.15) reads

$$\left[\nu_t^{2D}\right]_{m,n}\left(\frac{U^n_{m,n+1}-U^n_{m,n}}{\Delta y}+\frac{V^n_{m+1,n}-V^n_{m,n}}{\Delta x}\right)^2+$$

$$2\left[\nu_t^{2D}\right]_{m,n}\left(\frac{U^n_{m+1,n}-U^n_{m,n}}{\Delta x}\right)^2+2\left[\nu_t^{2D}\right]_{m,n}\left(\frac{V^n_{m,n+1}-V^n_{m,n}}{\Delta y}\right)^2 \qquad (3.12)$$

Now, averaging to depth points is required for

$$2\left[\nu_t^{2D}\right]_{m,n}\left(\frac{U^n_{m+1,n}-U^n_{m,n}}{\Delta x}\right)^2+2\left[\nu_t^{2D}\right]_{m,n}\left(\frac{V^n_{m,n+1}-V^n_{m,n}}{\Delta y}\right)^2 \qquad (3.13)$$

which are considered to be less important than the other terms in Eq. (3.12). We remark that in Eqs. (3.10-11) averaging is also required for the computation of $\Delta x$ and $\Delta y$. This averaging is straightforward.

Finally, we describe the discretization of the dissipation terms, in which Newton linearization is applied. For the turbulent energy $\overline{k}$ and energy dissipation $\overline{\varepsilon}$ we have, respectively,

$$\frac{2\,\overline{k}^{*}_{m,n}}{\overline{k}^{\wedge}_{m,n}}\,\overline{\varepsilon}^{\wedge}_{m,n}-\overline{\varepsilon}^{\wedge}_{m,n}$$

$$2\,c_{2\varepsilon}\,\frac{\overline{\varepsilon}^{*}_{m,n}\,\overline{\varepsilon}^{\wedge}_{m,n}}{\overline{k}^{\wedge}_{m,n}}-c_{2\varepsilon}\,\frac{\left(\overline{\varepsilon}^{\wedge}_{m,n}\right)^2}{\overline{k}^{\wedge}_{m,n}} \qquad (3.13)$$

As can be seen in Eq. (3.13), the discretization of the dissipation term for both $\overline{k}$ and $\overline{\varepsilon}$ is treated partly explicitly and partly implicitly to guarantee positivity.

For both $\bar{k}$ and $\bar{\varepsilon}$ the above described discretizations lead to a tridiagonal system of equations, because of the partly implicit treatment of the diffusion term. This system is solved by a double sweep algorithm, see also Chapter 8 in (Zijlema, 1998).

Above, we have described the space and time discretization of the first stage. At the second stage almost the same discretization is applied. Only the explicit/implicit treatment of the horizontal diffusion term is interchanged.

***Differences with implementation of (Bijvelds, 1997)***

The above described space and time discretization for the implementation of a 2D k-ε turbulence model in TRIWAQ slightly differs from the discretization used in (Bijvelds, 1997). Only the time integration is slightly different. In (Bijvelds, 1997) an explicit time integration method is applied, whereas in this project an ADI time integration method is applied for the horizontal eddy-diffusion term, which is more in line with the implicit approach followed in TRIWAQ. Furthermore, the treatment of open boundaries has been slightly improved in this project, which will be discussed in the next section. Summarizing, the differences between the implementation of (Bijvelds, 1997) and the implementation in this project are very small.

***Thin dams***

Finally, we should remark that for the discretization of the horizontal $k$-$\varepsilon$ turbulence model one fundamental problem exists, viz. the treatment of thin dams. For thin dams it is not clear which velocities (on both sides of the thin dam) and eddy-viscosities should be used in the computation. It is evident that some ad hoc solution has to be chosen. On the other hand, one can also argue whether the representation of thin dams by infinitely small walls is still acceptable at the spatial scales that are of interest to horizontal $k$-$\varepsilon$ turbulence modelling. In the present implementation of the $k$-$\varepsilon$ turbulence model the horizontal eddy-viscosity is set to zero at thin dams (and also at closed boundaries). In such a case there is no fundamental problem with respect to the implementation for thin dams.

## 3.4 Boundary conditions

In case of the 3D $k$-$\varepsilon$ turbulence model, at an open boundary that goes through the water level points just outside the domain, both $k$ and $\varepsilon$ are determined by mirroring the values of the corresponding turbulence quantities, located just inside the domain, at the boundary, see Section 7.2.11 in (Zijlema, 1998). However, for the horizontal $k$-$\varepsilon$ turbulence model we propose a different approach because of the different location of the turbulent quantities.

In case of outflow the Neumann boundary condition

$$\frac{\partial \bar{k}}{\partial n} = \frac{\partial \bar{\varepsilon}}{\partial n} = 0 \tag{3.14}$$

is prescribed, where $n$ denotes the normal direction to the closed boundary. Thus, in case of open boundaries the same approach as for the 3D $k$-$\varepsilon$ turbulence model is used. However, in

case of inflow fixed values for the turbulent energy $\overline{k}$ and the energy dissipation $\overline{\varepsilon}$ are applied:

$$\overline{k} = 1.10^{-5} \quad and \quad \overline{\varepsilon} = 4.10^{-4} \tag{3.15}$$

These values have been taken from the implementation of Bijvelds. It should be remarked that these values are a rather arbitrary choice. As an indication, the ratio $\overline{k}/\overline{\varepsilon}$ corresponds to a time scale. For the choice of $\overline{k}$ and $\overline{\varepsilon}$ in Eq. (3.15) we arrive at a time scale of a few seconds, which means that $\overline{k}$ and $\overline{\varepsilon}$ will rapidly disappear. Thus, in the present implementation the horizontal viscosity is not advected/dissipated into the model domain via the open boundaries, but the horizontal viscosity should be generated via the production term in the interior of the model domain. As an alternative, the values of $\overline{k}$ and $\overline{\varepsilon}$ might be chosen in such a way that the ratio $\overline{k}/\overline{\varepsilon}$ is sufficiently large to avoid a rapid decrease of $\overline{k}$ and $\overline{\varepsilon}$. If we, for example, assume that

$$\frac{\overline{k}}{\overline{\varepsilon}} = \alpha \quad and \quad \frac{\overline{k}^2}{\overline{\varepsilon}} = 1 \tag{3.16}$$

with $\alpha$ some time scale, then we arrive at

$$\overline{k} = 1/\alpha \quad and \quad \overline{\varepsilon} = 1/\alpha^2 \tag{3.17}$$

Finally, the implementation of the discretization of the advective and diffusion term is such that no values at closed boundaries are required. In other words, these terms are neglected near a closed boundary. We remark that this approach is similar to the treatment of thin dams. In numerical experiments we have observed that the choice of the type of boundary conditions is not critical. Alternative implementations, based on a estimate for $\overline{k}$ and $\overline{\varepsilon}$ at closed boundaries, yielded quite similar results.

# 4 Test models

In this chapter we will describe the numerical results of the horizontal $k$-$\varepsilon$ turbulence model for the following three test models:

- Yacht harbour "t Steel" (Bijvelds, 1997)
- Shallow-water mixing layer model (Tukker, 1997)
- MOHA (Monding Haringvliet) model (Soerdjbali, 1999)

These test models have been specified by RIKZ. For all three test models measurements are available. These measurements will be used for validation.

The yacht harbour "t Steel" (Bijvelds, 1997) simulation has already been performed with a horizontal $k$-$\varepsilon$ turbulence model. In this simulation a research version of Delft3D-FLOW, developed by Bijvelds, was used (Bijvelds, 1997). This implementation of a horizontal $k$-$\varepsilon$ turbulence model is almost identical to the one described in Chapters 2 and 3 of this report. We will carry out the TRIWAQ simulations with a horizontal $k$-$\varepsilon$ turbulence model. We therefore expect that the results of the TRIWAQ version will be very similar to the results of Bijvelds obtained with the Delft3D-FLOW version.

In the first two test models, namely the yacht harbour "t Steel" and the shallow-water mixing layer experiments of Uijttewaal and Booij (1999) a shallow-water mixing layer has been observed in which horizontal turbulent structures develop with characteristic length scales much larger than the water depth. These quasi-two-dimensional turbulent structures contribute to the transfer of mass and momentum across the mixing layer, hence the mixing layer plays an important role in the exchange of mass and momentum in many practical situations where two flows with different velocity meet. In the test model "t Steel" a mixing layer occurs in the harbour entrance because the water velocity in the river is larger than in the harbour itself. Caused by the velocity difference at the harbour entrance instabilities occur which eventually leads to the generation of turbulence. In the second test model, the velocity difference is imposed by the inflow boundary conditions at each side of the splitter plate. At the inlet of the physical scale model two flows with a different velocity are separated by a so-called splitter plate. At the end of the splitter plate a mixing layer starts to develop because of the difference in velocity below and above the splitter plate. Then, large (quasi two-dimensional) horizontal turbulence structures are generated in the regions of horizontal shear.

## 4.1 Yacht harbour "t Steel"

In April 1997 laboratory measurements were carried out at the Hydromechanics Laboratory of the Civil Engineering Faculty of Delft University of Technology with a scale model of yacht harbour "t Steel". This harbour is located in the river Meuse between kilometer 78.4 and 78.9. In this laboratory model a scale factor of 1:50 was used both in horizontal and vertical direction. This physical scale model was set-up to investigate a possible reduction of the harbour siltation by slightly changing the harbour geometry (Van Schijndel, 1997).

In the laboratory experiment horizontal velocities $U$ and $V$ were measured simultaneously, which allows for the determination of the horizontal Reynolds shear stress, which is an important quantity to validate the two-length-scale turbulence model.

As mentioned above, the velocity of the river flow is larger than in the harbour entrance. This velocity difference results from the separation of the flow in the river at the upstream corner of the harbour entrance. The shear layer is unstable and a mixing layer develops. Part of the water of the mixing layer flows into the harbour, where it encounters a downstream harbour wall. The location of the stagnation point is determined by the amount of river water and the harbour water that is entrained into the mixing layer. In the harbour a circulating flow, a so-called gyre, arises. The gyre in the harbour is induced by the entrainment of harbour water into the mixing layer and the supply of water from the mixing layer into the harbour near the stagnation point.

In the laboratory experiment the existence of large turbulent structures was visualized by injecting upstream of the mixing layer dissolved KMnO4 into the water, see Figure 4.1.3. In this figure four (developing) quasi 2D structures and a gyre can be distinguished with a characteristic length scale of several times the water depth.

Figure 4.1.3 Top view of a shallow-water mixing layer and flow pattern in a harbour entrance at laboratory scale. Taken from Bijvelds (1997).

### 4.1.1 Model characteristics

In Figure 4.1.1 bathymetry of the numerical "t Steel" model is shown. The size of this laboratory model is approximately 9 m by 3.5 m. The width of the harbour entrance (roughly 1 m) is approximately ten times the average water depth. Figure 4.1.2 contains the employed curvilinear grid. Special attention has been paid to the (stair-case) boundary locations at the harbour entrance. It is known that stair-case boundaries introduce computational errors. However, owing to the complexity of the geometry stair-case boundaries can not be avoided completely. The model contains 81 by 75 grid points in the horizontal direction. In the vertical ten non-uniformly distributed layers are applied. The vertical column is distributed in ten layers, representing 15,15, 14, 14,12, 10, 8, 6,4 and 2 percent of the water depth. Thus, near the bottom the resolution is higher, which allows for an accurate representation of sharp gradients near the bottom.

At the inflow boundary a flow rate of 0.041 $m^3/s$ was imposed for the whole inflow boundary. A non-uniform discharge distribution along this open boundary was applied. The flow rate of 0.041 $m^3/s$ corresponds to a bulk Reynolds number $Uh/\nu$ based on the average velocity in the river of approximately 40000, which means that the flow is evidently turbulent. The Froude number $U/\sqrt{gH}$ yields a value of 0.28, which corresponds to a subcritical condition. For the bottom friction a constant Chezy value of *70* is applied. At outflow a water level boundary of *0 m* is prescribed. A (background) value of $10^{-6}$ is used for the horizontal eddy-viscosity, which represents the kinematic viscosity. This value for the horizontal eddy-viscosity is increased by the turbulent viscosity, which is computed by the horizontal $k$-$\varepsilon$ turbulence model.

Owing to the fact that the boundary conditions are constant in time, a steady state solution is reached. The simulation period of ten minutes is long enough to reach the steady state. In the experiments it has been observed that after approximately six minutes the steady state is reached. The time step is 0.024 sec. Such a small time step is required because of the explicit integration of the horizontal viscosity.

In this application the turbulent viscosity, which depends on the flow and on the intensity of the turbulence, is dominant over the kinematic viscosity (assumed to be $10^{-6}$ $m^2/s$). From literature several formulations are known to estimate the turbulent viscosity. For example, the estimate of Booij (1991) for a laboratory model with a *square* harbour reads

$$\nu_t^{2D} = 0.0014\ U\ B \tag{4.1}$$

which yields a value of approximately $4.\ 10^{-4}\ m^2/s$.

In the laboratory measurements two gyres have been observed. The primary gyre is at the harbour entrance. Deeper into the harbour a second gyre is observed, which rotates in the other direction (anti clock-wise). We remark that the flow velocities in the harbour were observed to be very low and the corresponding Reynolds number was approximately as low as 1000.

### 4.1.2 Model results

In Figure 4.1.4 the steady state surface layer velocities at the harbour entrance (in black), computed with TRIWAQ, are plotted together with the steady state bottom layer velocities (in red). The primary gyre is clearly visible. The variation in vertical direction of the horizontal velocities is small. Thus, the flow is more or less two-dimensional. In Figures 4.1.5-6 the velocities are compared with measurements. It can be seen that velocities in the harbour entrance, down of the stagnation point, are significantly underestimated by the model simulation, which is in agreement with conclusions drawn in (Bijvelds, 1997). The centre and shape of the primary gyre are, however, correctly predicted by the horizontal $k$-$\varepsilon$ turbulence model.

As a consequence of the lower velocities in the primary gyre, the computed velocities in the secondary mixing layer are considerably lower as well, see Figure 4.1.7. The location of the secondary mixing layer differs in comparison with the measurements.

In (Bijvelds, 1997) it was suggested that the difference in velocities between the measurements and the model computations may be due to the rather crude representation of the model boundary at the upstream part of the harbour entrance. It is known that stair case boundaries introduce additional friction which decelerate the flow. Furthermore, it was suggested in (Bijvelds, 1997) that the turbulent kinetic energy near the stagnation point and consequently the horizontal eddy-viscosity may be overestimated.

As an illustration, at the bottom of the inflow boundary a continuous tracer was released in the simulations. Figure 4.1.8 represents a contour plot of the tracer concentrations for the steady state situation. One clearly observes that part of the tracer enters the harbour. The highest concentrations correspond to the location of the primary mixing layer. Furthermore, the tracer has the tendency to follow the secondary gyre, see the left bottom part of the harbour entrance. However, due to the low velocities of the secondary gyre, hardly any tracer substance enters the secondary mixing layer.

Figure 4.1.9 contains contours of the horizontal turbulent kinetic energy, dissipation and viscosity, respectively. The values at the end of the simulation period are plotted, for which the steady state has been reached. For the river part and for the primary mixing layer the results are in close agreement with the ones in (Bijvelds, 1997). This is the case for both the horizontal turbulent kinetic energy, the dissipation and the horizontal viscosity. Both the absolute values and the horizontal distribution are rather similar. For the sake of completeness we have added Figure 4.1.10, which shows the numerical solution computed by Bijvelds. However, further into the harbour, which more or less corresponds to the secondary mixing layer, a large difference is observed between the Delft3D-FLOW results of Bijvelds (Figure 4.1.10) and the solution computed with TRIWAQ (Figure 4.1.9). After detailed checking of both implementations, it was concluded that the large difference in results was caused by a different implementation of the restart functionality. In the TRIWAQ implementation the restart functionality has been computed correctly, which means that also the turbulent quantities of the horizontal $k$-$\varepsilon$ turbulence model are part of the restart file, which was not the code for the ad hoc Delft3D-FLOW implementation that was used in (Bijvelds, 1997). As a result, the numerical solution in Figure 4.1.9 corresponds

to the steady state solution of the TRIWAQ simulation, whereas the results in Fig. 4.1.10 are based on a steady state solution for the hydrodynamic flows but not for the turbulent kinetic energy and the dissipation rate (and also for the horizontal viscosity ).

In the primary mixing layer the computed turbulent viscosity is roughly $10^{-3}$ $m^2/s$, which is in the same order of magnitude as the estimate of Booij (see Eq. (4.1)), which is satisfying. Unfortunately, in the steady state solution the highest values for the horizontal viscosity occur in the eastern part of the harbour. In this part there is hardly any flow, see Figure 4.1.7 and the so-called Reynolds number are therefore laminar and clearly not turbulent. The horizontal turbulent kinetic energy and the dissipation rate computed by the horizontal $k$-$\varepsilon$ turbulence model are much smaller than, for example, the values in the primary mixing layer. However, the ratio $k^2/\varepsilon$ is much too large in the secondary mixing layer. It appears that for the area deep into the harbour the horizontal $k$-$\varepsilon$ turbulence model has been applied beyond its limits of applicability.

To circumvent the high viscosities in regions of hardly any flow, a lot of possible remedies have been tested (in arbitrary order):

- different boundary conditions at closed boundaries
- a lower bound for the dissipation rate
- examine influence of wall friction
- upper limit for the horizontal viscosity based on the Reynolds number
- upper limit for the horizontal viscosity based on the mixing length
- changing of the Prandtl Schmidt number for the dissipation rate
- addition of so-called external dissipation (dependent on bottom friction)
- different time integration levels (explicit or implicit) for $\overline{k}$ and $\overline{\varepsilon}$
- other integration scheme for advection

None of the possible remedies yielded a satisfactory solution for the problem of unrealistically high value of the horizontal viscosity. It was observed that in this area of laminar flow the dissipation, diffusion, production and advection are (off course) in equilibrium. The dissipation and the diffusion is roughly three times and twice as large as the production term, respectively. The advection is an order of magnitude smaller than the other terms. This also explains why a different advection scheme did not yield a satisfactory solution. Summarizing, no satisfactory remedy has been found yet to solve, *for this specific application,* the problem of a high horizontal viscosity in the eastern part of the harbour. We remark that this problem is observed for a laboratory model with very low velocities in part of the model area. In advance, this does not mean that the same problem also occurs for realistic, larger scale, test models.

## 4.2 Shallow-water mixing layer model

In (Uijttewaal et al., 2000) an extensive set of measurements was presented for a shallow-water mixing layer. In this laboratory model the development of large quasi two-dimensional turbulence structures was observed and analysed. For example, the influence of bottom friction and shallowness was examined. In this section we will simulate this

experiment with the TRIWAQ code containing the implementation of a horizontal $k$-$\varepsilon$ turbulence model.

At the Laboratory of Fluid Mechanics at the Delft University of technology a mixing layer has been studied with a depth of 67 mm (Uijttewaal et al., 2000). The inlet section of the flume consists of two separate parts divided by a splitter plate of 3 m. The velocities at both sides of the splitter plate are 0.14 and 0.32 m/s, respectively. These velocities correspond to Reynolds numbers, defined by $Uh/\nu$, of 9400 and 21400, respectively. The splitter plate has been modelled by dam points. Thus, in this experiment the splittter plate has a thickness of 6 cm (1 grid cell). As described in Chapter 3, in the present implementation of the horizontal k-ε model there is no fundamental problem for thin dams. So, the splitter plate could have been modelled by a thin dam as well.

In the numerical experiment we have used a model dimension of 18 m by 3 m. An equidistant grid is applied with a mesh size of 0.06 m. A long simulation period is required to reach the steady state. Therefore, we have chosen a simulation period of 50 minutes with a time step of 0.001 min. Furthermore, a 2D model has been simulated, because even for such a 2D model the required computation time is already huge. In the simulation we have released a continuous tracer just below and above the splitter plate. In this way, the turbulent behaviour of the flow beyond the splitter plate can be followed.

As a consequence of the initial velocity difference a mixing layer starts to develop beyond the end of the splitter plate. It is known that a system of two parallel streams with different flow velocity is subject to the so-called Kelvin-Helmholtz instability, which means that wave-like disturbances that grow in the downstream direction and roll-up to become vortices that form a mixing layer. In Figure 4.2.1, which shows the tracer concentration after one minute of simulation, the instable behaviour of the flow can be easily identified. Next, Figure 4.2.2 contains the tracer concentration after 50 minutes. Although the numerical solution is still not fully steady state, it can be seen that such a situation has almost been reached. In Figure 4.2.3 contours of the horizontal turbulent kinetic energy, dissipation and viscosity are presented, respectively. Owing to the larger velocities in the upper part of the splitter plate, the mixing layer has shifted towards the lower velocity side.

In (Uijttewaal et al., 2000) values were presented for, among others, the velocities on both sides of the splitter plate, the width of the mixing layer and the Reynolds stress. We will now compare the measurements in (Uijttewaal et al., 2000) with the numerical results computed by the horizontal $k$-$\varepsilon$ turbulence model.

| | measurements | | model results | |
|---|---|---|---|---|
| x(m) | $u_1$ (m/s) | $u_2$ (m/s) | $u_1$ (m/s) | $u_2$ (m/s) |
| 0.0 | 0.14 | 0.32 | 0.14 | 0.32 |
| 2.0 | 0.16 | 0.32 | 0.16 | 0.32 |
| 5.8 | 0.18 | 0.31 | 0.16 | 0.30 |
| 11.0 | 0.21 | 0.30 | 0.20 | 0.27 |

Table 4.1: Velocities on both sides of the mixing layer at several downstream positions.

In Table 4.1 $u_1$ and $u_2$ represent the low and high velocities at both sides of the splitter plate, respectively. From Table 4.1 it is evident that the measurements are in good agreement with the model results. We remark that, although the velocities on both sides of the mixing layers are slightly smaller in the model results than in the measurements, the discharge in lateral direction is identical.

Next, we will compare the width of the mixing layer. In (Uijttewaal et al., 2000) the width $\delta$ was defined by

$$\delta = \frac{u_1 - u_2}{(\partial u / \partial y)_{max}} \tag{4.2}$$

with $u_1$ and $u_2$ defined above. For the same positions as in Table 4.1 we now list the width of the mixing layer, see Table 4.2.

| | measurements | model results |
|---|---|---|
| x(m) | $\delta$ (m) | $\delta$ (m) |
| 2.0 | 0.19 | 0.24 |
| 5.8 | 0.31 | 0.45 |
| 11.0 | 0.45 | 0.60 |

Table 4.2: Width of the mixing layer at several downstream positions.

We remark that the measured values have been estimated from Figure 6 in (Uijttewaal et al., 2000). Furthermore, one should take into account that in the model simulation a constant mesh size of 0.06 m has been used. This means that the computation of the velocity gradient in Eq. (4.2) can be rather inaccurate. With this in mind, one can conclude that the measured and computed width of the mixing layer are in satisfactory agreement.

Finally we will compare measured and computed Reynolds stress. Figure 4.2.5 contains the computed Reynolds stress for the steady state solution. Measured values of the Reynolds stress for this experiment can be found in Figure 14 in (Uijttewaal et al., 2000). In Table 4.3 we have given a overview of the Reynolds stresses at several downstream positions.

| | measurements | model results |
|---|---|---|
| x(m) | $u'v'$ $(m/s)^2$ | $u'v'$ $(m/s)^2$ |
| 2.0 | $3.0\ 10^{-4}$ | $7.0\ 10^{-4}$ |
| 5.8 | $2.5\ 10^{-4}$ | $2.5\ 10^{-4}$ |
| 11.0 | $2.0\ 10^{-4}$ | $1.5\ 10^{-4}$ |

Table 4.3: Reynolds stress at several downstream positions.

Owing to variations in the measurements the measured values in Table 4.3 should be considered as rough estimations. Our only goal is verify whether the Reynolds stresses are in the same order of magnitude, which is clearly the case.

In conclusion, for the shallow-water mixing layer test model the computed and measured results are in good agreement. This is the case for all quantities (velocity, width of the mixing layer and in particular the Reynolds stress) that have been compared.

## 4.3 MOHA (MOnding HAringvliet) model

We will now verify the TRIWAQ implementation of the horizontal $k$-$\varepsilon$ turbulence model for a realistic test model, namely a MOHA (MOnding HAringvliet) model. The MOHA model has been set-up to examine the changes in hydrodynamics due to the construction of a dam in the Haringvliet. As a result, the change in hydrodynamics has a large effect on the ecological environment in the Haringvliet. The quality of the bottom has deteriorated considerably since the closure of the Haringvliet. In the "MER Haringvlietsluizen" several alternatives to partially re-open the Haringvliet sluices have been examined. In this project we selected one of these scenarios to investigate the influence of the horizontal k-ε turbulence model on the numerical results.

The MOHA model consists of 102 by 149 grid points in the horizontal direction. In the vertical direction an equidistant eight layer distribution is applied. Figure 4.3.1 contains the bathymetry of the MOHA model. The simulation period is from 3 March 1997 10:00 hour to 16 March 1997. During the period of 10-15 March the Haringvliet sluices are open. For this period measurements are available from the measuring campaign "Meetproef 1997". The time step in the MOHA model is 30 sec.

Two simulations have been carried out, a reference simulation (without horizontal $k$-$\varepsilon$ turbulence closure model) and a simulation with the horizontal $k$-$\varepsilon$ turbulence model. In the latter simulation it has been observed that the computed horizontal viscosities are extremely small, even much smaller than the molecular eddy-viscosity, which is assumed to be $10^{-6}$. Thus, no differences of any importance have been observed between the reference simulation and the simulation with the horizontal $k$-$\varepsilon$ turbulence closure model. The increase in computation time, which is caused by the computation required for the horizontal $k$-$\varepsilon$ model, is about 15%.

In Figures 4.3.2-3 time histories of the velocity magnitude and the salinity are shown. For the time histories of magnitudes at two stations (sluizen-7 en sluizen-12) close to the Haringvliet sluices have been selected, because the highest velocities occur in that area. In Figure 4.3.2 it can be seen that magnitudes of several m/s occur. The time histories of salinity are shown at locations at which stratification occurs, namely stations MTP 1-3 and PUT-4 (see Figure 4.3.3) and at Paal 2 W and Paal 2 O (see Figure 4.3.4).

The main differences with two previous test models is that the mesh sizes in the MOHA model considerably differ from the ones in the two other test models. For the yacht harbour "t Steel" and for the shallow-water mixing layer model the mesh sizes are in the order of 5 to 10 cm. For the MOHA model, however, the average mesh size is more than 100 m with

a smallest mesh size of approximately 30-40 m in the near surrounding of the Haringvliet sluices. A second important difference is that in the first two test models constant open boundary conditions, which yielded a steady state situation, whereas in the MOHA test model time varying conditions were simulated. Furthermore, in the MOHA test model drying and flooding plays a role, which might cause problems for the turbulence model.

The 3D MOHA test model is the first one in which the horizontal $k$-$\varepsilon$ turbulence model of (Bijvelds, 1997) was applied for a model schematization with mesh sizes that are commonly used in 3D model simulations (mesh sizes in the order of 50 m). The fact that a very low horizontal eddy-viscosity is computed clearly indicates that further research is required to examine the applicability of this method for mesh sizes that are used in practice. Thus, at first the limits of applicability of the implementation of the horizontal $k$-$\varepsilon$ turbulence model should be investigated. In Appendix A already alternatives are discussed.

# 5 Conclusions

The present concept in TRIWAQ for the horizontal eddy-viscosity is a constant value in both space and time, which should be specified by the user. Such a formulation for the horizontal eddy-viscosity has clearly an empirical character. For relatively simple flow configurations it is acceptable to specify a somewhat arbitrary value for this coefficient, because this term has little effect. However, for applications such as the simulation of flows in mixing layers, wakes and jets, such a simple formulation is considered to be unsuitable, because then the eddy-viscosity does not depend on the flow characteristics and there is no history effects.

Therefore, RIKZ has commissioned WL | Delft Hydraulics, in co-operation with Delft University of Technology and EDS, to implement in this project a more sophisticated formulation for the horizontal eddy-viscosity in TRIWAQ. In particular, the two-length-scale model, in which both 2D and 3D $k$-$\varepsilon$ models occur, developed in (Bijvelds, 1997) has been employed. The two-length-scale model requires a sufficiently fine horizontal grid to resolve the horizontal velocity gradients of the mean flow. We remark that such a two-length-scale model does not bridge the gap between the horizontal turbulent eddies and the grid size. For that purpose a subgrid scale model should be implemented.

In this project the horizontal eddy-viscosity has been defined as the superposition of three eddy-viscosities, representing the eddy-viscosity specified by the user, the quasi 2D (large scale) and the 3D (small-scale) turbulence, respectively. The 3D turbulence is computed in TRIWAQ by a turbulence model, for example the already operational 3D $k$-$\varepsilon$ turbulence model. In general, the small-scale (3D) turbulence strongly depends on the velocity gradients in vertical direction, bed friction, wind and possible stratification.

Quasi 2D (large-scale) turbulence corresponds to length scales larger than the water depth. In this project a two-length-scale model has been implemented in TRIWAQ in which not only for the 3D turbulence, but also for the quasi 2D turbulence a $k$-$\varepsilon$ turbulence closure model is applied. In Chapters 2 and 3 a conceptual model and algorithmic implementation for this horizontal $k$-$\varepsilon$ turbulence model has been specified. This model is almost identical to the one described in (Bijvelds, 1997). A slightly more implicit time integration method has been applied for the horizontal eddy-diffusion term, which is more is in line with the implicit approach followed in TRIWAQ.

The implementation of the horizontal $k$-$\varepsilon$ turbulence model has been tested for the following three test models:

- Yacht harbour "t Steel" (Bijvelds, 1997)
- Shallow-water mixing layer model (Tukker, 1997)
- MOHA (Monding Haringvliet) model (Soerdjbali, 1999)

The yacht harbour "t Steel" model has already been simulated with a horizontal $k$-$\varepsilon$ turbulence model, viz. the implementation described in (Bijvelds, 1997). In that project a research version of Delft3D-FLOW, developed by Bijvelds, was used.

The TRIWAQ version with the implementation of a horizontal $k$-$\varepsilon$ turbulence model has been tested in this project for the yacht harbour "t Steel". As expected the numerical results are in close agreement with the ones in (Bijvelds, 1997). Accurate eddy-viscosities are computed in the primary gyre, which is located at the harbour entrance. However, a problem was observed with respect of the computation of the horizontal eddy-viscosity in the harbour, which was not detected in (Bijvelds, 1997). In the steady state solution the highest values for the horizontal viscosity occur in the eastern part of the harbour. In this part there is hardly any flow and the so-called Reynolds number are therefore laminar and clearly not turbulent. The horizontal turbulent kinetic energy and the dissipation rate computed by the horizontal $k$-$\varepsilon$ turbulence model are much smaller than, for example, the values in the primary mixing layer. However, the ratio $k^2/\varepsilon$ is much too large in the secondary mixing layer. A lot of possible remedies have been tested. However, none of them yielded a satisfactory solution.

For the second test model, a shallow-water mixing layer, an extensive set of measurements was presented in (Uijttewaal et al., 2000). The inlet section of the flume consists of two separate parts divided by a splitter plate of 3 m. The depth of the scale model was 67 mm. That research was carried out at the Laboratory of Fluid Mechanics at the Delft University of Technology. In this laboratory model the development of large quasi two-dimensional turbulence structures was observed and analysed.

In the simulation a model domain of 18 m by 3 m has been used with a constant mesh size of 0.06 m. For this shallow-water mixing layer test model the model results computed with the horizontal $k$-$\varepsilon$ turbulence model and are in good agreement with the measurements. This is the case for all quantities (velocity, width of the mixing layer and in particular the Reynolds stress) that have been compared.

Finally, a simulation with a 3D MOHA (MOnding HAringvliet) model has been carried out. The main difference with the two previous test models is that the mesh sizes in the MOHA model considerably differ from the ones in the other two test models. For the yacht harbour "t Steel" and for the shallow-water mixing layer model the mesh sizes are in the order of 5 to 10 cm. For the MOHA model, however, the average mesh size is more than 100 m with a smallest mesh size of 30 m in the near surrounding of the Haringvliet sluices. For this application the horizontal viscosity computed by the horizontal $k$-$\varepsilon$ turbulence model is even smaller than the molecular viscosity, which is assumed to be $10^{-6}$. Such small eddy-viscosities are, off course, unrealistic. The increase in computation time is about 15%.

The 3D MOHA model is the first one in which the horizontal $k$-$\varepsilon$ turbulence model of (Bijvelds, 1997) has been applied to a model schematization with mesh sizes that are commonly applied in practical situations (in the order of 50 m). Furthermore, time varying boundary conditions have been used in the 3D MOHA test model, whereas in most of the previous simulations with the horizontal $k$-$\varepsilon$ turbulence model a steady state situation was

simulated. Also drying and flooding plays a role in the MOHA test model, which might lead to complications for the turbulence model.

These first results of the 3D MOHA model clearly indicate that further research is required. At least, the limits of applicability of the implementation of the horizontal $k$-$\varepsilon$ turbulence model should be investigated. Other aspects that might be investigated are, see also (Bijvelds et al., 1999):

- **The model is based on the k-ε model**. The k-ε model has been developed for three-dimensional turbulent flow characterized by the energy cascade process. The vortex stretching related to the cascade process is impeded in case of quasi-2D turbulence and therefore the model is applied beyond its limits of applicability.
- **Standard coefficients of the depth-averaged k-ε model are used**. These coefficients have been derived for flows that deviate strongly from the ones described in this report.
- **Transfer of energy neglected**. The transfer of energy from the large scale turbulent structures to the small scale turbulent structures and vice versa have been neglected. The neglect of transfer of energy from the large scale turbulent structures to the small scale turbulent structures is justified, based on comparison with the production term in the turbulence model. Interaction via the mean flow equations exists.
- **Use of the eddy-viscosity**. The use of the eddy-viscosity concept for quasi-2D turbulence meets difficulties due to the possible reverse flow of energy from small scales to large scales.
- **Not applicable for stratified flows.** The model has been developed for unstratified flows. Extension of the model for application in stratified flows, however, is not trivial and requires additional research.

In Appendix A alternatives to resolve above described problems are discussed. The main conclusion of the additional research described in Appendix A is that the horizontal $k$-$\varepsilon$ turbulence model is able to compute realistic horizontal eddy-viscosities for the MOHA model if

- a first-order upwind discretization (implicit in time) is used instead of the directional upwind method,
- model coefficient $c_{\varepsilon 2}$ is tuned slightly (from a default value of 1.92 to 1.8),
- molecular viscosity $\nu_{mol}$, which is set to $10^{-6}$, is added to the production term,
- the implementation of closed boundaries is slightly changed.

The first three changes, especially the adaptation of the advection method, are far more important than the change in implementation of closed boundaries. It should be investigated in more detail why the combination of an explicit time integration method for the advection (either the directional upwind method or the first-order upwind method) with an ADI time integration method for the diffusion term yields large values for the horizontal eddy-viscosity in the MOHA model, leading to convergence problems for the iterative Red-Black Jacobi solver for the momentum equations. For some reason this problem does not occur when the first-order upwind method (implicit in time) is used.

Although it has not been tested in detail yet, it is believed that the horizontal *k*-ε turbulence model will produce adequate horizontal eddy-viscosities for other realistic test models as well. This should be investigated in future.

# 6 References

Bijvelds, M.D.J.P., 1997: Recirculating steady flow in harbours: comparison of numerical computations to laboratory measurements, Fac. of Civil Eng., Delft University of Technology, Tech. Report 1-97.

Bijvelds, M.D.J.P., 1999: 3D numerical computations of the Haringvliet estuary using different vertical co-ordinates, Fac. of Civil Eng., Delft University of Technology, Tech. Report 16-99.

Bijvelds, M.D.J.P. and Kranenburg, C. and Stelling, G.S., 1999: 3-D numerical simulation of turbulent shallow-water flow in square harbor, J. Hydr. Eng., Vol. 125, No. 1, 26-31.

Bijvelds, M.D.J.P. and De Goede, E.D., 1999: On the use of a horizontal k-ε model for shallow-water flow. Literature study, WL | Delft Hydraulics, Report Z2747.10.

Booij, R., 1989: Depth-averaged k-ε model in ODYSSEE, Delft University of Technology, No. 1-89.

Delft Hydraulics, 1999: Delft3D-FLOW manual, Release 3.05, September 1999.

Eijkeren, J.C.H. Van, Haan, B.J. De, Stelling, G.S. and Stijn, Th.L. Van, 1993: Linear upwind biased methods. Numerical methods for advection-diffusion problems, Eds. Vreugdenhil, C.B. and Koren, B.,55-91.

Goede, E.D. de, and Bijvelds, M.D.J.P., 1999: On the use of a horizontal k-ε model for shallow-water flow. Conceptual and numerical description, WL | Delft Hydraulics, Report Z2747.20/Z2747.30.

Kester, J.A.Th.M. van, 1994: Validatie Delft3D voor menglaagproef. Fase 1: verbeterde numerieke implementatie k-ε model, WL | Delft Hydraulics, Report Z810 (in Dutch).

Launder, B.E., and Spalding, D.B., 1974: The numerical computation of turbulent flows, Comput. Meth. Appl. Mech. Engng., Vol 3., 269-289.

Rastogi, A.K. and Rodi, W., 1978: Predictions of heat and mass transfer in open channels, J. Hydr. Eng., Vol. 104, No. 3, 397-420.

Rodi, W., 1980: Turbulence models and their applications in hydraulics - A state of the art review, International Association of Hydraulic Research, Delft, The Netherlands.

Rodi, W., 1985: Calculation of stable stratified shear-layer flows with a buoyancy-extended k-ε turbulence model, Ed. Hunt, J.C.R., Turbulence and diffusion in stable environments, Clarendon, Oxford, 111-140.

Schijndel, S.A.H. van, 1997: Siltation of a river harbour. M. Sc. Thesis, Delft University of Technology (in Dutch).

Smagorinsky, J., 1963: General circulation model experiments with the primitive equations, Monthly Weather Review, Vol. 91, No. 3, 99-164.

Soerdjbali, M., 1999: Detailmodel Mond Haringvliet, Werkdocument RIKZ/OS-99.117X (in Dutch).

Tukker, J, 1997:Turbulence structures in shallow free-surface mixing layers, Ph. D. Thesis, Delft University of Technology.

Uijttewaal, W.S.J. and Booij, R., 2000: Effects of shallowness on the development of free-surface mixing layers. Physics of fluids. Vol. 12, No. 2.

Uittenbogaard, R.E. and van Kester, J.A.Th.M. and Stelling, G.S., 1992: Implementation of three turbulence models in TRISULA for rectangular horizontal grids, Delft Hydraulics Laboratory, Report Z162.

Zijlema, M., 1998: TRIWAQ-three-dimensional shallow-water flow model, technical documentation, Rijkswaterstaat/RIKZ, Version 1.1, May 1998.

# A Further research

In Section 4.3 it has been described that for the MOHA application the horizontal $k$-ε turbulence model is not able to compute horizontal viscosities larger than the molecular value of $10^{-6}$. It appears that for mesh sizes in the order of a few meter and larger this problem occurs. Therefore, the implementation described in Chapters 2 and 3 has been closely examined and alternatives have been examined to solve this problem. We remark that for the other two test model in this report, namely the yacht harbour "t Steel" and the shallow-water mixing layer model, the mesh sizes are approximately 5 to 10 cm.

***Smagorinsky model***

At first experiments have been carried out in which the application the horizontal $k$-ε turbulence model is combined with the well-known Smagorinsky model (Smagorinsky, 1963). This model uses a mixing-length concept in which the eddy-viscosity is assumed to be proportional to the subgrid characteristic length scale equal to the mesh width $\Delta x$ and to a characteristic turbulent velocity $\Delta x\sqrt{(2S_{ij}S_{ij})}$. Then, the eddy-viscosity reads

$$\nu_t^{2D} = \left(C_s \Delta x\right)^2 \sqrt{(2S_{ij}S_{ij})} \quad i,j = 1,2 \tag{A.1}$$

in which $C_s$ is a constant, which is often set to 0.1. This model is based on local balance between production and dissipation. No history effects are present in this model, which are likely to be important in case of large-scale turbulence.

In the experiments a switch has been implemented between the Smagorinsky model and the horizontal $k$-ε model that is based on the cell Peclet number, with

$$\begin{aligned} &for \ \frac{|U|\,\Delta x}{\nu_t^{2D}} > 10^5 \quad \text{Smagorinsky model} \\ &for \ \frac{|U|\,\Delta x}{\nu_t^{2D}} \le 10^5 \quad \text{horizontal } k-\varepsilon \text{ model} \end{aligned} \tag{A.2}$$

For this implementation the above described problem of exceptionally small viscosities computed by the horizontal $k$-ε model is no longer present. By using such a high criterion (of $10^5$) it has been observed that only in a very few occasions the Smagorinsky model was used. This appeared to be sufficient "to keep the horizontal viscosity alive" in the horizontal $k$-ε model. However, another problem is now observed. The horizontal viscosities computed by the horizontal $k$-ε model are now too large.

As an alternative, the following implementation has been used for the discretization of the production term, cf. (2.18):

$$\overline{P_k} = (\nu_t^{2D} + \nu_{mol}) \left[ \left( \left( \frac{\partial U}{\partial y} \right) + \left( \frac{\partial V}{\partial x} \right) \right)^2 + 2 \left( \frac{\partial U}{\partial x} \right)^2 + 2 \left( \frac{\partial V}{\partial x} \right)^2 \right] \quad \text{(A.3)}$$

with the molecular viscosity $\nu_{mol}$ equal to $10^{-6}$. In experiments it has been shown that such a small value was sufficient "to keep the horizontal viscosity alive". Such an approach is identical to the one in the vertical k-ε model, in which the molecular viscosity is also used in the discretization of the buoyancy term, see (Zijlema, 1998).

In the simulations with implementations (A.2) or (A3) it has been observed that now too large viscosities are generated by the horizontal k-ε model. Therefore, possible remedies have been tested to resolve this problem. It was observed that the model results are very sensitive to the choice of the coefficient $c_{\varepsilon 2}$, see Eq. (2.13). We tried to calibrate the model results by tuning the value of $c_{\varepsilon 2}$. The default value of 1.92 for this coefficient has been determined under circumstances which are questionable in case of large scale horizontal turbulence. It is therefore worthwhile to examine the influence of the value of $c_{\varepsilon 2}$ on the numerical results. In Appendix A.2 this issue will be addressed.

## A.1 MOHA model with Smagorinsky implementation

The Smagorinsky model can be seen as a simplified alternative for the horizontal k-ε model, which is widely applied in 3D shallow-water modelling. In this model Eq. (A.1) is used for the computation of the quasi 2D (large scale) turbulence $\nu_t^{2D}$, instead of Eq. (2.15).

The MOHA model described in Section 4.3 has been simulated with a TRIWAQ version in which the Smagorinsky model is used for the computation of the horizontal eddy-viscosity. In Figures A.1.1-3 time histories of the velocity magnitude and the salinity are shown. For the time histories of magnitudes at two stations (sluizen-7 en sluizen-12) close to the Haringvliet sluices have been selected, because the highest velocities occur in that area. In Figure 4.3.2 it can be seen that magnitudes of several m/s occur. The time histories of salinity are shown at locations at which stratification occurs, namely stations MTP 1-3 and PUT-4 (see Figure A.2) and at Paal 2 W and Paal 2 O (see Figure A.1.2). For both the reference simulation, in which a constant eddy-viscosity of 1 $m^2/s$ is used, and the simulation with the Smagorinsky model results are shown.

The differences between these two simulations are small. This is explained by the fact that the horizontal viscosities computed by the Smagorinsky model are in the same order of magnitude. In general, the computed eddy-viscosities are maximally about 10 $m^2/s$. In Figure A.1.4 the horizontal viscosities computed by the Smagorinsky model are shown at 11 March (00:00, 12:00 and 24:00 hour). It is known that for the grid sizes used in the MOHA model viscosities in this order of magnitude (0-10 $m^2/s$) have little effect on the flow.

Figures A.1.5-7 contain contour plots of salinity (both at the top and the bottom layer) for the same three times, i.e. on 14 March 00:00, 12:00 and 24:00 hour. The differences between the two simulations are again very small. It can be seen that salt water is entering

the Haringvliet. At the bottom layer the salt concentrations are clearly higher than at the surface layer.

This MOHA experiment has shown that realistic horizontal eddy-viscosities are computed by the Smagorinsky model. Furthermore, it appears that for applications in which only global flow and transport patterns are of interest, the model formulation for the horizontal eddy-viscosity is not critical. The model results computed by the Smagorinsky model are in close agreement with the model results for a (space and time) constant eddy-viscosity (of 1 $m^2/s$).

## A.2 Sensitivity analysis for the horizontal k-ε model

As discussed in Chapter 5 and in Appendix A.1, the application of the two-length-scale turbulence model may yield unrealistic values for the horizontal turbulent kinetic energy, the horizontal energy dissipation and thus for the horizontal eddy viscosity. To analyse and improve the performance of the model a sensitivity analysis has been performed. The following aspects of the model have been addressed:

- implementation of closed boundaries
- model coefficient $c_{\varepsilon 2}$
- grid resolution

In order to reduce the turn-around time of the computations, only a part of the MOHA-model of Section 4.3 has been used for this analysis. Moreover, an artificial thin dam upstream of the sluices and an artificial island downstream of the sluices have been added to the model to introduce extra velocity gradients. At the inflow boundary at the western side of the model a stationary current of 1 m/s is imposed. At the outflow boundary the water elevation is set to zero. Thus, a steady state solution will be reached, whereas in Section 4.3 the numerical solution of the MOHA model is time dependent.

***Reference simulation***

As described in Chapter 5, the concept of the horizontal $k$-ε turbulence model is formally used beyond its limits of applicability. The behaviour of large-scale quasi-two-dimensional turbulence is essentially different from three-dimensional turbulence. In order to assess the effects of the various changes in the turbulence model, a reference simulation has been carried out by using the standard formulation presented in Chapters 2 and 3. For this reference simulation a typical distribution of the magnitude of the horizontal velocity is shown in Figure A.2.1. In Figure A.2.2 the computed horizontal turbulent kinetic energy and the horizontal eddy-viscosity are shown. The values of $\overline{k}$ are locally too large. The turbulent fluctuations of the horizontal velocity are of the same order of magnitude as the mean velocity, which is physically unsound. Although it is more difficult to assess the value of this quantity it is clear that the standard code generates excessively high values for the horizontal eddy-viscosity.

In the remainder of this section, model results of various alternatives will be compared with the results of the reference simulation.

***Implementation of closed boundaries***

In the present formulation of the model, no values at closed boundaries are required for $\overline{k}$ and $\overline{\varepsilon}$, see Section 3.4. As a consequence, the value of $\overline{k}$ is determined by internal shear only and closed boundaries have no effect on the distribution of the turbulent kinetic energy. By imposing Dirichlet type boundary conditions for $\overline{k}$ and $\overline{\varepsilon}$ with a value of zero, $\overline{k}$ and $\overline{\varepsilon}$ may be reduced significantly, especially near closed boundaries. The values imposed at the closed boundary are transported into the domain by means of diffusion only. So, the zero values for $\overline{k}$ and $\overline{\varepsilon}$ at closed boundaries are not used in the discretization of the advective terms.

In Figure A.2.3 the horizontal eddy viscosity is shown in case of zero values for $\overline{k}$ and $\overline{\varepsilon}$ at closed boundaries. The adjustment of the boundary conditions seems to prevent exceptionally large values for the horizontal turbulent kinetic energy and is therefore preferred. The remaining model simulations will therefore make use of this implementation for closed boundaries. We remark that this approach of zero values for $\overline{k}$ and $\overline{\varepsilon}$ are also applied at "internal" closed boundaries such as dam points and dry areas.

***Model coefficient $c_{\varepsilon 2}$***

The model coefficients in the two-length-scale turbulence model are equal to the coefficients of the three-dimensional standard k-ε model. Within the standard k-ε model the coefficient $c_{\varepsilon 2}$ has been determined from grid-turbulence experiments. The constant $c_{\varepsilon 2}$ has been derived from the measured rate of decay behind a grid and was found to lie between 1.8 and 2.0. Since the energy transfer of large-scale turbulence is essentially different from the energy transfer in three-dimensional turbulence, is seems justified to change the value of the coefficient $c_{\varepsilon 2}$ in order to improve the model results. Three different values of $c_{\varepsilon 2}$ have been tested, namely 1.6, 1.7 and 1.8. From Figure A.2.4 it can be concluded that the latter value gives the best results. Although the eddy viscosity still exhibits high values at certain parts of the domain, in most regions appropriate values of $\overline{k}$ and of the horizontal eddy-viscosity are computed. For smaller values of $c_{\varepsilon 2}$ the turbulence is damped too much.

***Grid resolution***

Three different grids have been used to examine the effect of the grid resolution on the model results. Apart from the original grid (which contains 63x84 grid points), a coarser grid (32x43 grid points) and a finer grid (124x166 grid points) have been tested. Although all three models generate values of horizontal eddy-viscosity that are of the same order of magnitude, the distribution of the horizontal eddy-viscosity in the coarse model is clearly different from the other two models, which use a higher resolution. These latter models yield more or less similar results. It may therefore be concluded that the original grid is sufficiently fine for the computation of the turbulent quantities.

***Conclusions***

From this sensitivity analysis it has been concluded that improvement of the model results compared to the reference simulation could be obtained by changing the implementation of closed boundaries and by decreasing the value of the model coefficient $c_{\varepsilon 2}$. It should be remarked that the sensitivity has been carried out for one test model only, namely a MOHA

model with a steady state solution. To validate the improvements other test models should be examined as well.

## A.3 MOHA model with first-order upwind advection

In Appendix A.1 it was concluded that after adaptation of the implementation of the production term, by adding the molecular viscosity, locally too large values for the horizontal eddy-viscosity were generated. Further tests have shown that this was caused by too small values for the horizontal energy dissipation $\overline{\varepsilon}$, being in the order of, for example, $10^{-15}$ with corresponding values for $\overline{k}$ of $10^{-5}$. In such situations, the ratio of $\overline{k}/\overline{\varepsilon}$ has no physical meaning and yields a exceptionally large value for the horizontal eddy-viscosity. In turn, this may lead to ill conditioned systems of equations for the momentum equations, for which the applied iterative solution method does not lead to a converged solution within the maximal number of iterations (in TRIWAQ equal to 100). Then, the simulation halts.

Further analysis has revealed that the problem of turbulent values very close to zero and an unrealistic ratio for $\overline{k}/\overline{\varepsilon}$ is related to the chosen numerical method for the discretization of the advective terms, namely the directional upwind method, see Section 3.2.1. In (Bijvelds, 1997) it was concluded that such a method was superior to a first-order upwind discretization for the modelling of a square harbour.

As an alternative, a simulation with the MOHA model has been carried out with a first-order upwind discretization (implicit in time) instead of the directional upwind method. Then, the above described problems do not occur. Figures A.3.1-5 contain contours of the horizontal turbulent kinetic energy, dissipation and viscosity, respectively, at 11 March 1997 0:00-12:00 hour with an interval of three hours. All figures show realistic values for the turbulent quantities.

In Figure A.3.6 the horizontal viscosities computed by the horizontal turbulence model are shown at 11 March (00:00, 12:00 and 24:00 hour). This MOHA simulation shows that realistic horizontal eddy-viscosities can be computed by the horizontal turbulence model.

Figures A.3.7-9 contain contour plots of salinity (both at the top and the bottom layer) for the same three times, i.e. on 14 March 00:00, 12:00 and 24:00 hour. The differences between the two simulations are rather small. It can be seen that salt water is entering the Haringvliet. At the bottom layer the salt concentrations are clearly higher than at the surface layer.

It should be investigated in more detail why the combination of an explicit time integration method for advection (either the directional upwind method or the first-order upwind method) with an ADI time integration method for the diffusion term yields large values for the horizontal eddy-viscosity in the MOHA model, leading to convergence problems for the iterative Red-Black Jacobi solver for the momentum equations.

We remark that for the 't Steel model, see Section 4.1, the first-order upwind discretization yield model results that are in close agreement with the ones of the directional upwind method.

***Conclusions***

Additional research has shown that the horizontal $k$-ε turbulence model is able to compute realistic horizontal eddy-viscosities values for the MOHA model if

- a first-order upwind discretization (implicit in time) is used instead of an explicit time integration method,
- model coefficient $c_{\varepsilon 2}$ is tuned slightly (from a default value of 1.92 to 1.8),
- molecular viscosity $\nu_{mol}$, which is set to $10^{-6}$, is added to the production term,
- the implementation of closed boundaries is slightly changed.

The first two changes, especially the adaptation of the advection method, are far more important than the change in implementation of closed boundaries. Although it has not been tested in detail within this project, it is believed that the horizontal $k$-ε turbulence model will produce adequate horizontal eddy-viscosities for other realistic test models as well. This should be investigated in future.

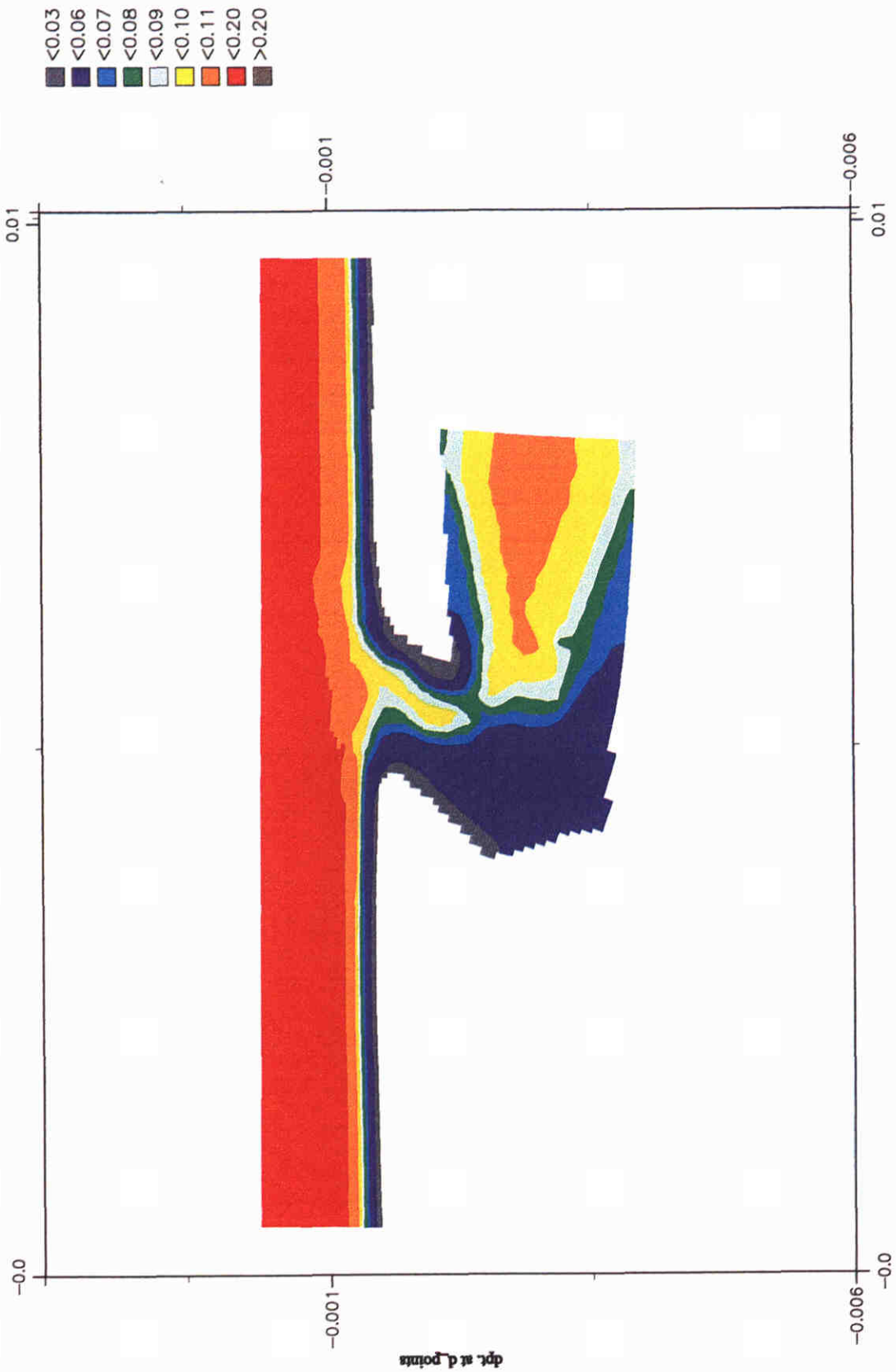


| | | |
|---|---|---|
| Yacht harbour t Steel<br>Bathymetry | | |
| | Fig. 4.1.1 | |
| WL \| DELFT HYDRAULICS | | Z2747.50 |

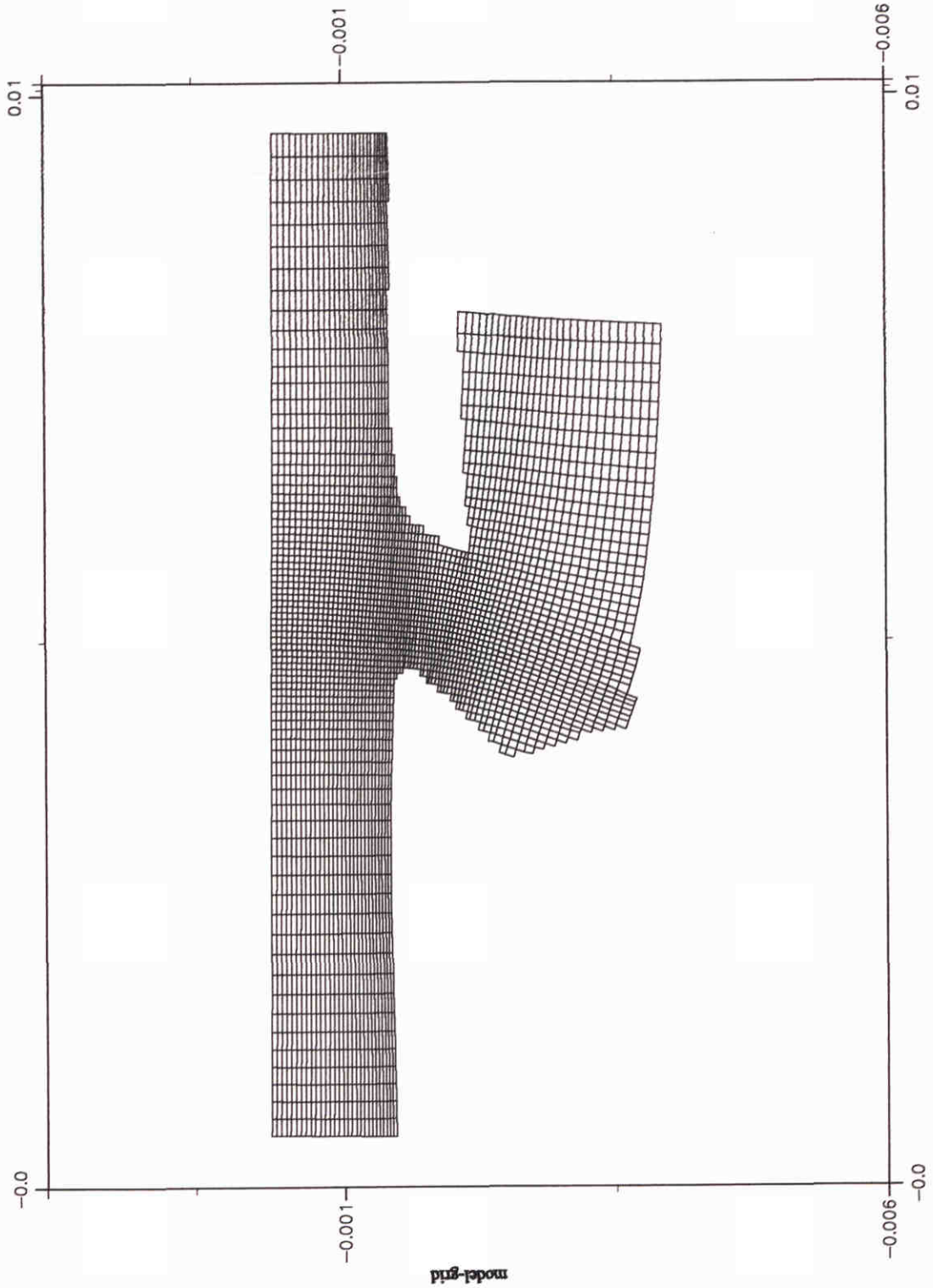


Yacht harbour t Steel
Computational grid

Fig. 4.1.2

WL | DELFT HYDRAULICS

Z2747.50

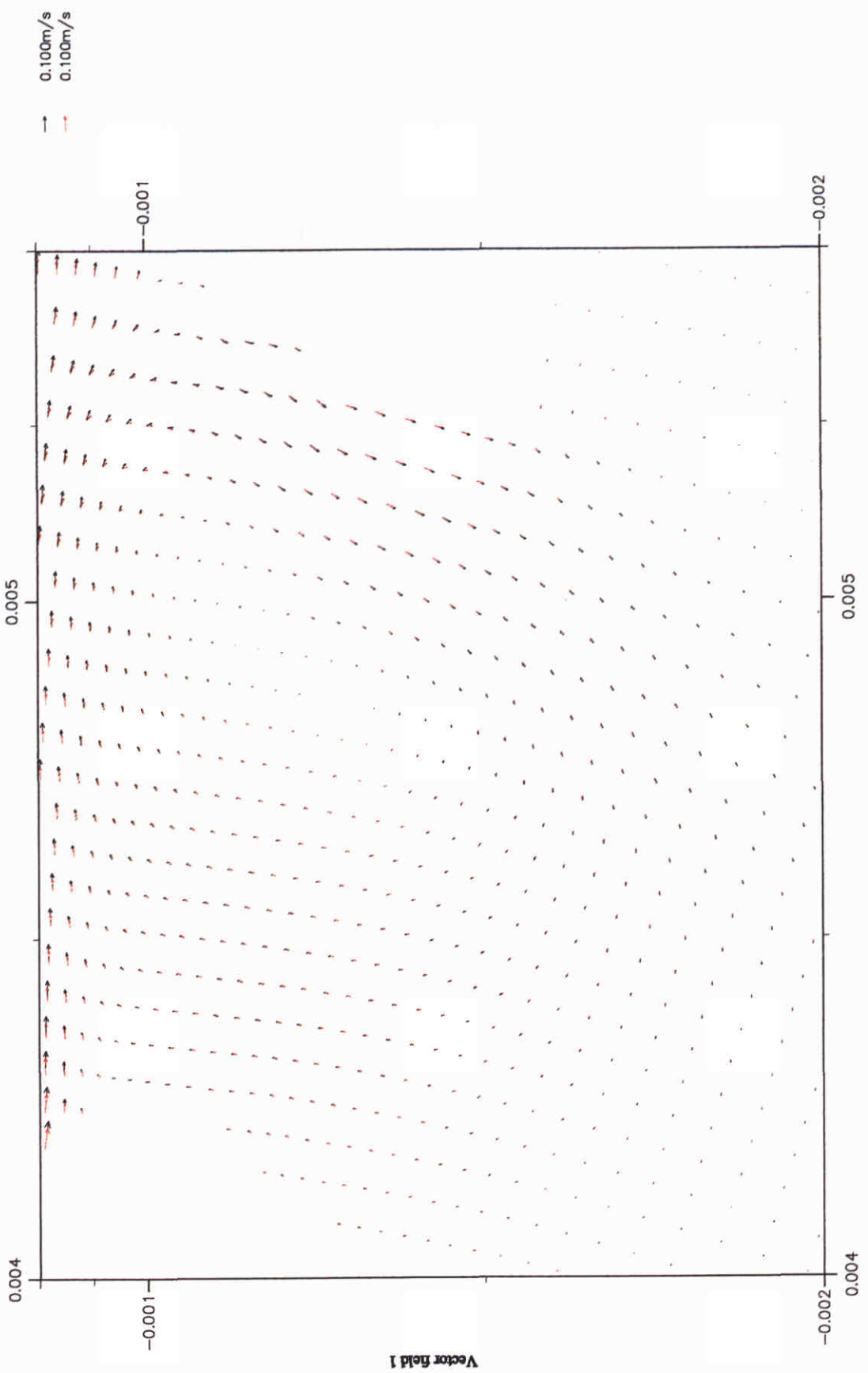


t steel model (3D); TRIWAQ with horizontal turbulence model
vector field
top layer (black) and bottom layer (red)

Fig. 4.1.4

WL | DELFT HYDRAULICS

Z2747.50

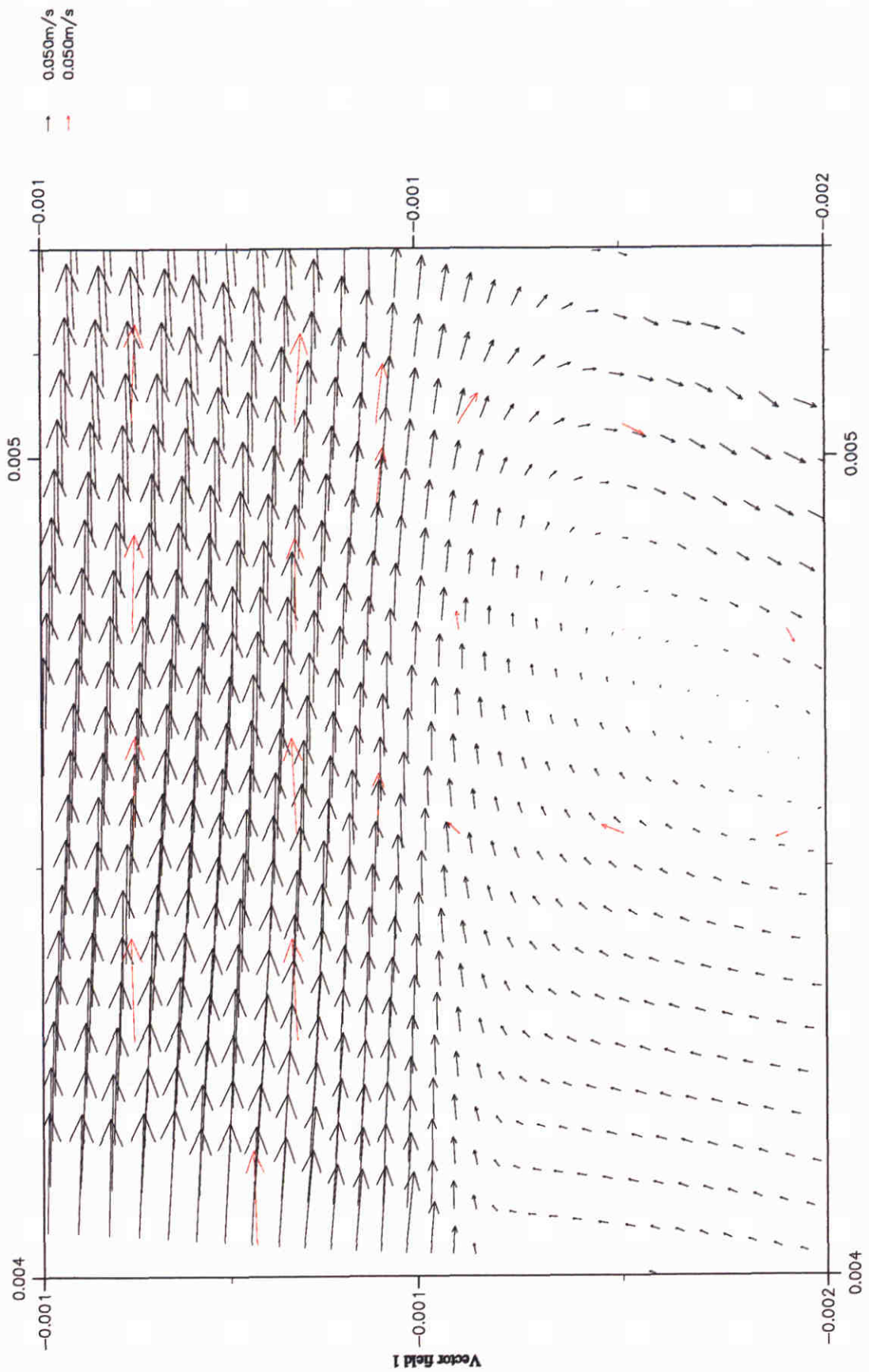


t Steel model (3D)
top layer velocity at harbour entrance (in black)
compared with measurements (in red)

Fig. 4.1.5

WL | DELFT HYDRAULICS

Z2747.50

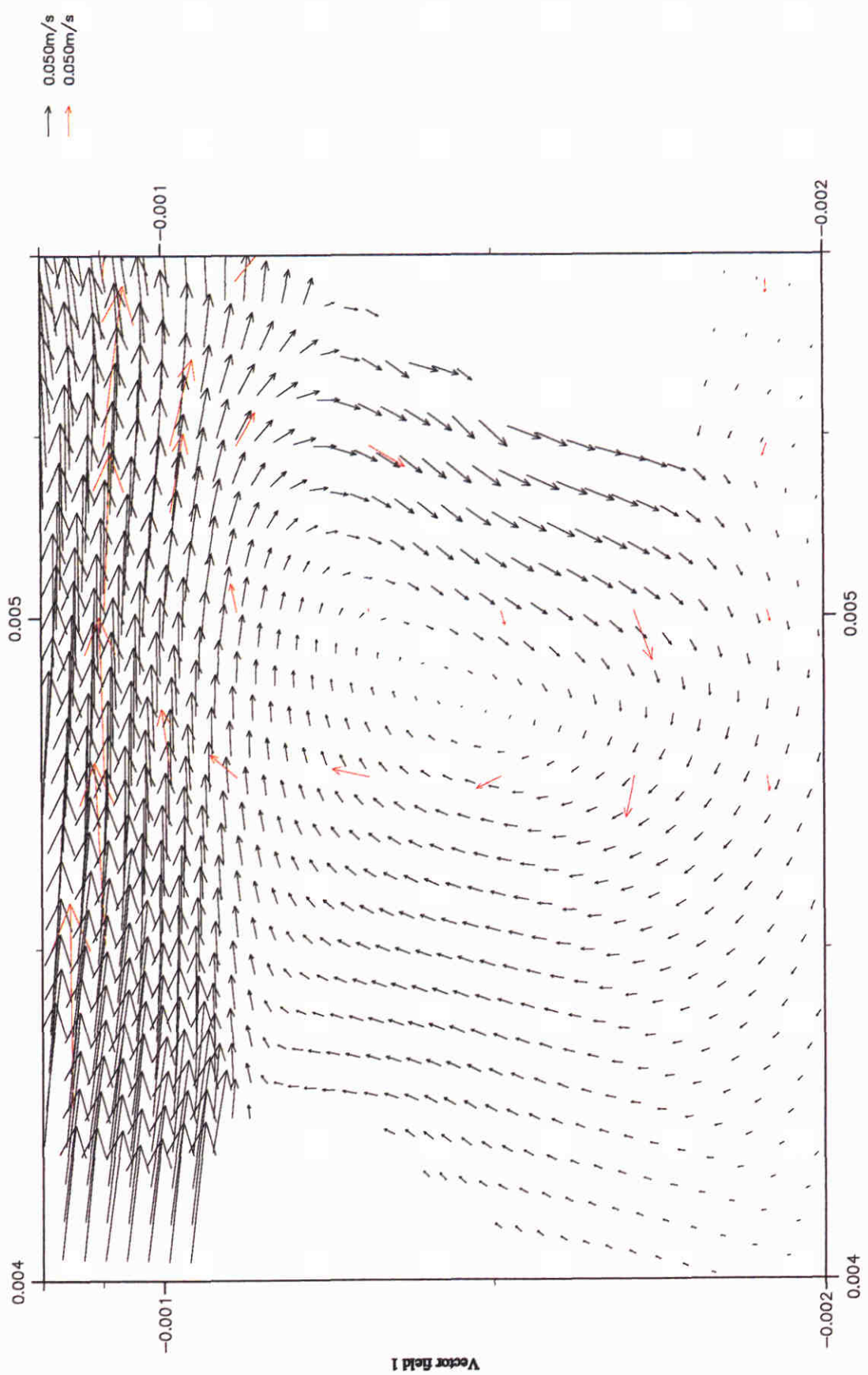


t Steel model (3D)
Velocities at mid depth (in black) compared with measurements (in red)

Fig. 4.1.6

WL | DELFT HYDRAULICS

Z2747.50

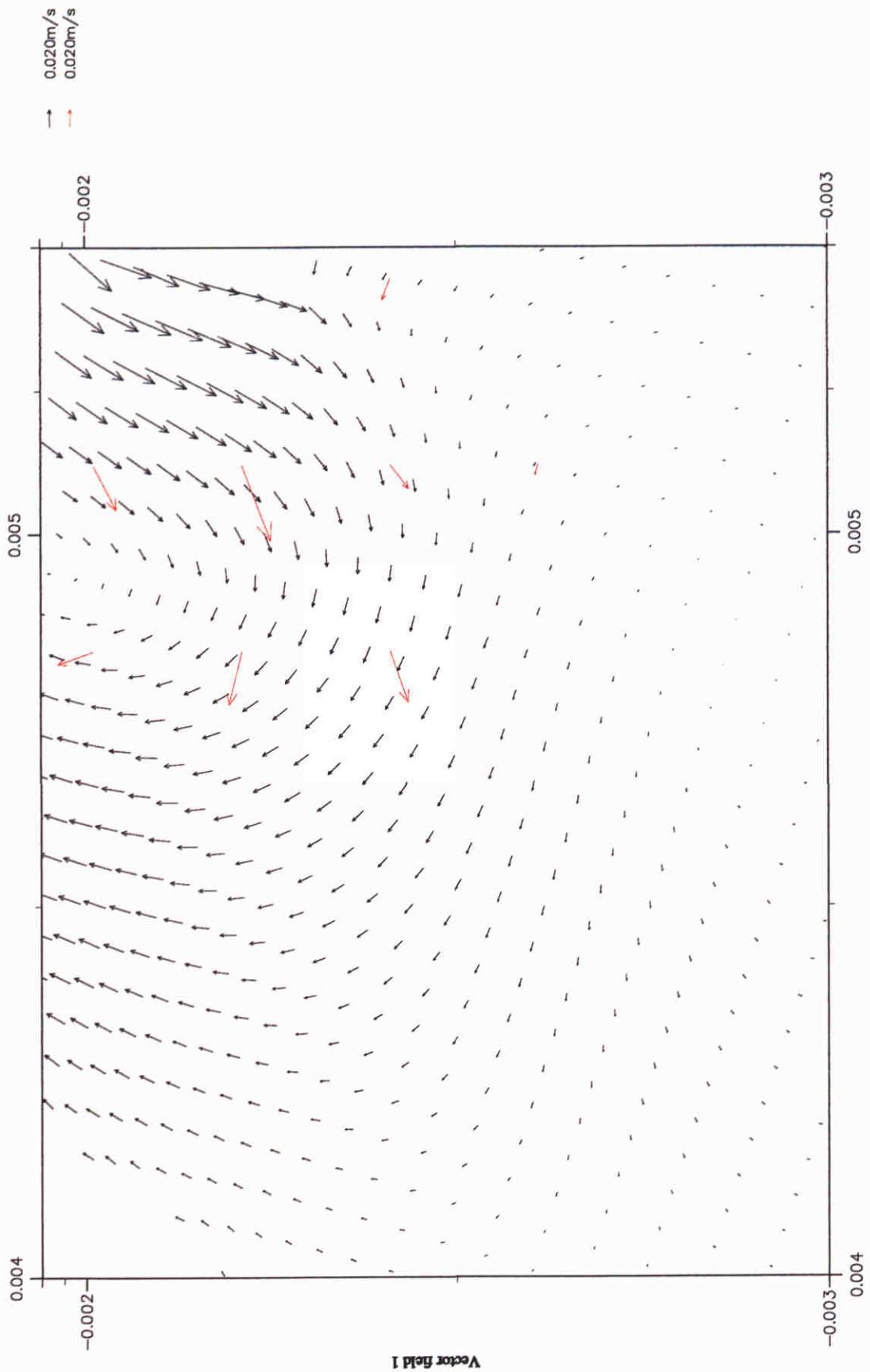


t Steel model (3D)
Velocities in harbour at the surface
Computed solution (in black), measurements (in red)

Fig. 4.1.7

WL | DELFT HYDRAULICS

Z2747.50

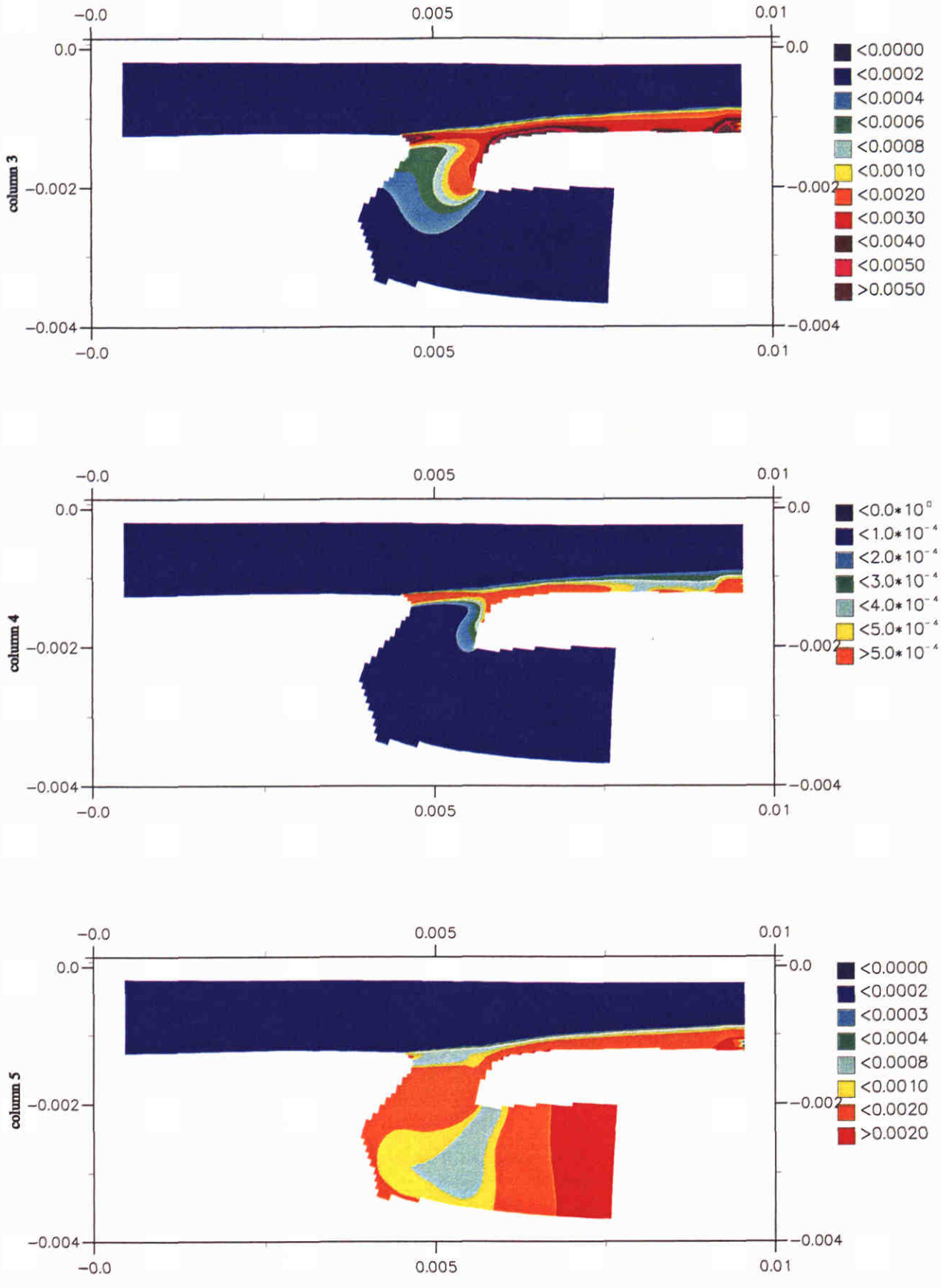


t steel model (3D); TRIWAQ with horizontal turbulence model

upper horiz. tke centre: horiz. dissipation lower horiz. viscosity

Fig. 4.1.8

WL | DELFT HYDRAULICS

Z2747.50

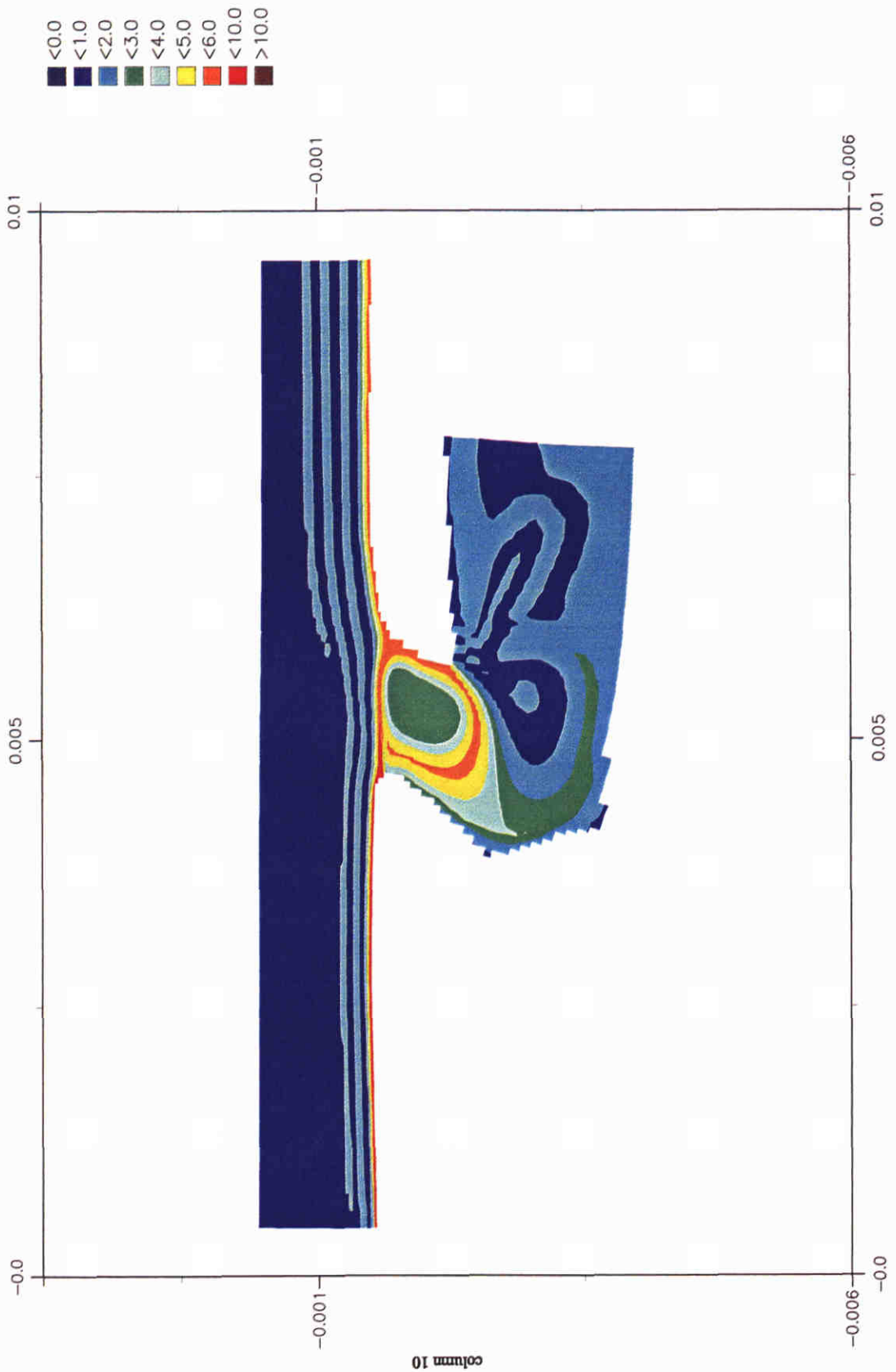


t Steel model (3D); TRIWAQ with horizontal k–eps turbulence model
continuous discharge at bottom of inflow boundary

Fig. 4.1.9

WL | DELFT HYDRAULICS

Z2747.50

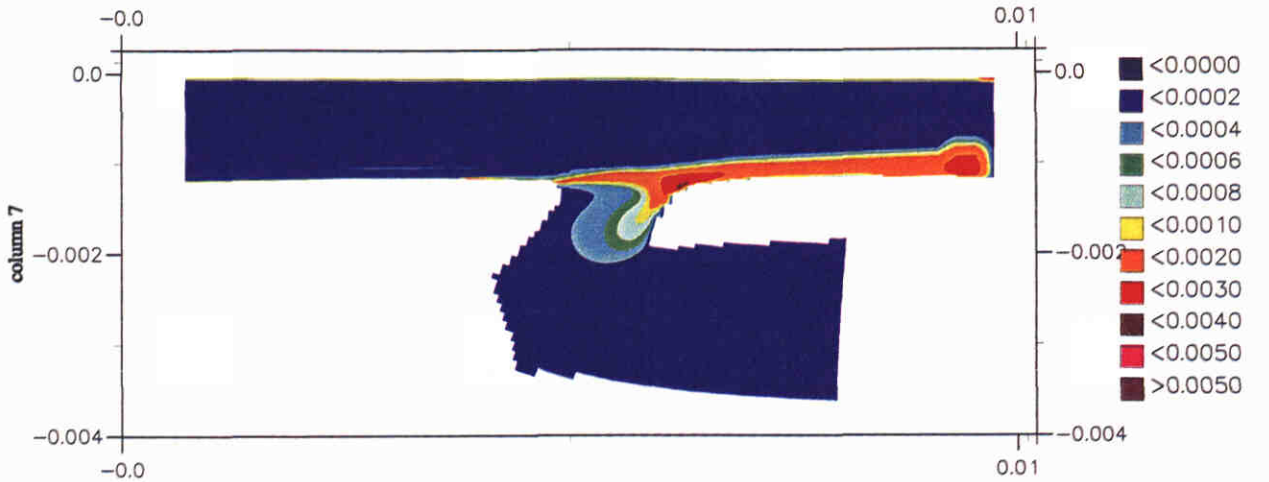


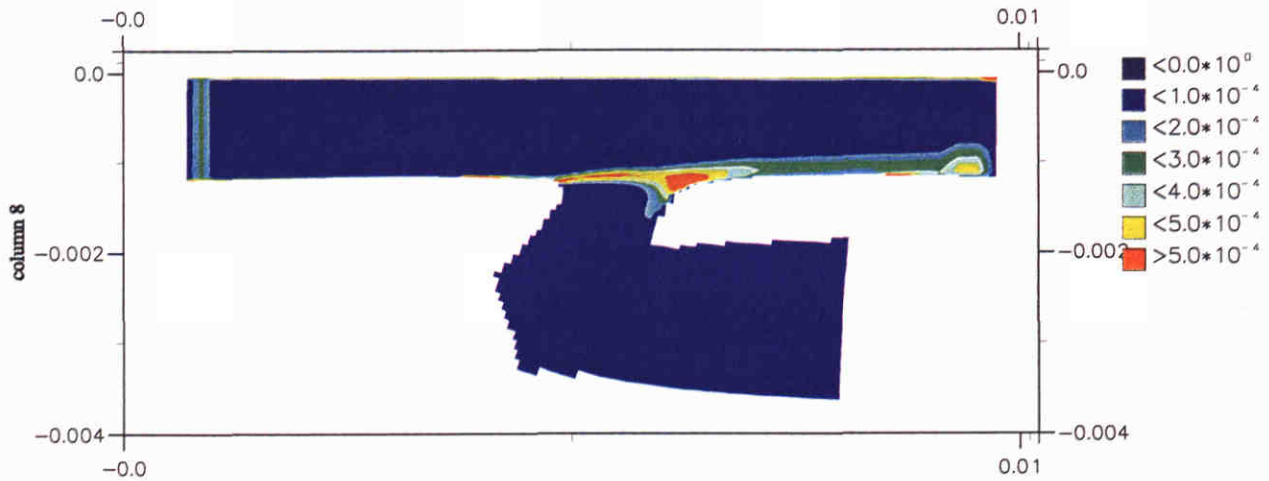


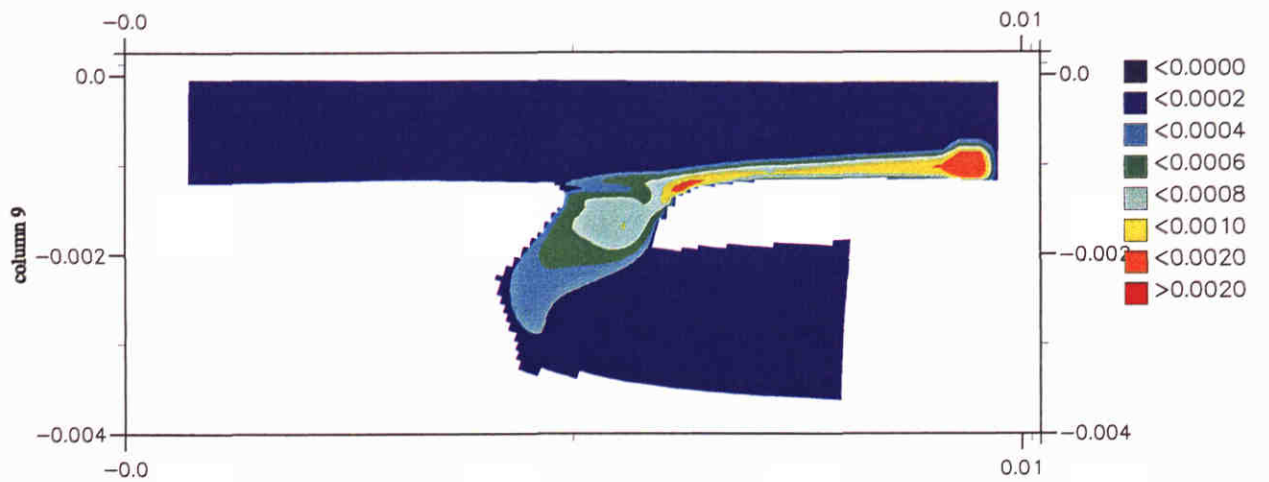


t Steel model (3D); solution computed in (Bijvelds, 1997)

top: horiz. tke centre: horiz. dissipation bottom: horiz. viscosity

Fig. 4.1.10

WL | DELFT HYDRAULICS

Z2747.50

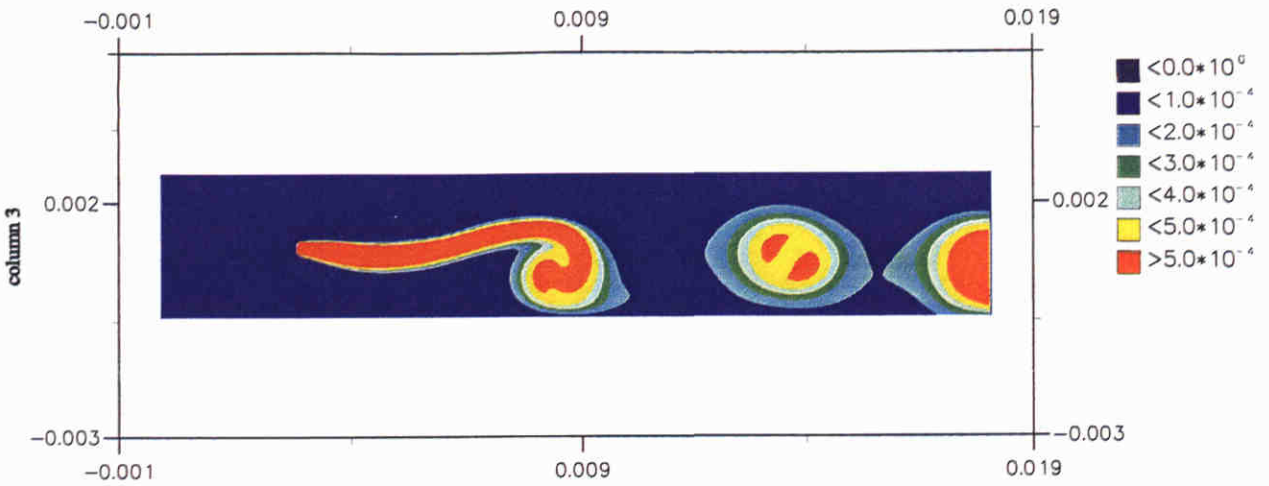


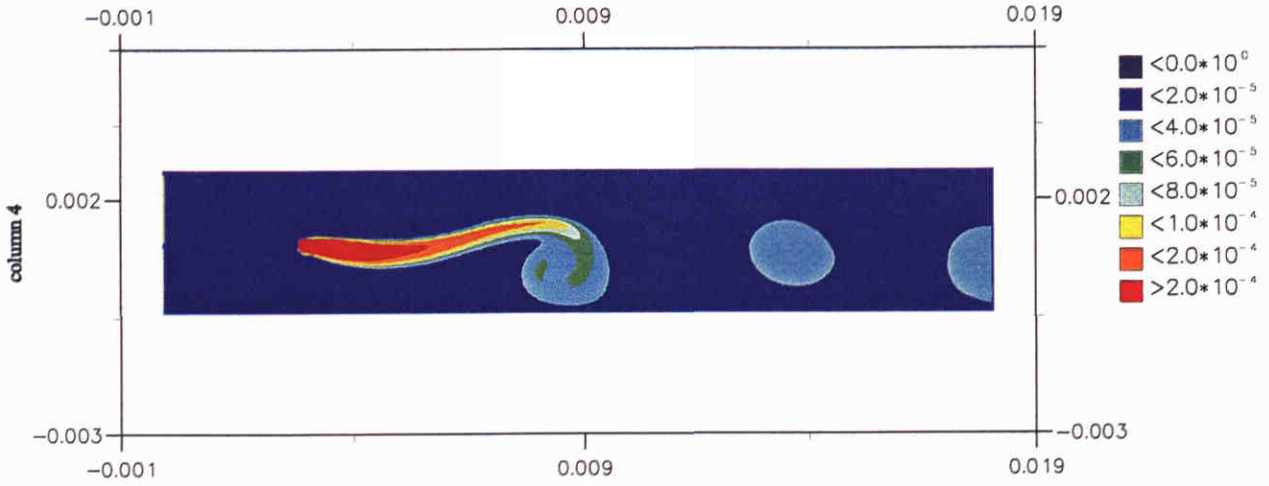


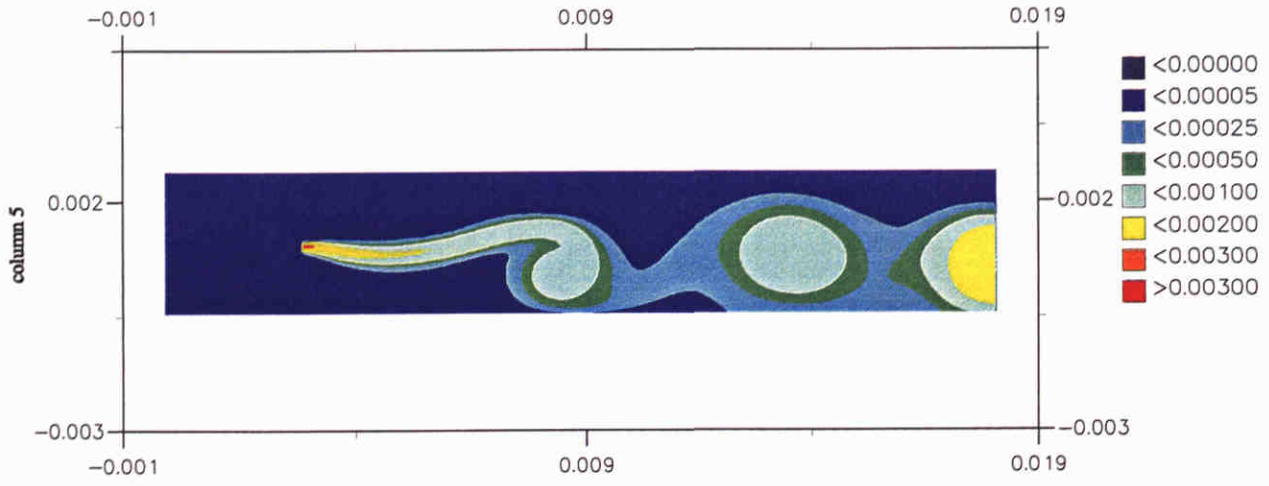


Splitter plate (2D); TRIWAQ with horizontal k–eps turbulence model

upper: horiz. tke centre: horiz. dissip lower: horiz. viscosity

after 1 minute

Fig. 4.2.1

WL | DELFT HYDRAULICS

Z2747.50


Splitter plate (2D); TRIWAQ with horizontal k–eps turbulence model
concentration of tracer after 1 minute

Fig. 4.2.2

WL | DELFT HYDRAULICS

Z2747.50

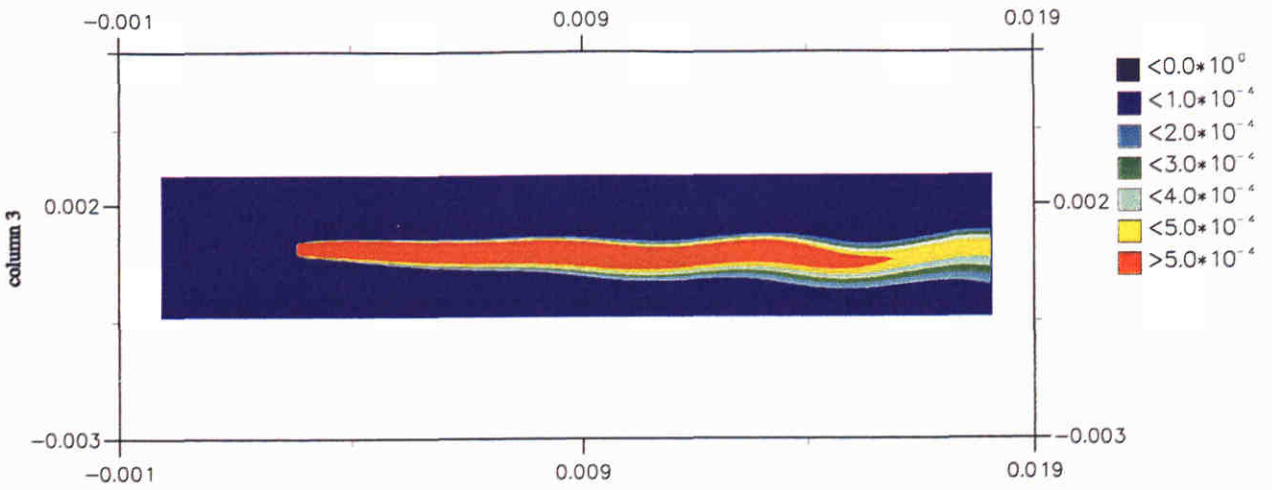


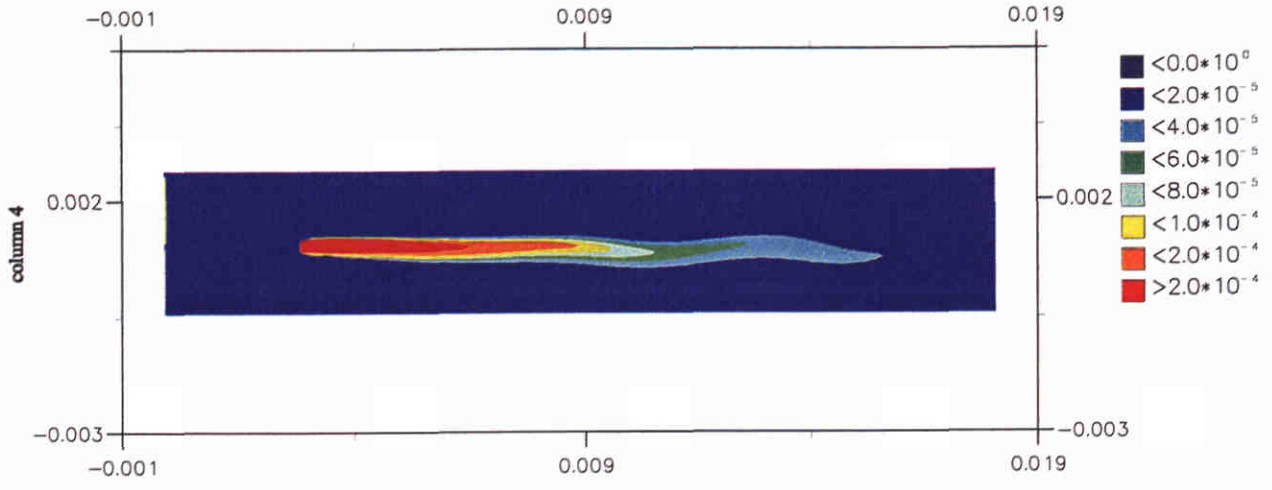


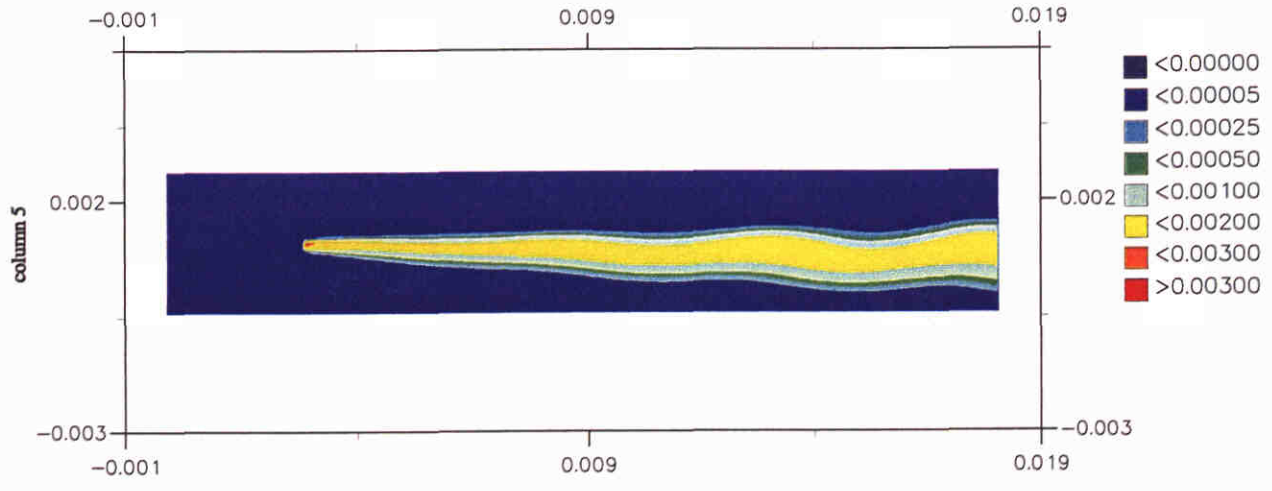


Splitter plate (2D); TRIWAQ with horizontal k–eps turbulence model
upper: horiz. tke centre: horiz. dissip lower: horiz. viscosity
after 50 minutes

Fig. 4.2.3

WL | DELFT HYDRAULICS

Z2747.50


Splitter plate (2D); TRIWAQ with horizontal k–eps turbulence model
concentration after 50 minutes

Fig. 4.2.4

WL | DELFT HYDRAULICS

Z2747.50

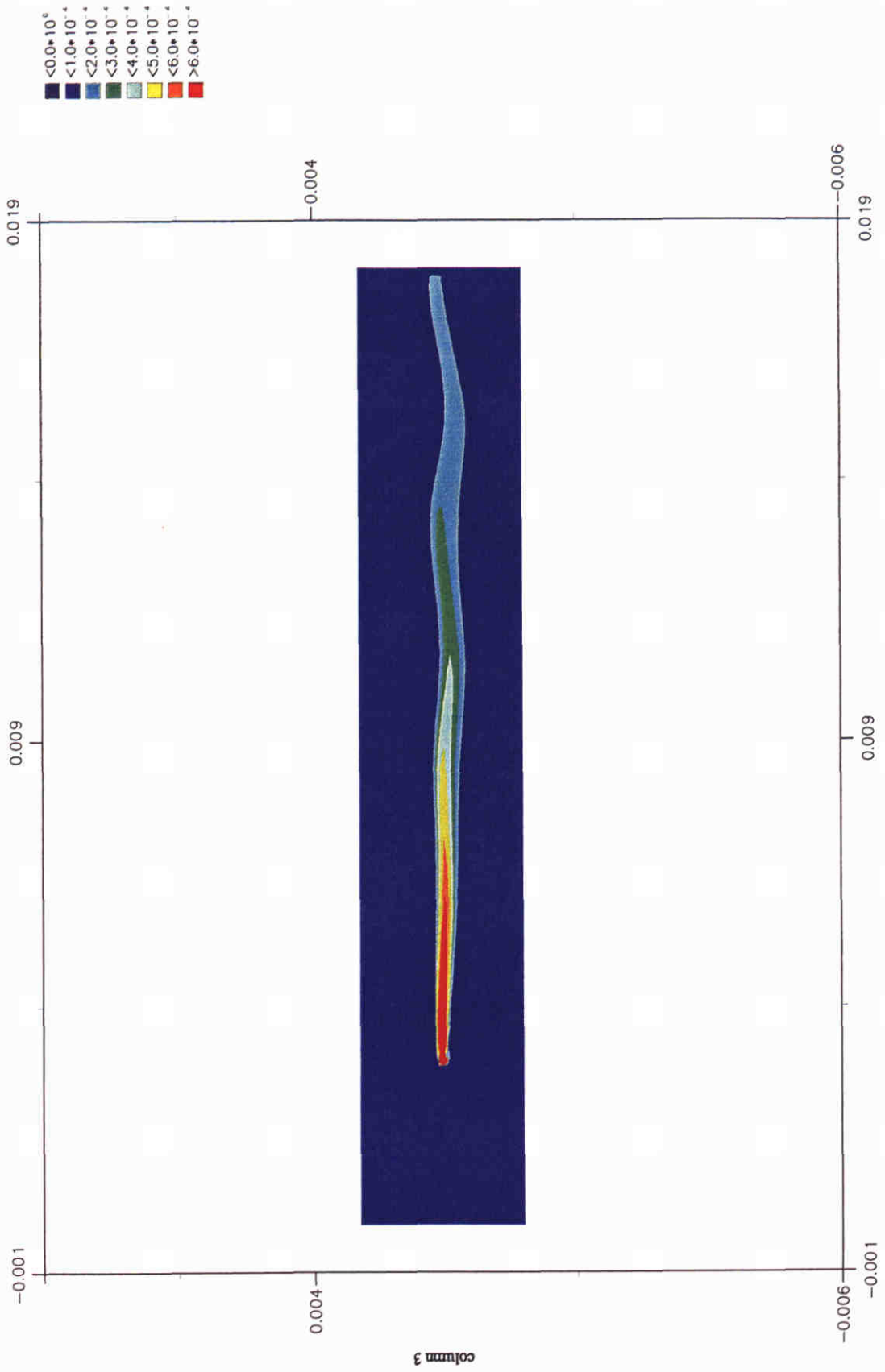


Splitter plate (2D)

Contourplot of Reynolds stress

Fig. 4.2.5

WL | DELFT HYDRAULICS

Z2747.50

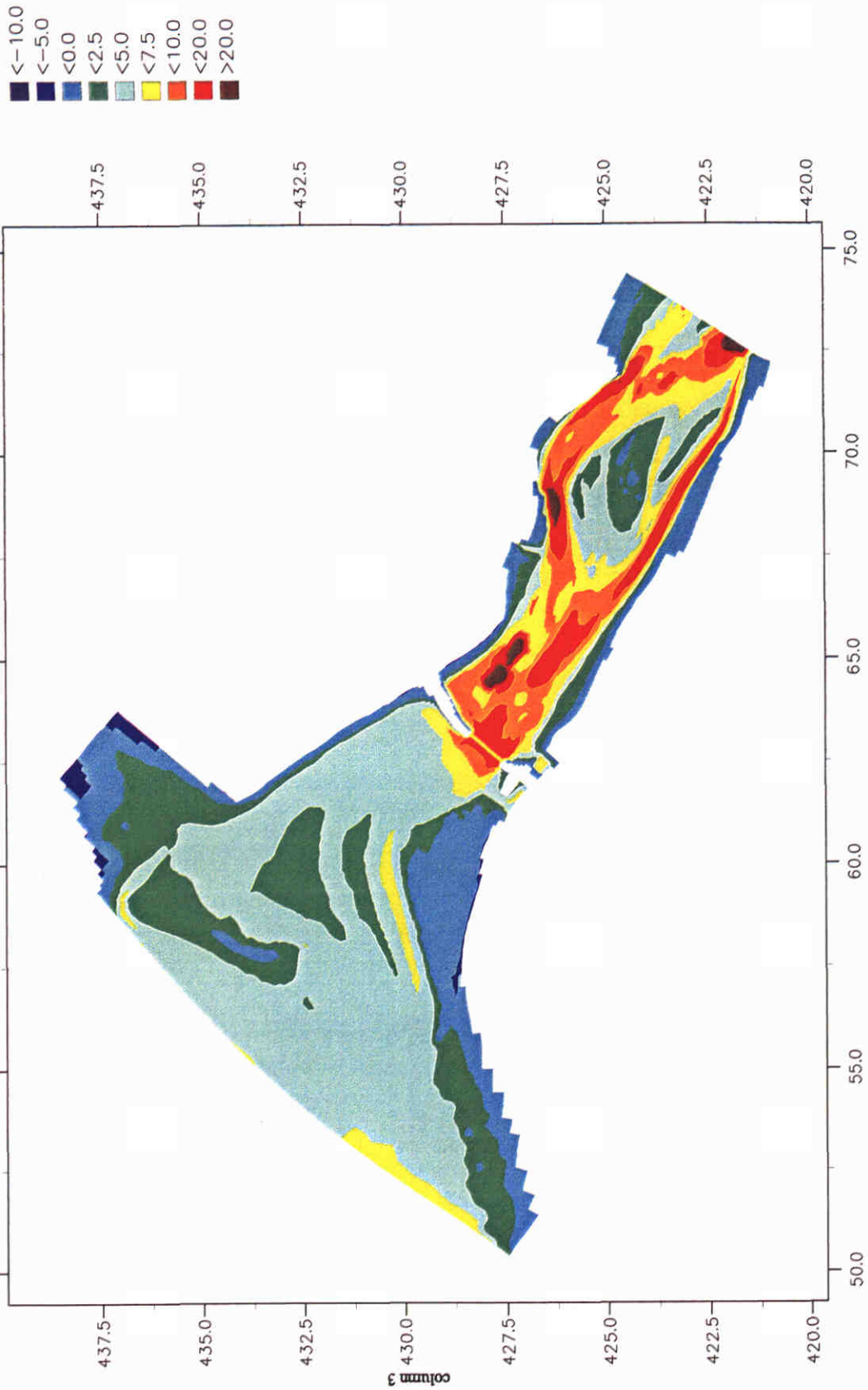


MOHA model
Bathymetry

Fig. 4.3.1

WL | DELFT HYDRAULICS

Z2747.50

DELFT HYDRAULICS

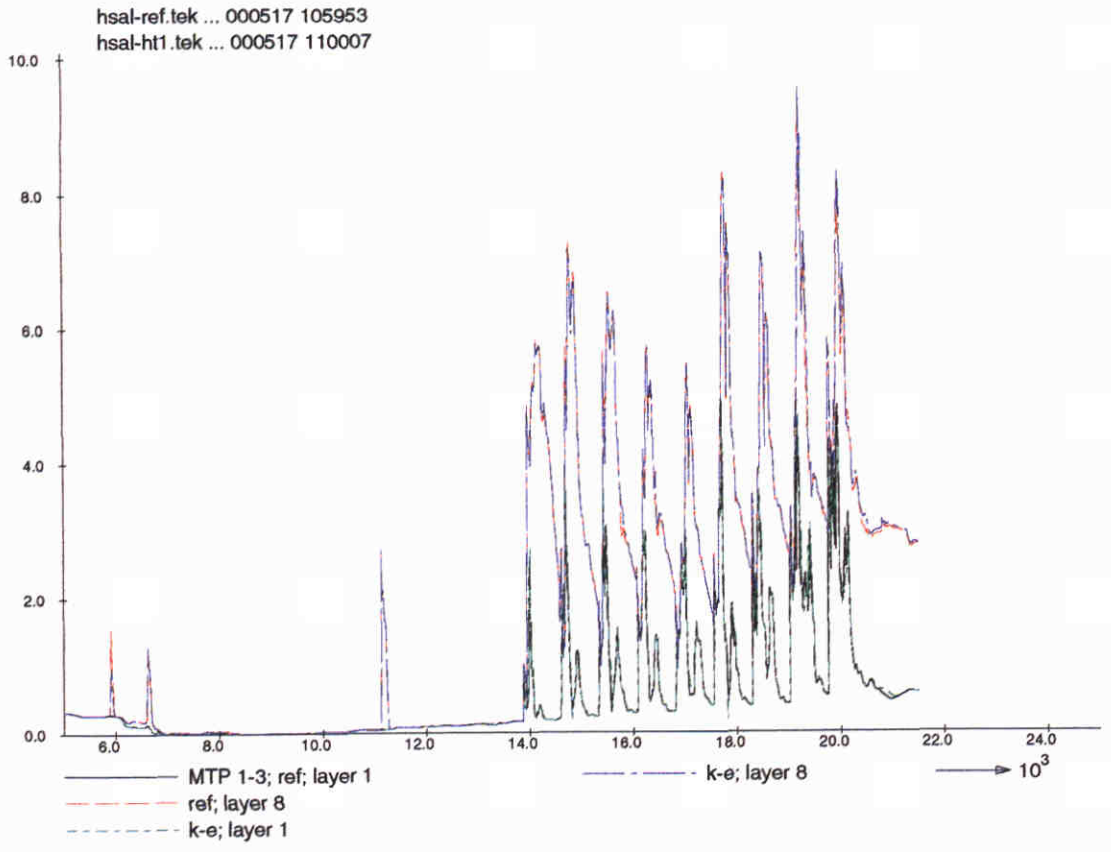


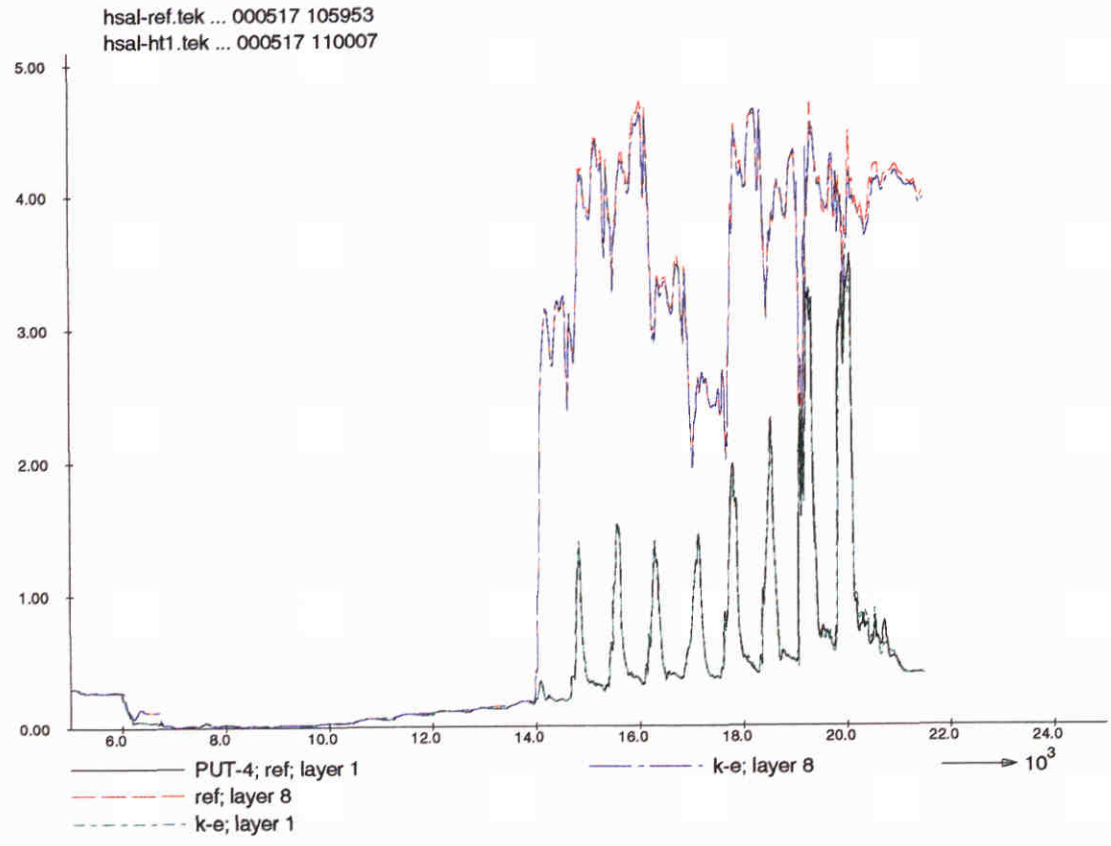


Time histories of salinity
for stations MTP 1-3 and PUT-4
for reference run and run with horizontal k-e model

DELFT HYDRAULICS

Fig. 4.3.3

DELFT HYDRAULICS

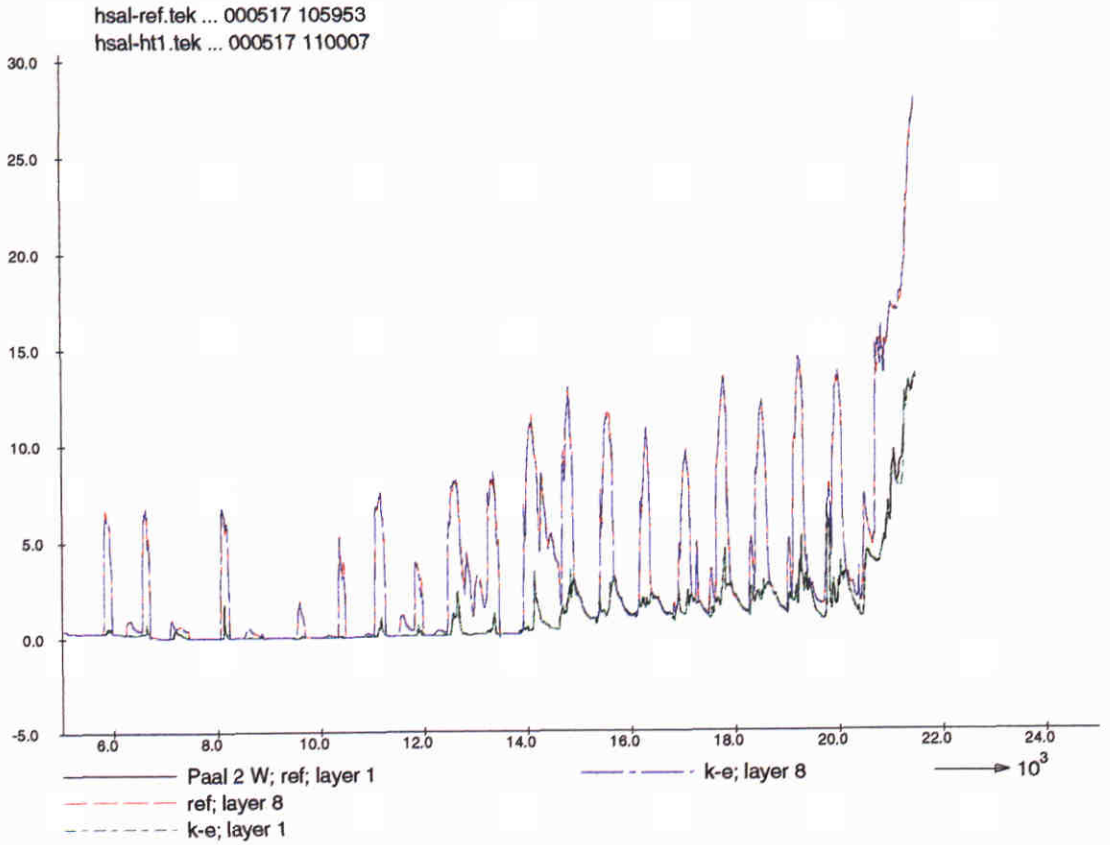


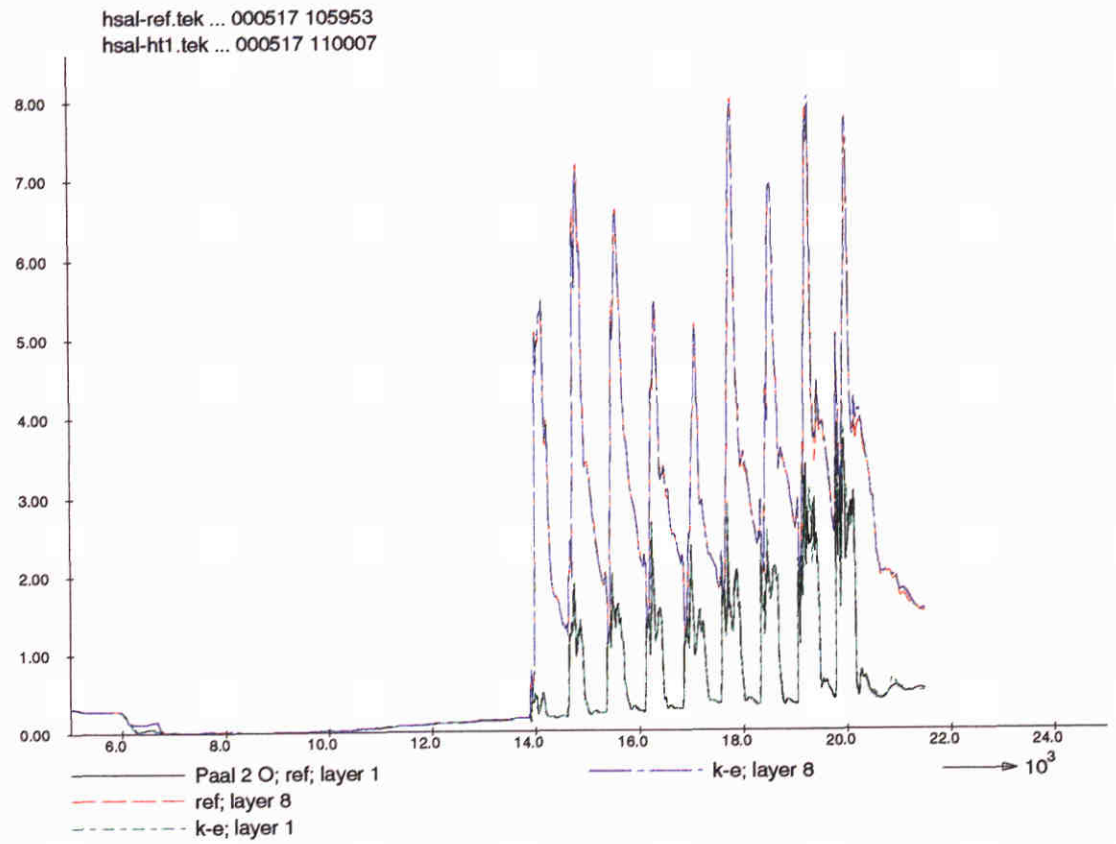


Time histories of salinity
for stations Paal 2 W and Paal 2 O
for reference run and run with horizontal k-e model

DELFT HYDRAULICS

Fig. 4.3.4

DELFT HYDRAULICS

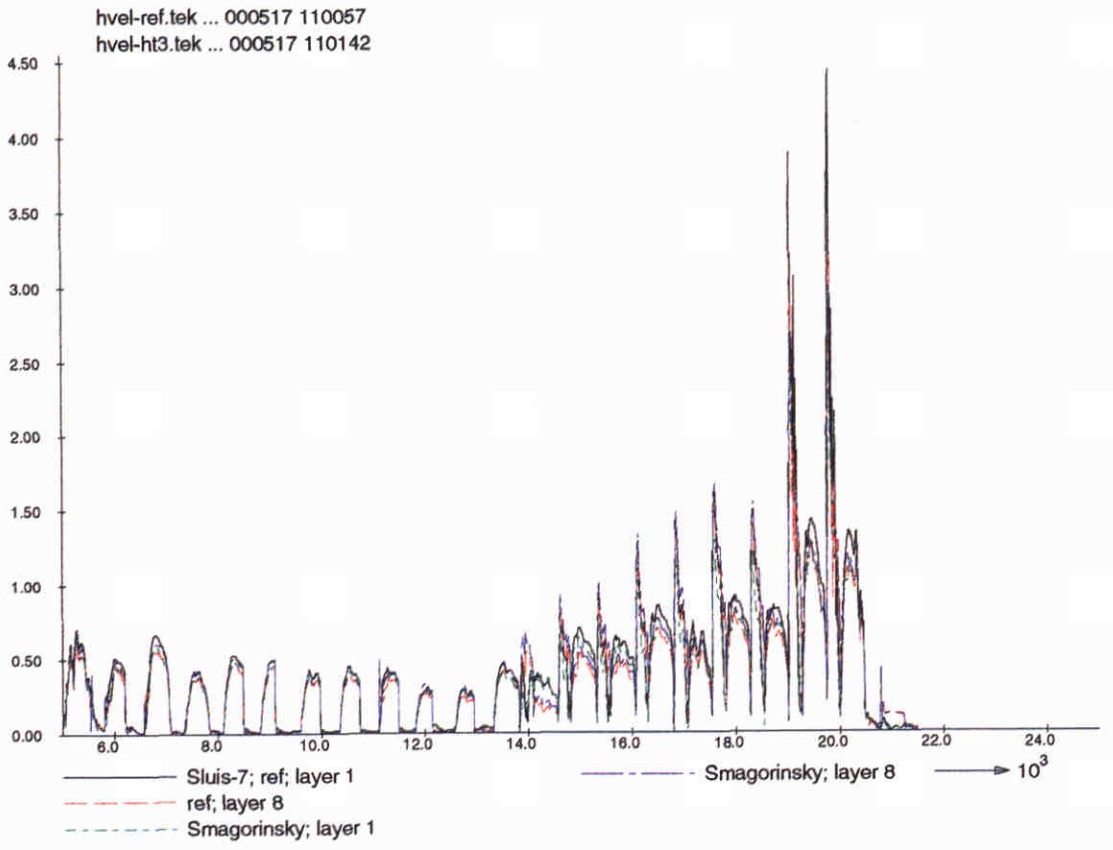


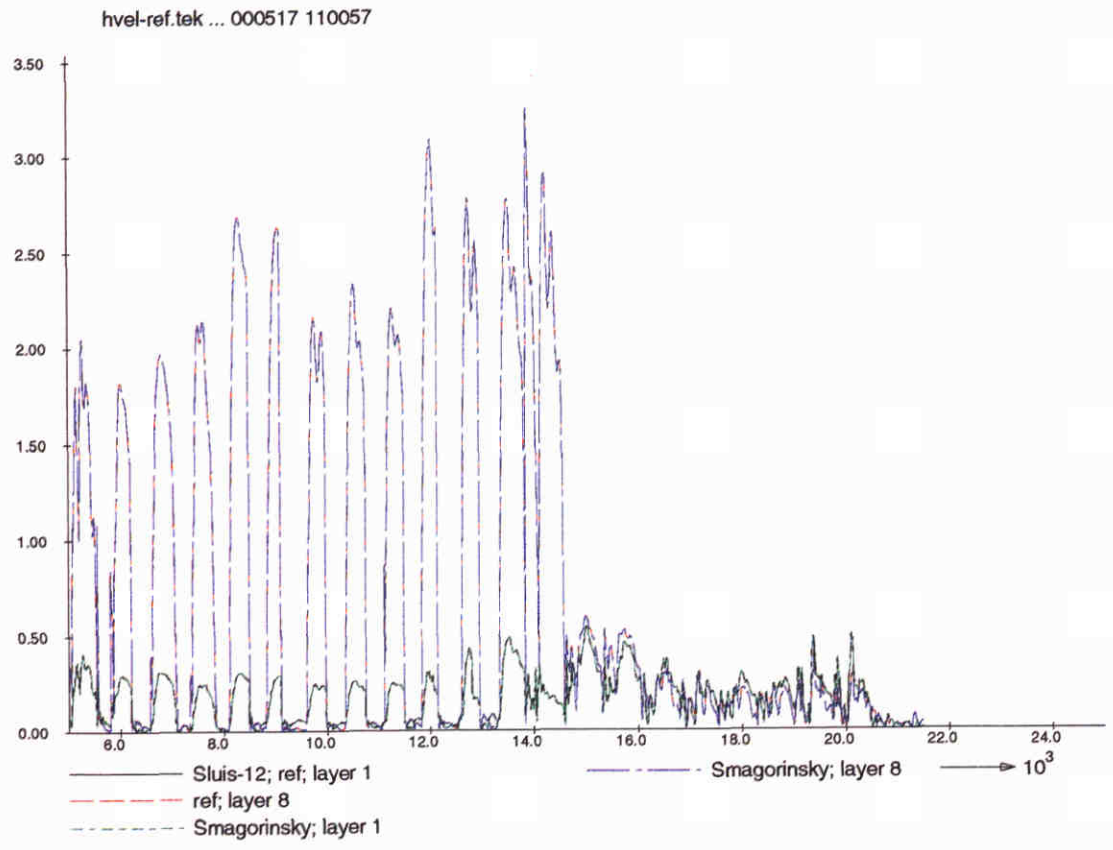


Time histories of velocity
for stations Sluis-7 and Sluis-12
for reference run and run with Smagorinsky model

DELFT HYDRAULICS

Fig. A.1.1

DELFT HYDRAULICS

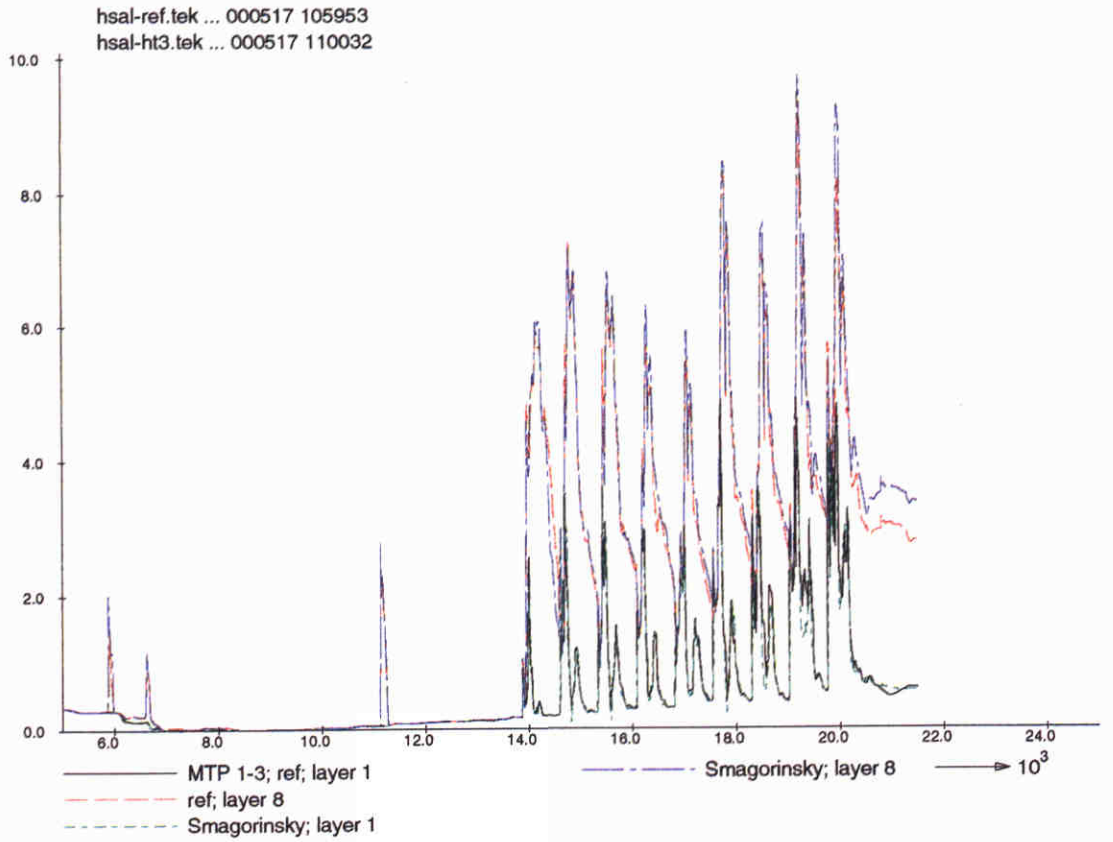


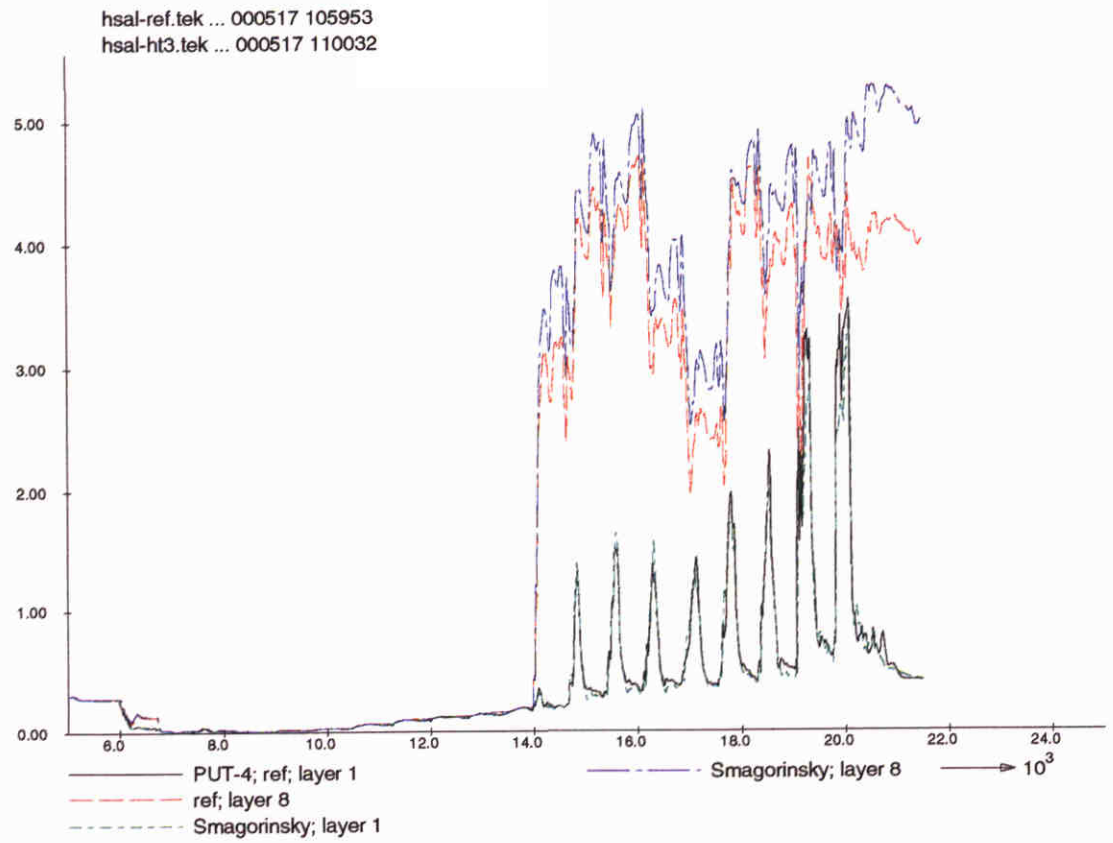


Time histories of salinity
for stations MTP 1-3 and PUT-4
for reference run and run with Smagorinsky model

DELFT HYDRAULICS

Fig. A.1.2

DELFT HYDRAULICS

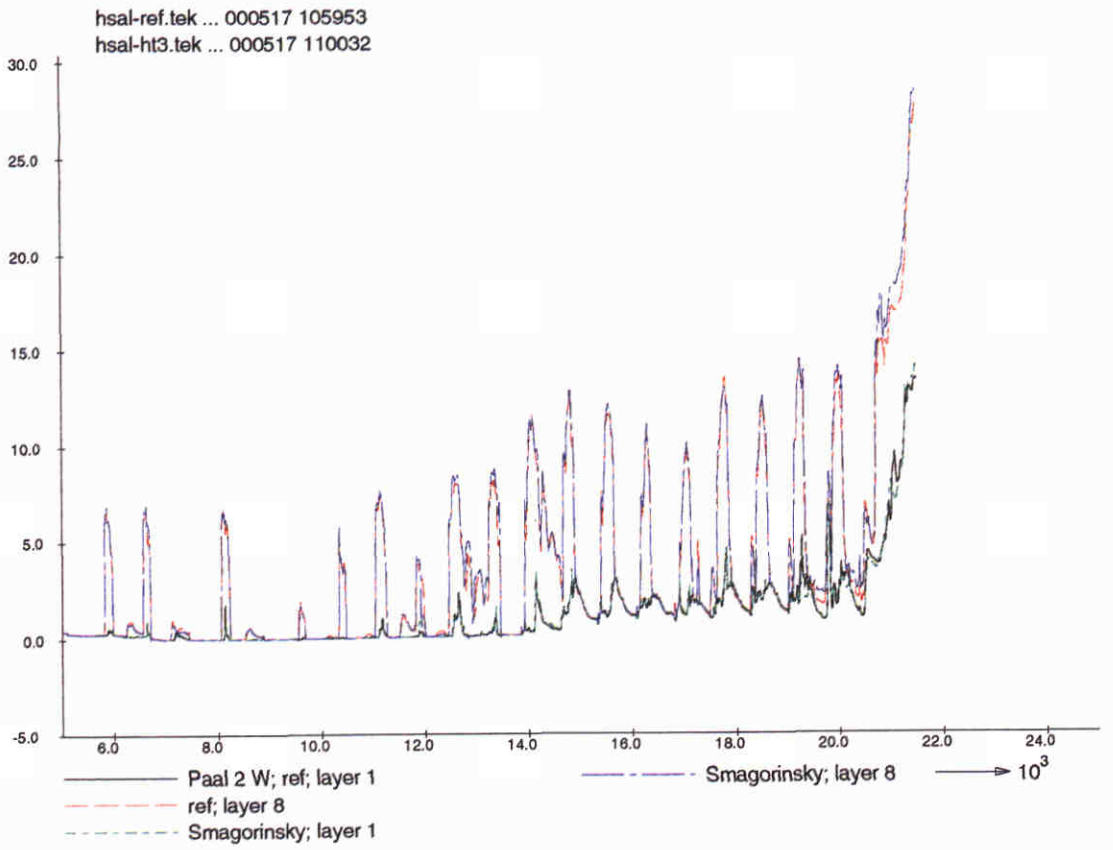


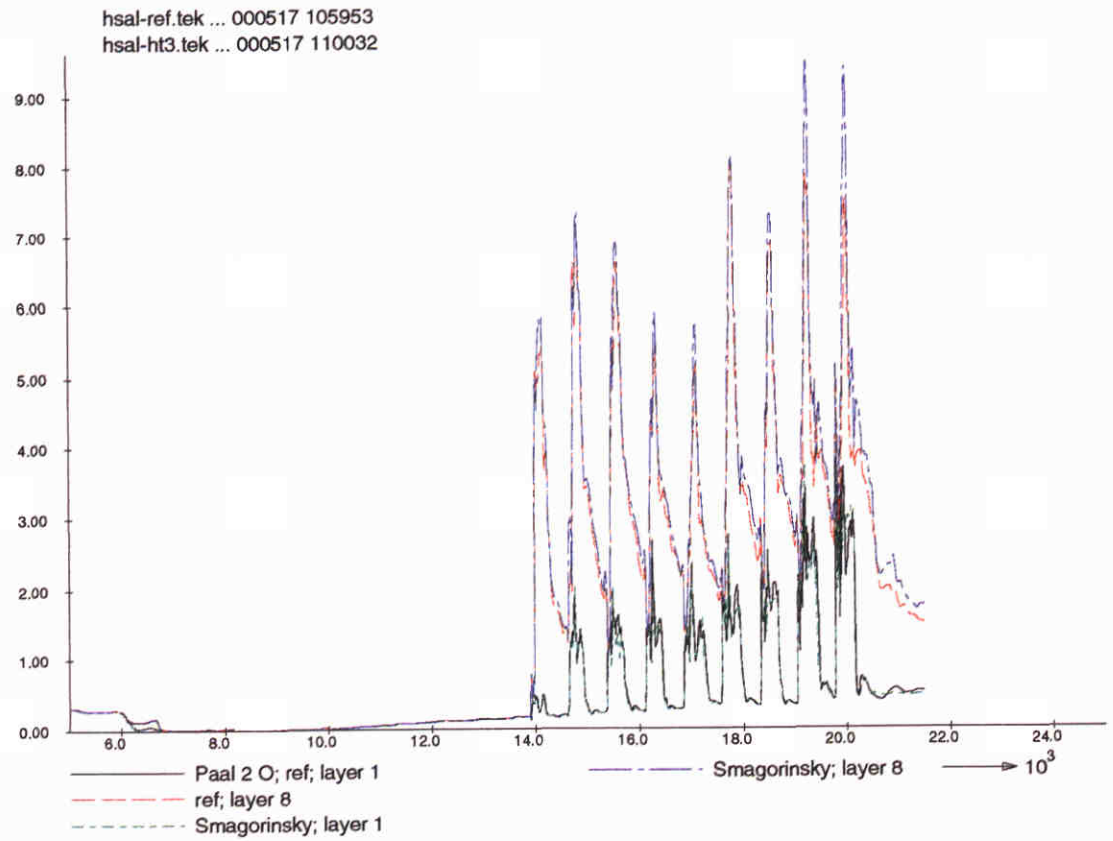


Time histories of salinity
for stations Paal 2 W and Paal 2 O
for reference run and run with Smagorinsky model

DELFT HYDRAULICS

Fig. A.1.3

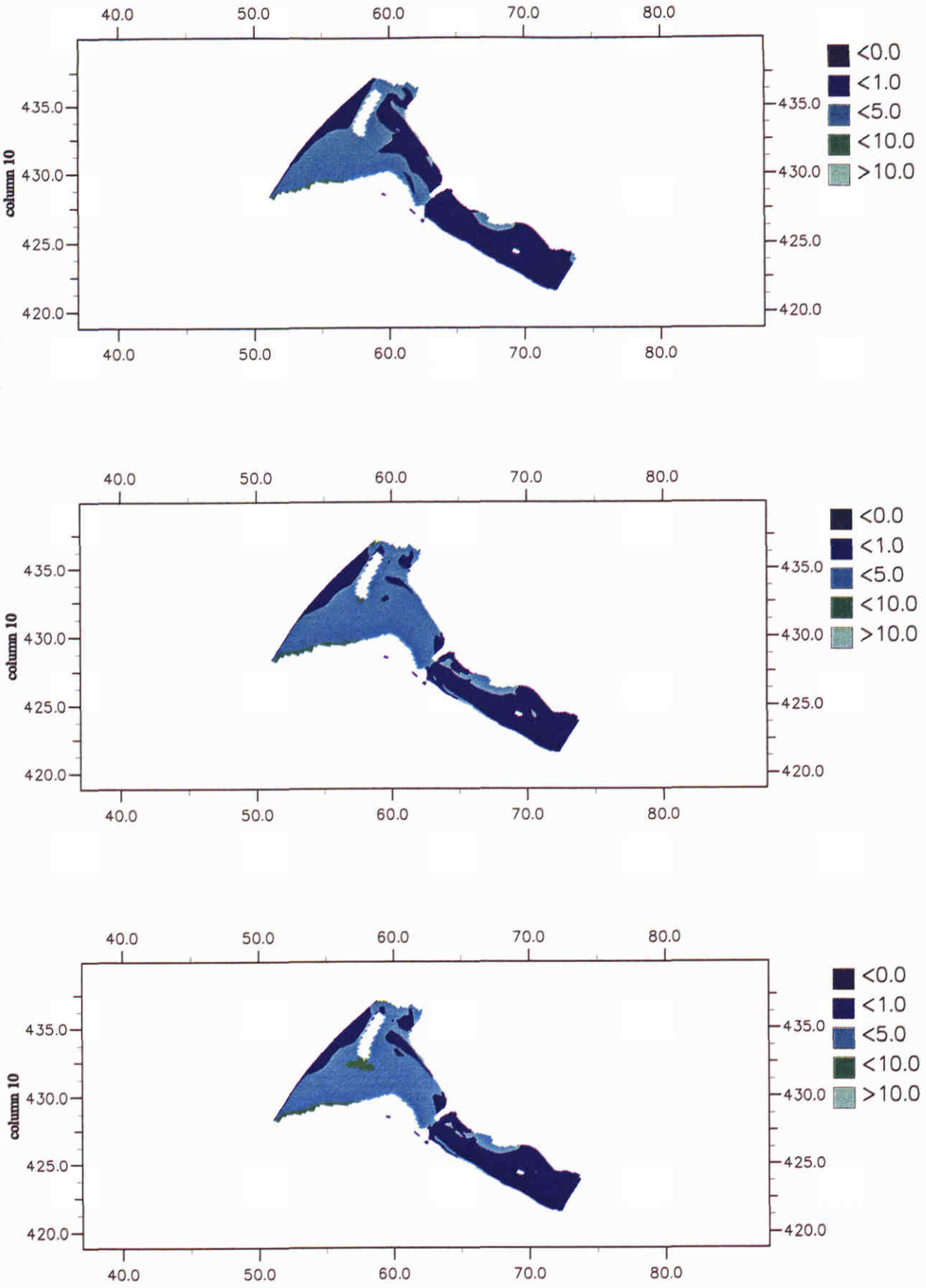


3D MOHA model;
Contour plots of horizontal viscosity computed by Smagorinsky
Upper: 00:00 hr Centre: 12:00 hr Lower: 24:00 hr on 11 March 1997

Fig. A.1.4

WL | DELFT HYDRAULICS

Z2747.50

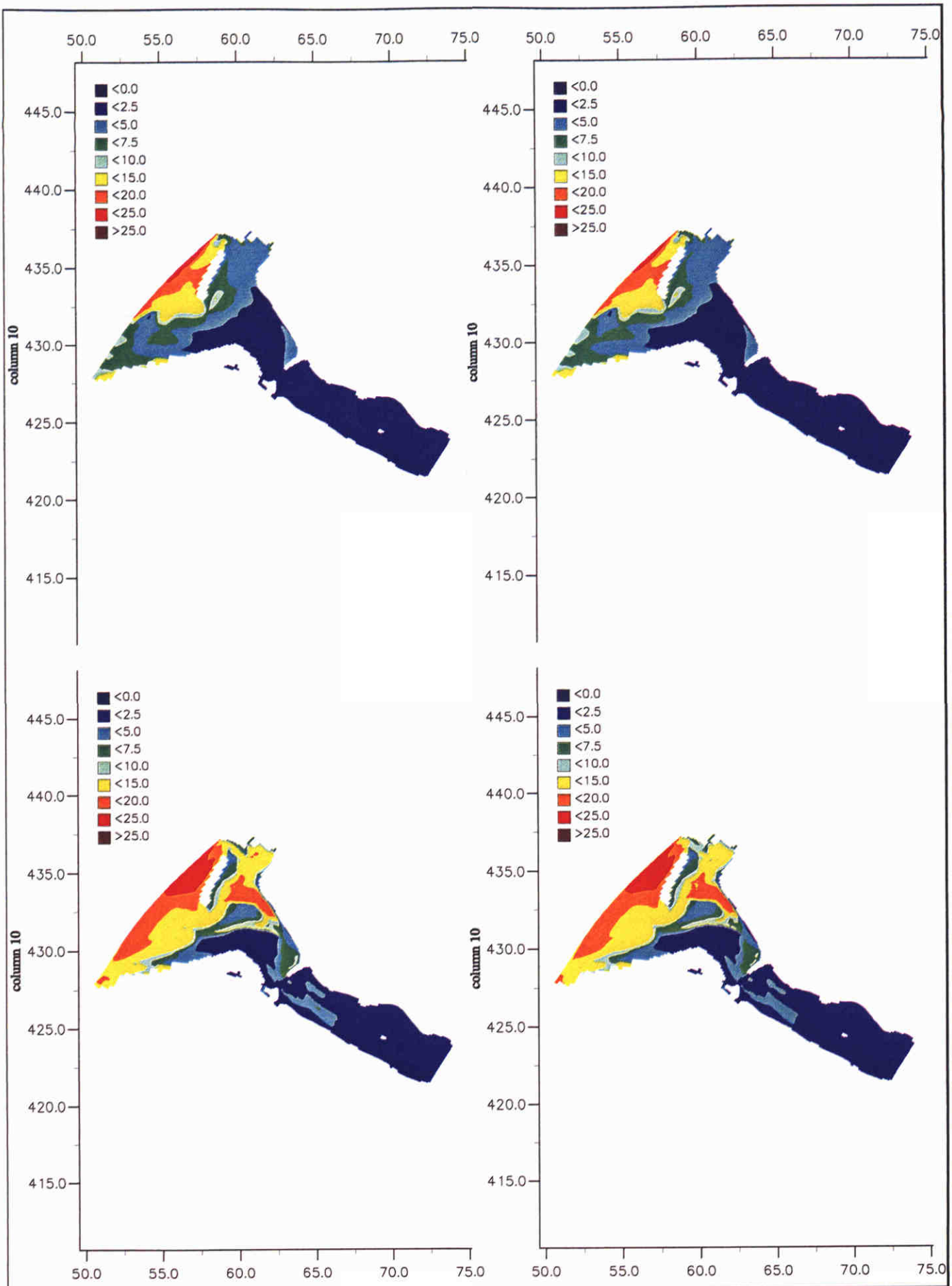


3D MOHA model; Contour plots of salinity at 11 March 00:00 hr.
Upper left: layer 1 (Smagorinsky); Upper right: layer 1 (Ref.)
Lower left: layer 8 (Smagorinsky); Lower right: layer 8 (Ref.)

Fig. A.1.5

WL | DELFT HYDRAULICS

Z2747.50

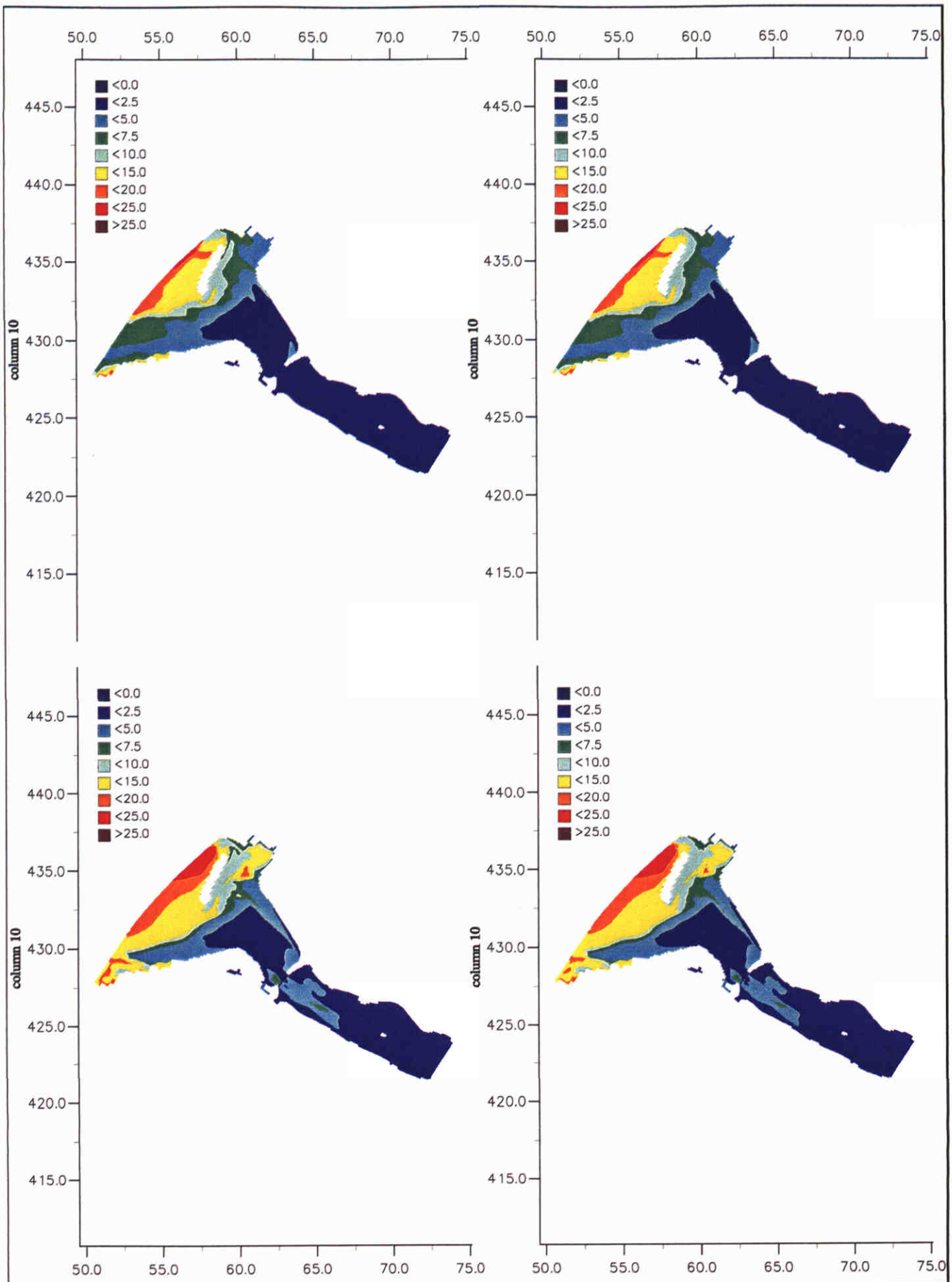


3D MOHA model; Contour plots of salinity at 11 March 12:00 hr.
Upper left: layer 1 (Smagorinsky); Upper right: layer 1 (Ref.)
Lower left: layer 8 (Smagorinsky); Lower right: layer 8 (Ref.)

Fig. A.1.6

WL | DELFT HYDRAULICS

Z2747.50

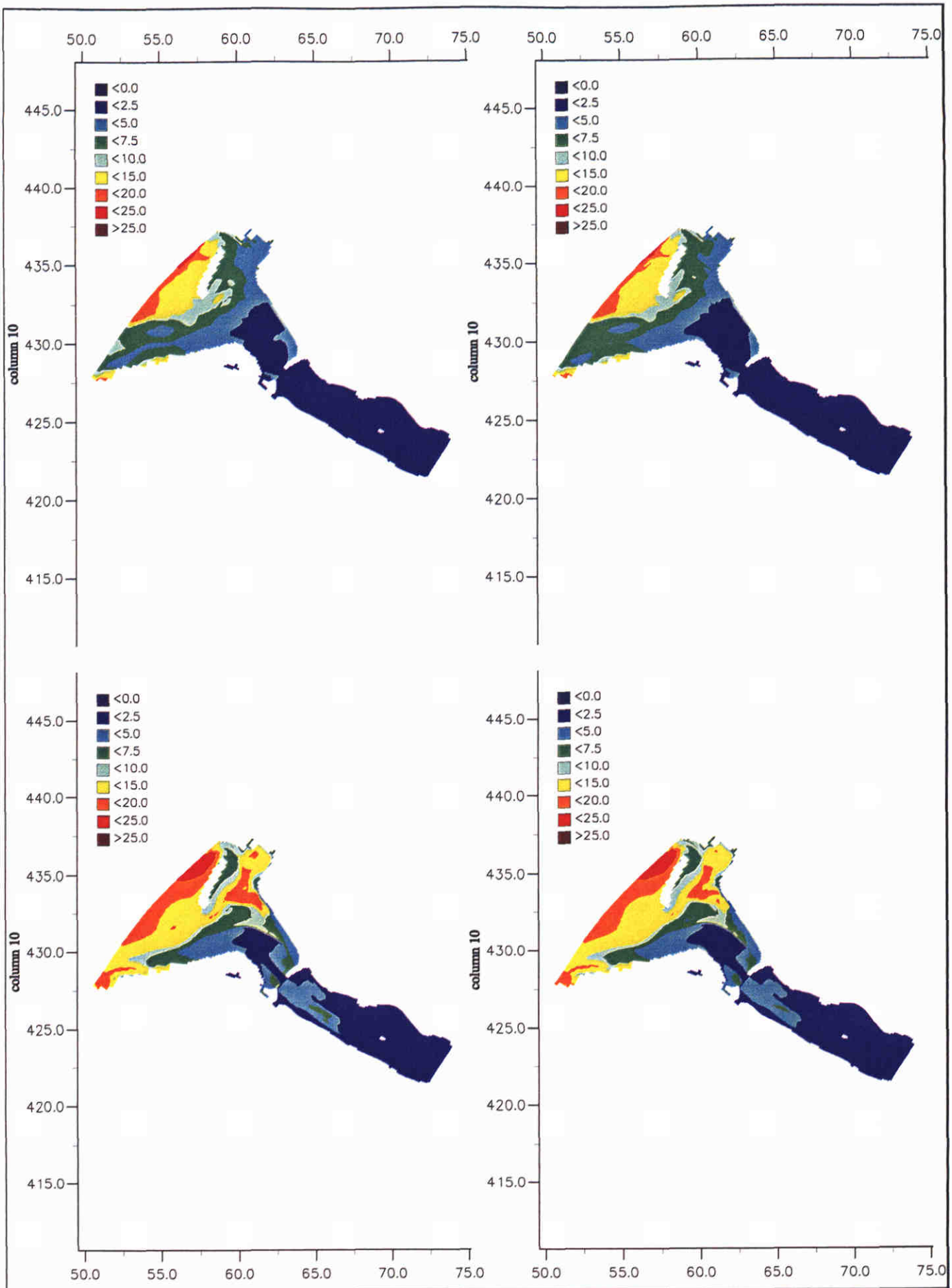


3D MOHA model; Contour plots of salinity at 12 March 00:00 hr.
Upper left: layer 1 (Smagorinsky); Upper right: layer 1 (Ref.)
Lower left: layer 8 (Smagorinsky); Lower right: layer 8 (Ref.)

Fig. A.1.7

WL | DELFT HYDRAULICS

Z2747.50

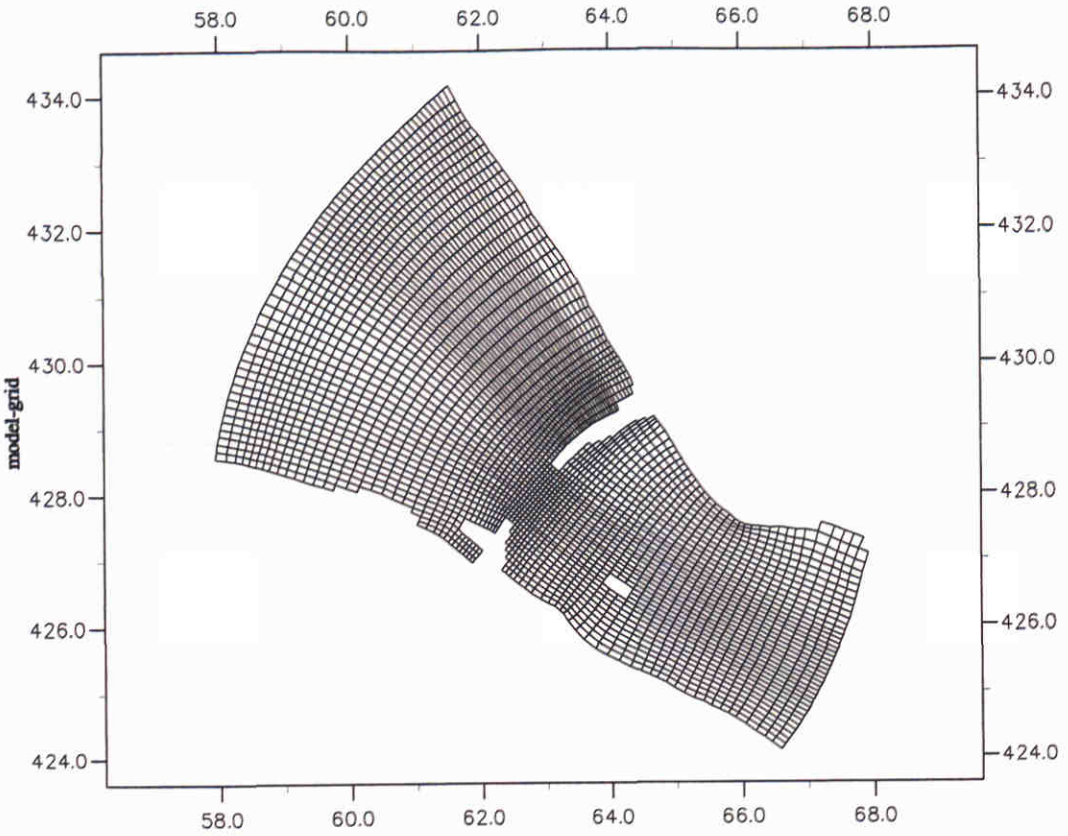


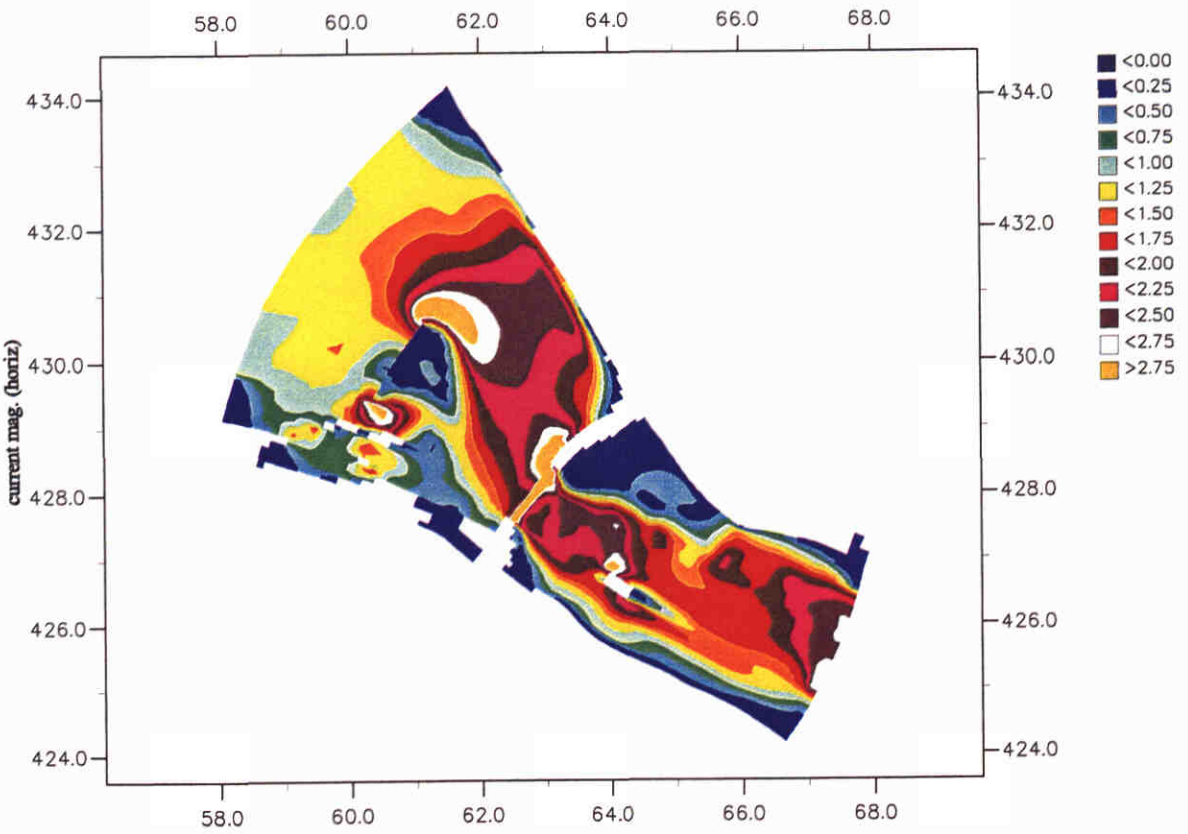


Upper figure: Computational grid

Lower figure: typical distribution of the magnitude of the horizontal velocity

Fig. A.2.1

WL | DELFT HYDRAULICS

Z2747.50

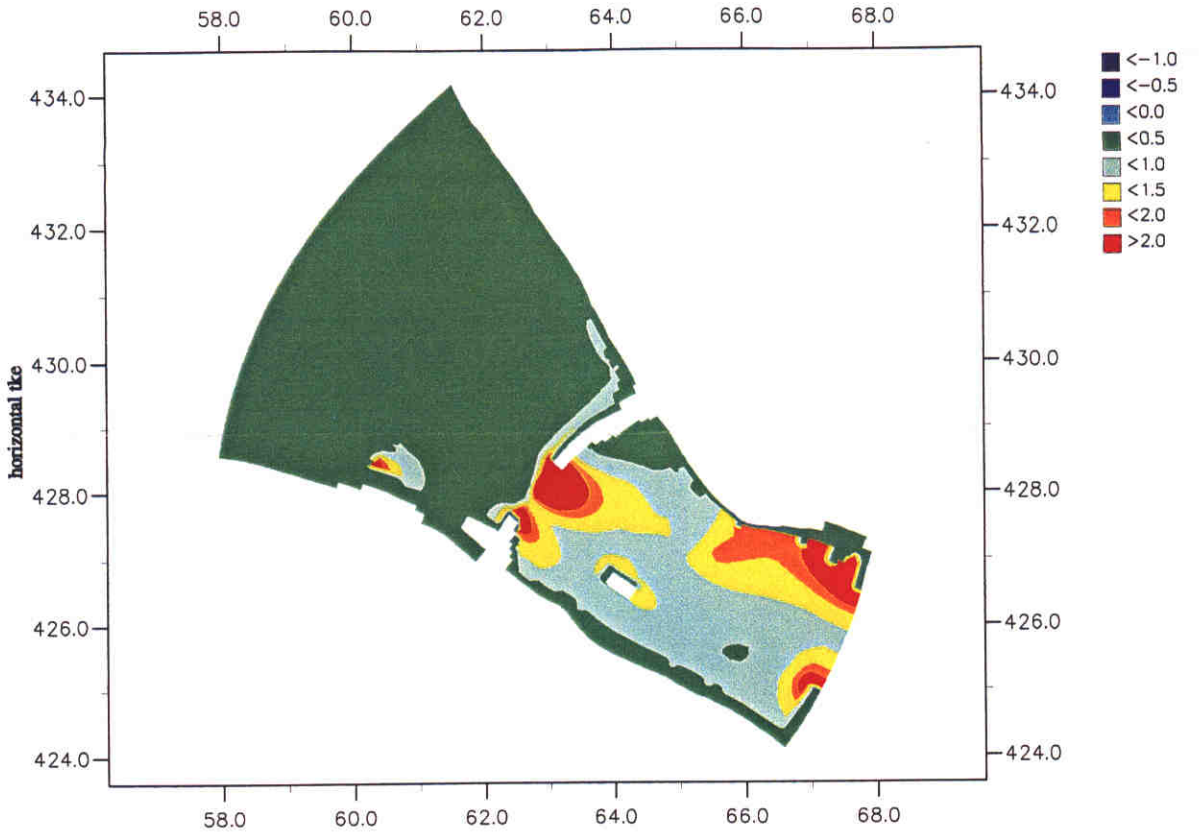


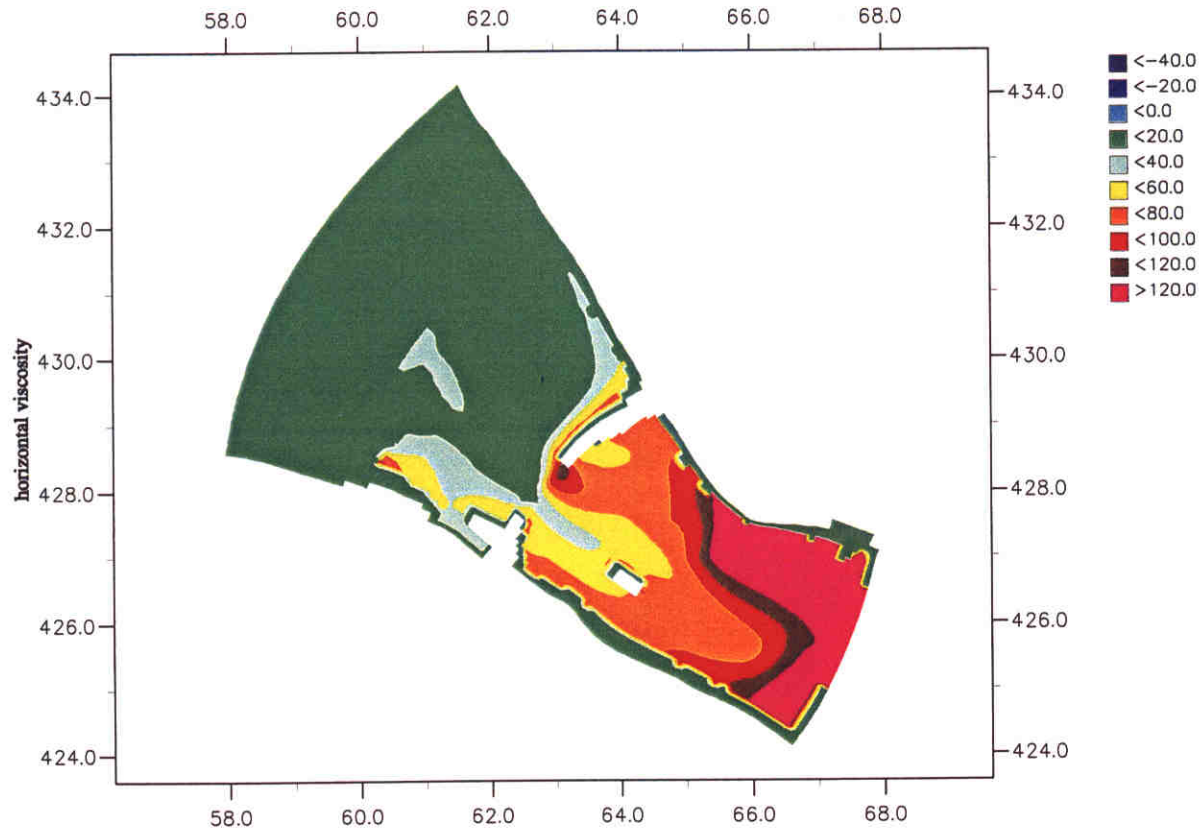


Upper: turbulent kinetic energy, standard model

Lower: horizontal eddy viscosity, standard model

Fig. A.2.2

WL | DELFT HYDRAULICS

Z2747.50

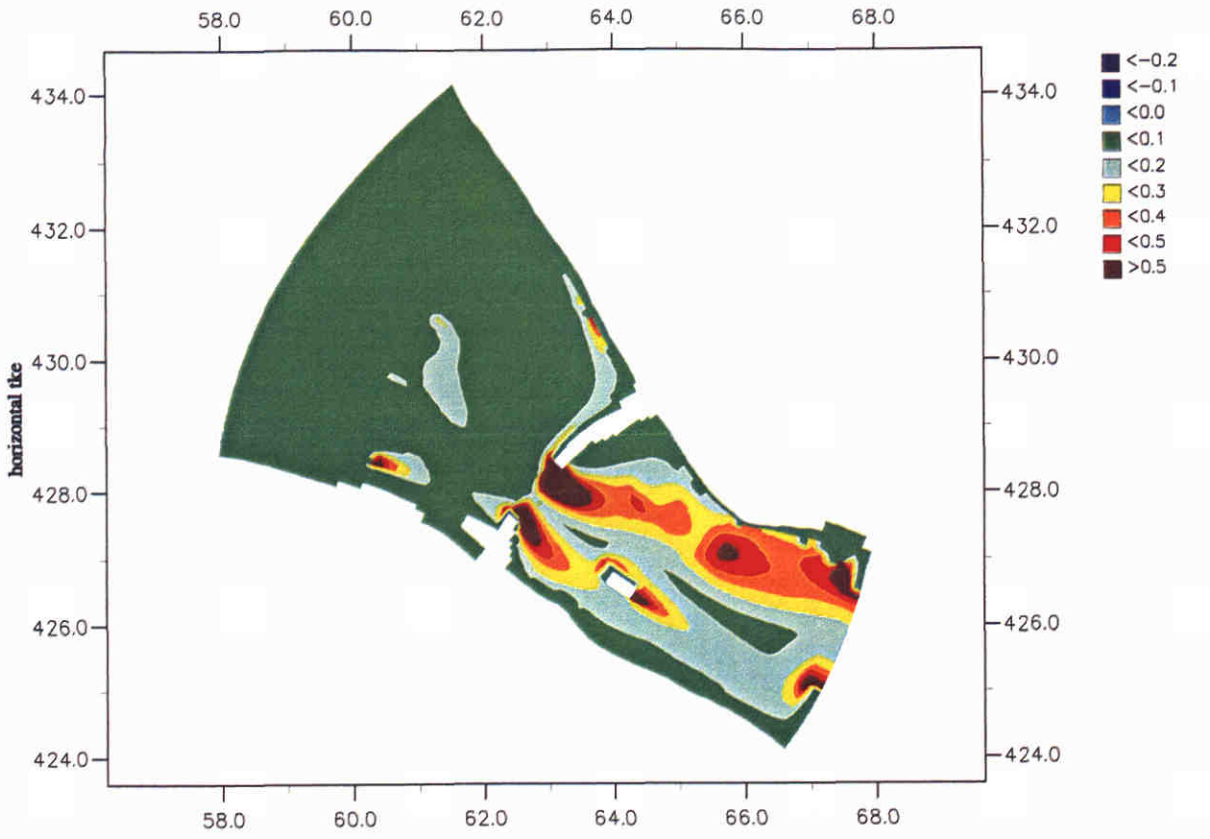


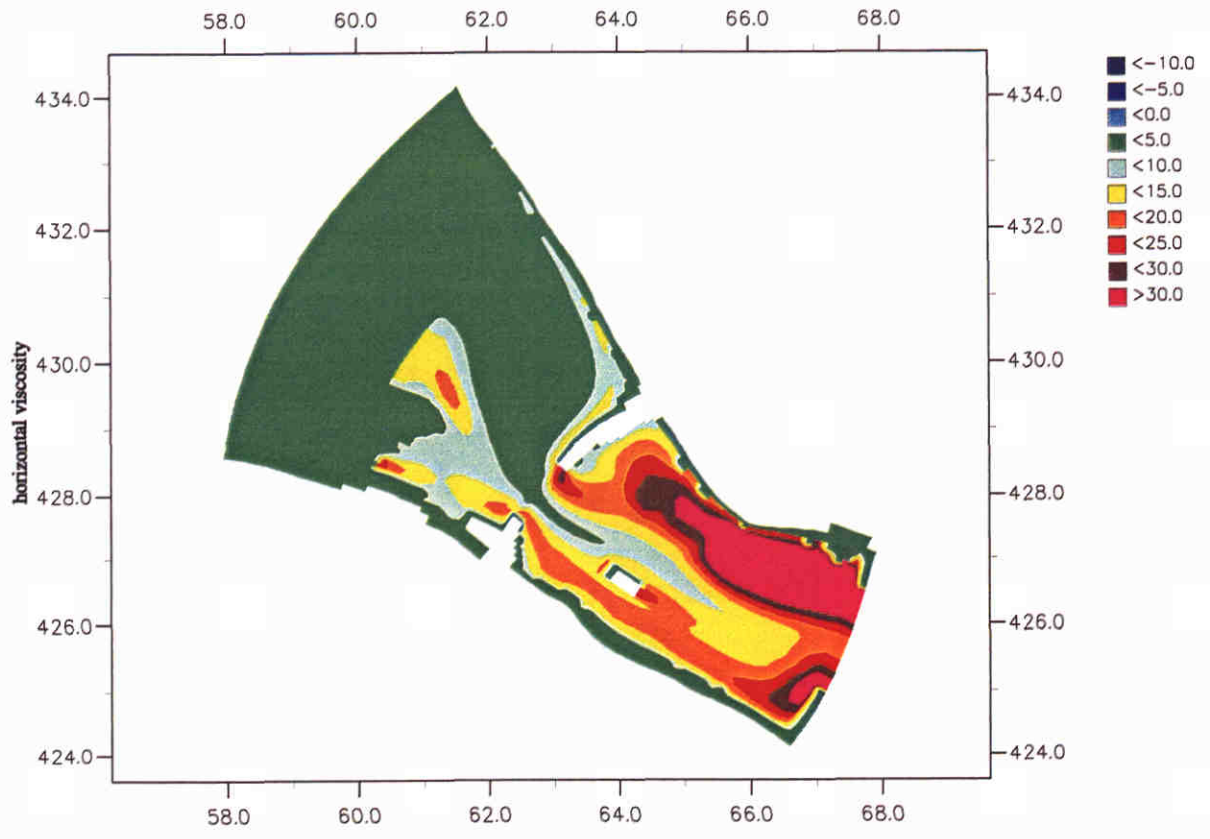


Upper: turbulent kinetic energy
Lower: horizontal eddy viscosity
homogeneous Dirichlet boundary conditions

Fig. A.2.3

WL | DELFT HYDRAULICS

Z2747.50

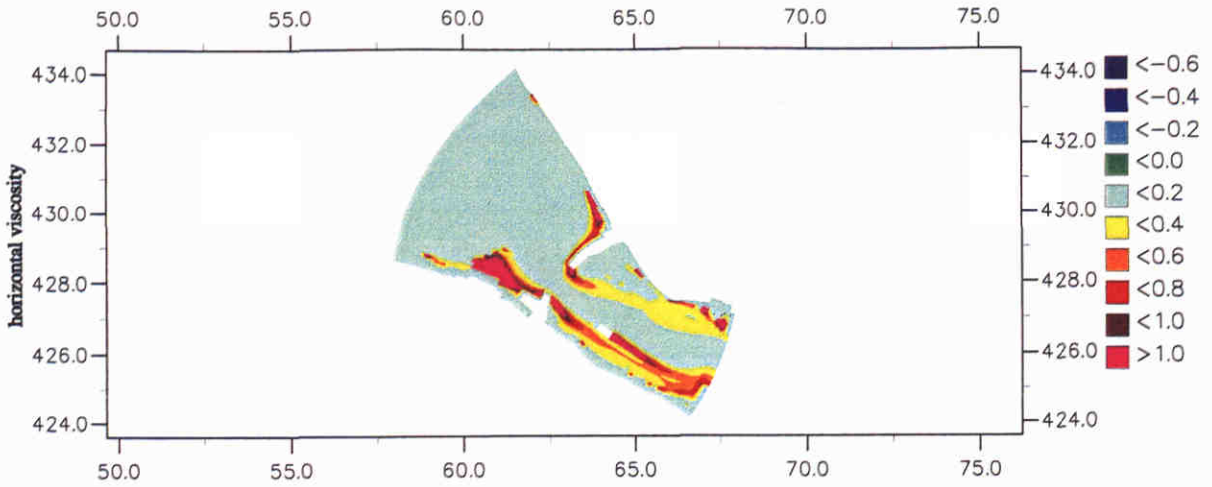


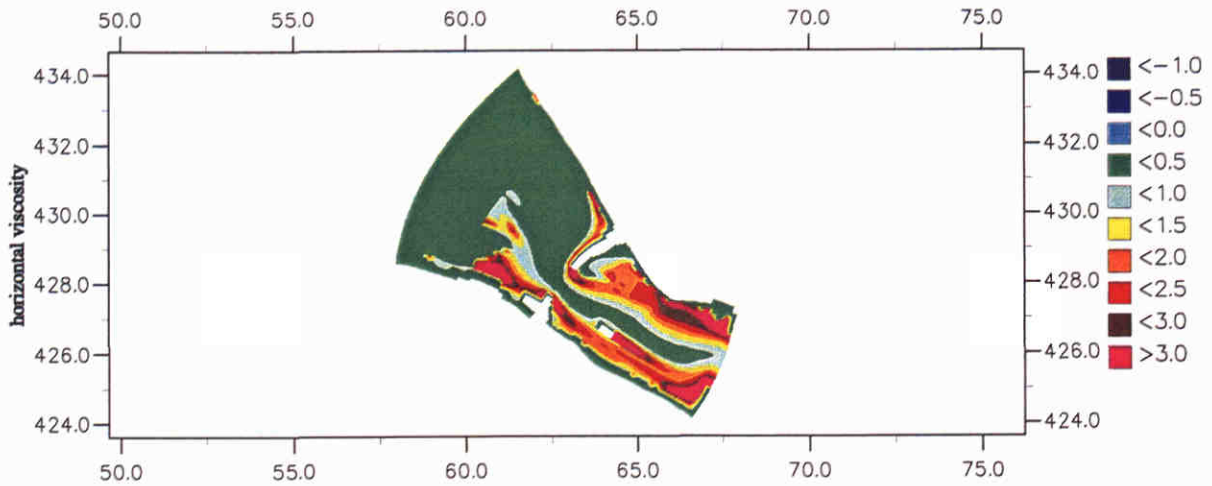


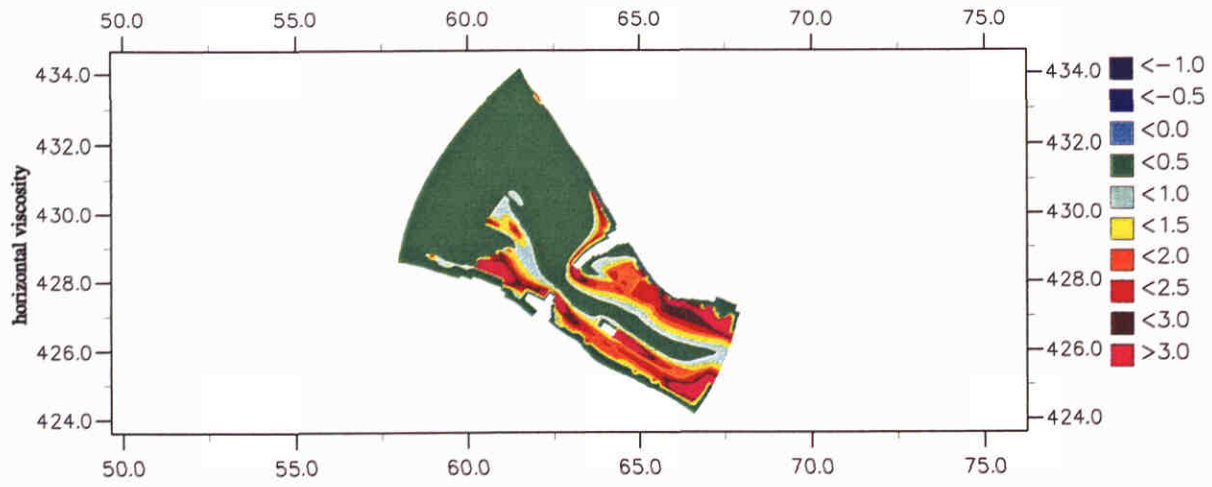


Horizontal eddy viscosity for c2e=1.6, c2e=1.7 and c2e=1.8 respectively

Fig. A.2.4

WL | DELFT HYDRAULICS

Z2747.50

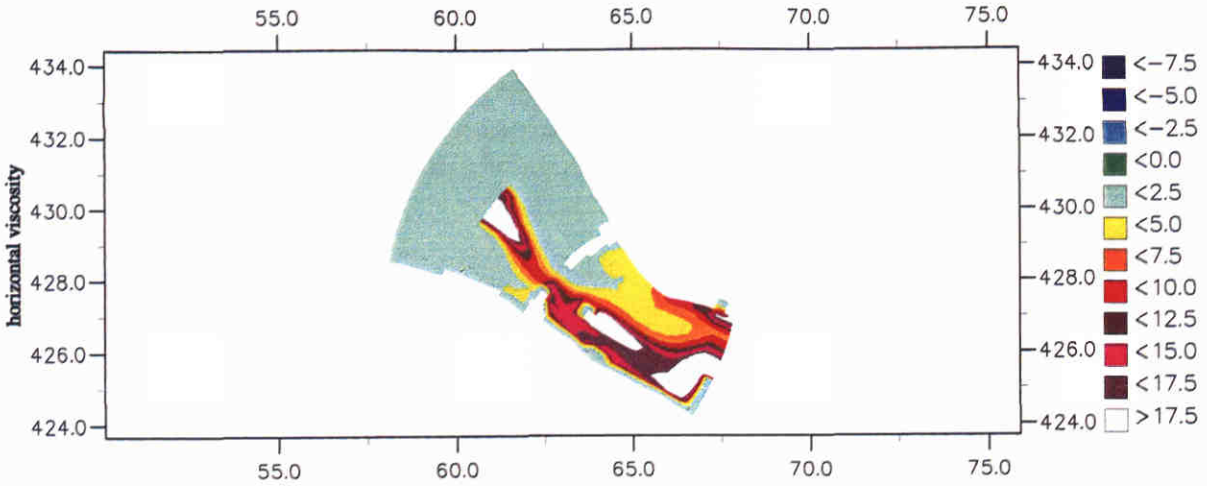


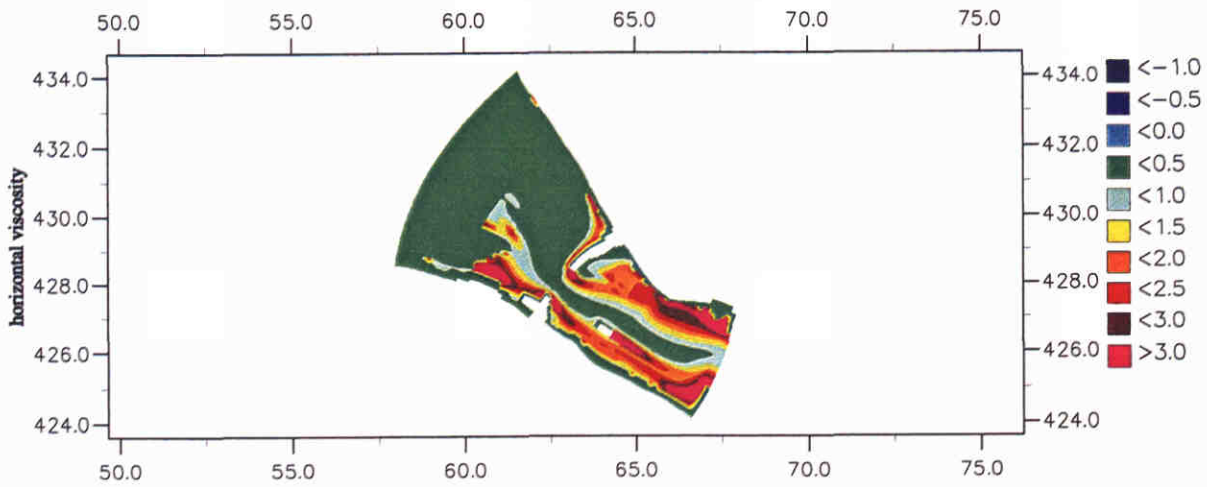


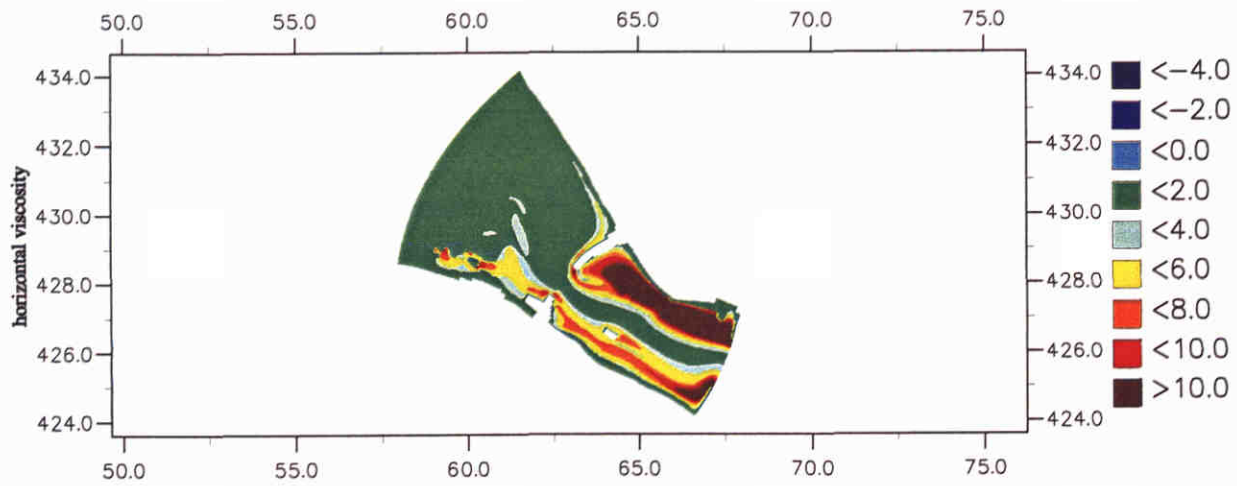


Horizontal eddy viscosity for three different grids, (M,N)=(32x43), (M,N)=(63x84), (M,N)=(124x166), respectively

Fig. A.2.5

WL | DELFT HYDRAULICS

Z2747.50

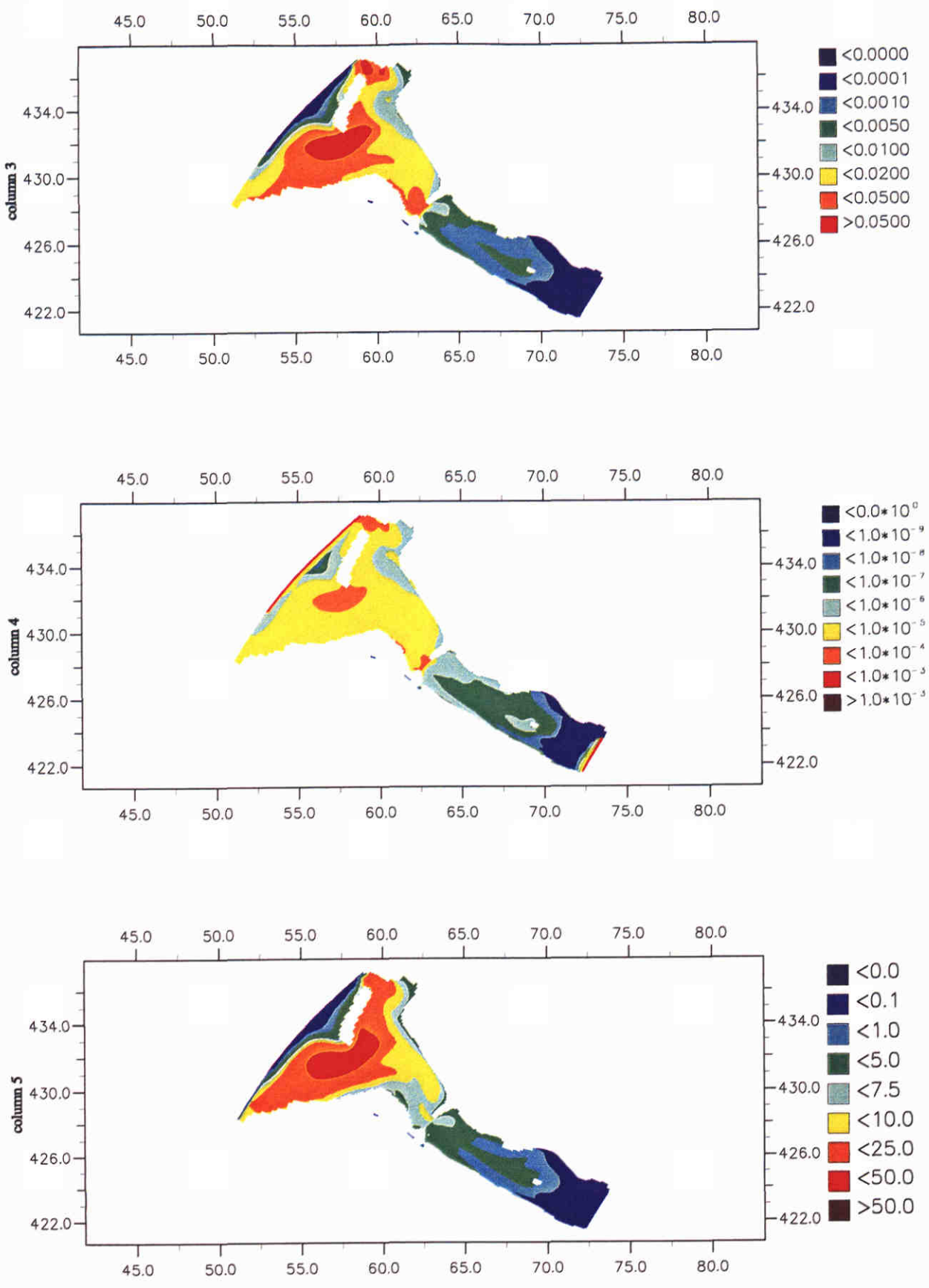


MOHA model (3D);
Horizontal TKE, dissipation and viscosity at 11 March 0:00 hr
Advection: first-order upwind (implicit in time)

Fig. A.3.1

WL | DELFT HYDRAULICS

Z2747.50

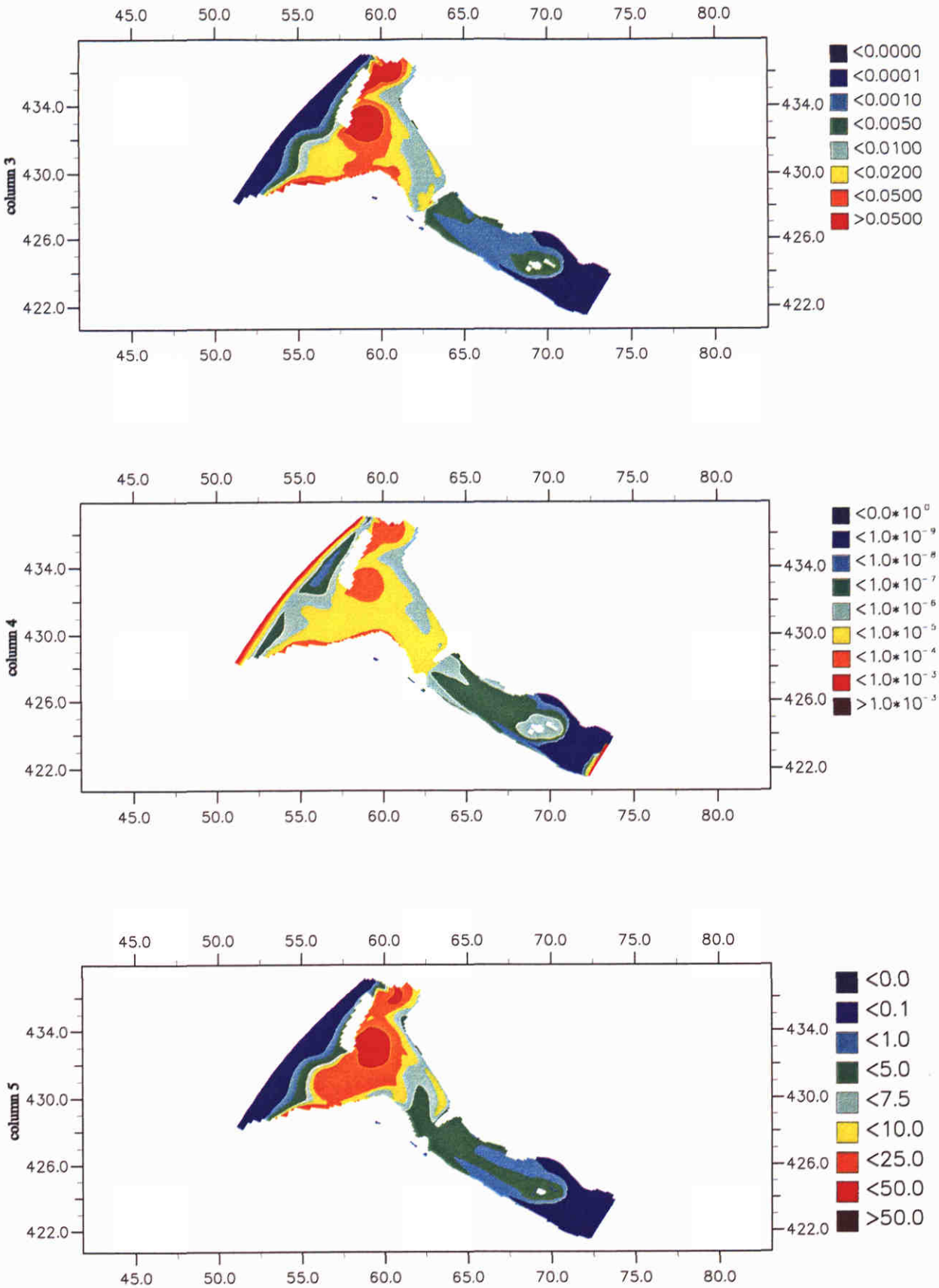


MOHA model (3D)
Horizontal TKE, dissipation and viscosity at 11 March 3:00 hour
Advection: first-order upwind (implicit in time)

Fig. A.3.2

WL | DELFT HYDRAULICS

Z2747.50

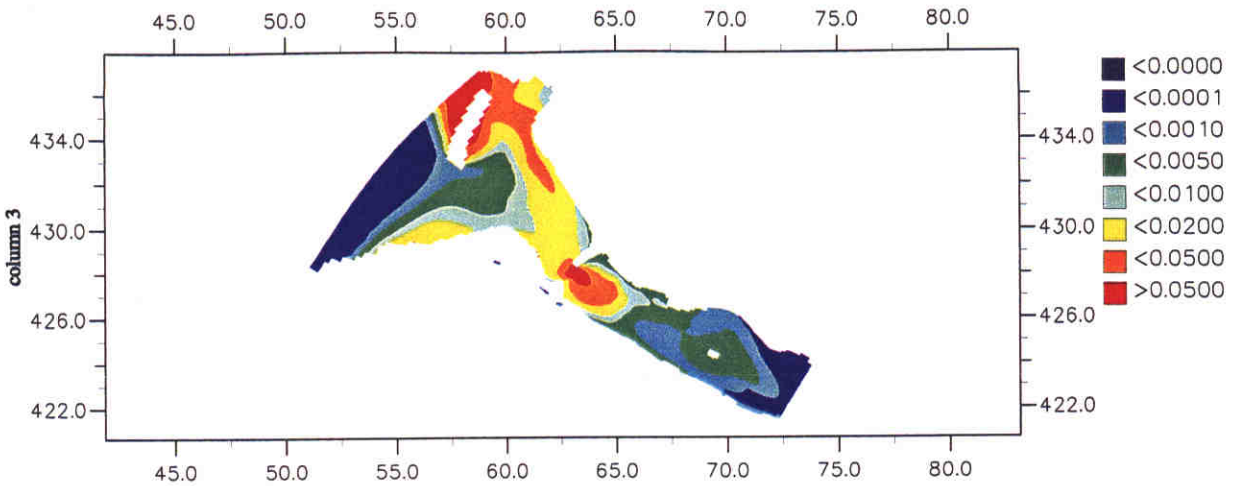


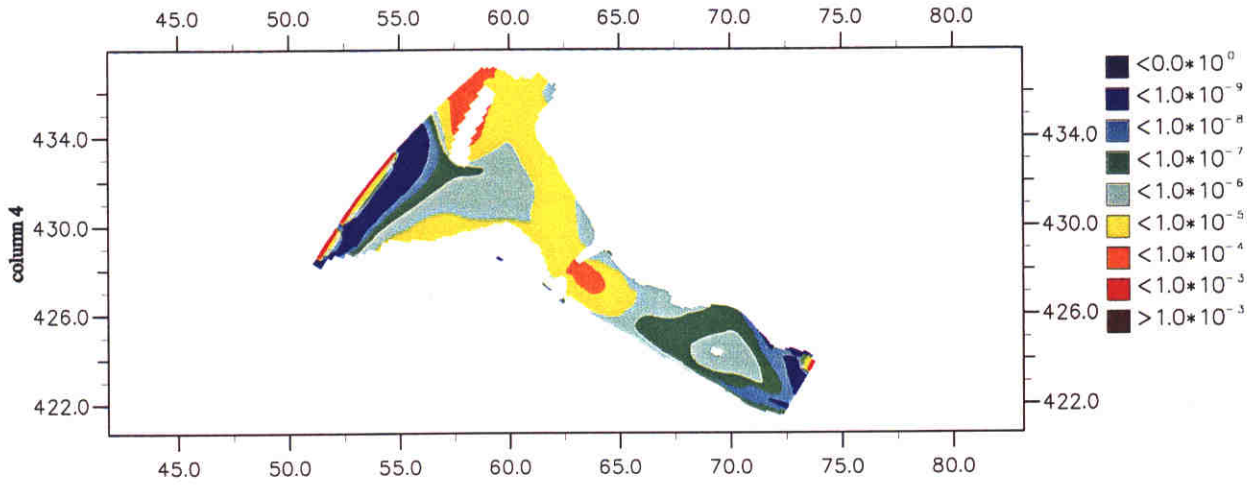


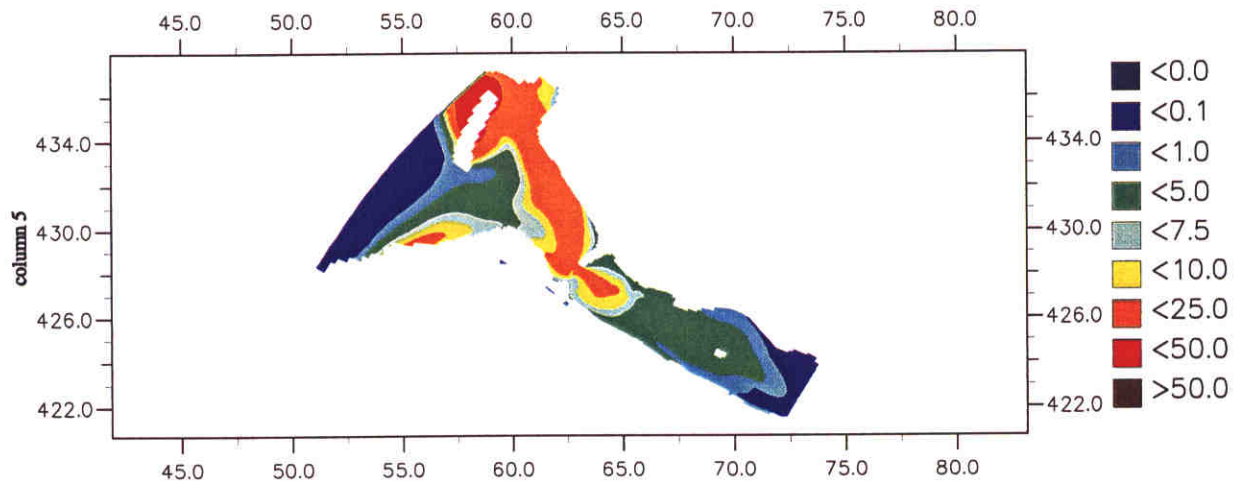


MOHA model (3D)
Horizontal TKE, dissipation and viscosity at 11 March 6:00 hour
Advection: first-order upwind (implicit in time)

Fig. A.3.3

WL | DELFT HYDRAULICS

Z2747.50

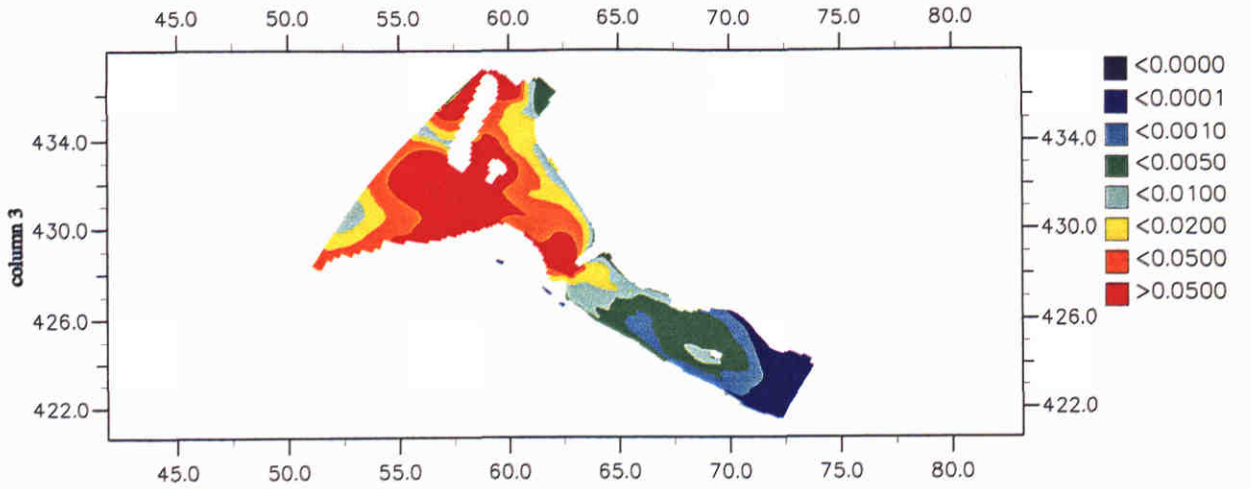


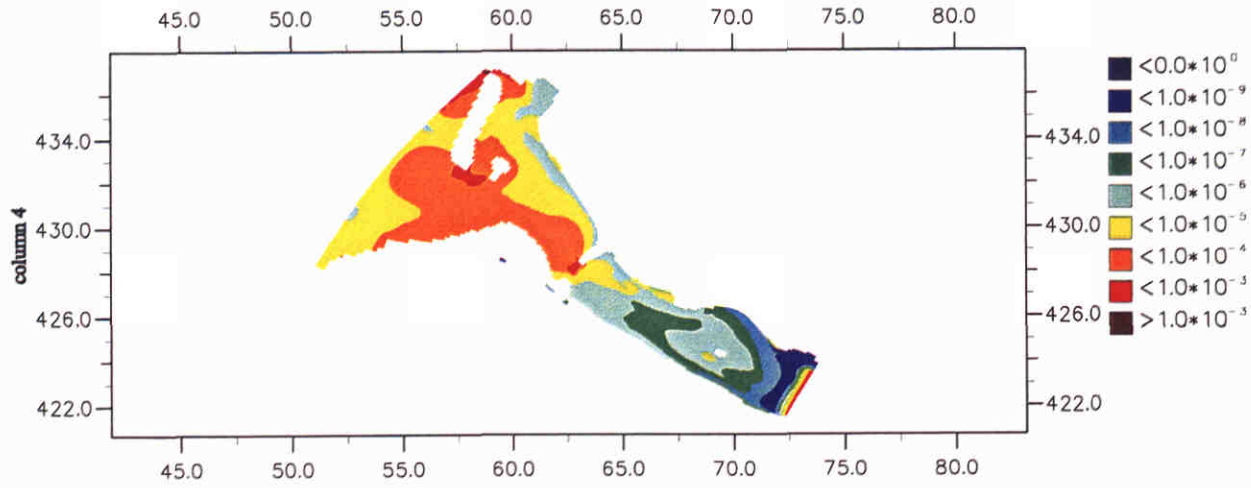


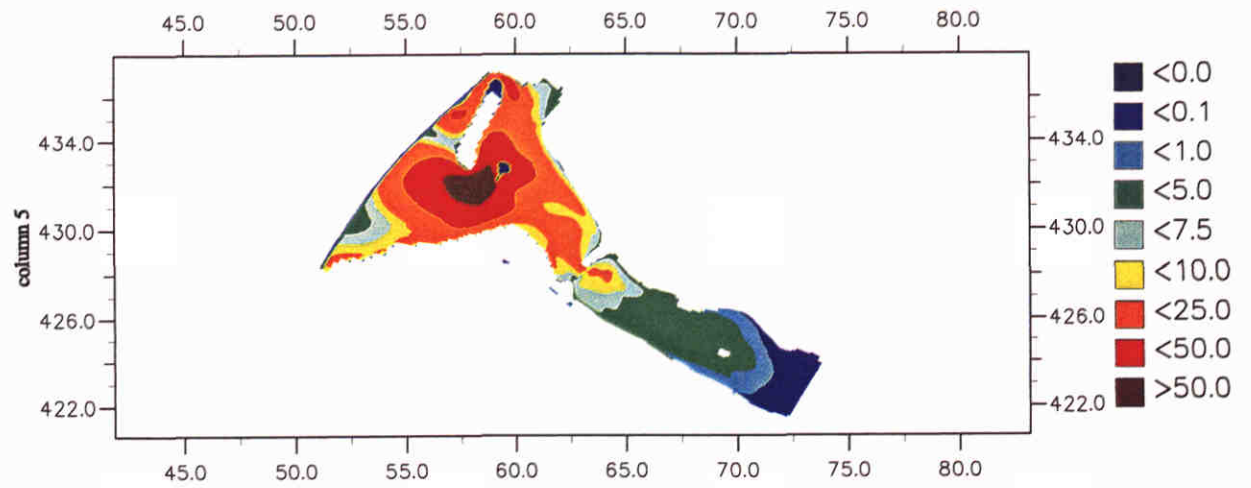


MOHA model (3D)

Horizontal TKE, dissipation and viscosity at 11 March 9:00 hour

Advection: first-order upwind (implicit in time)

Fig. A.3.4

WL | DELFT HYDRAULICS

Z2747.50

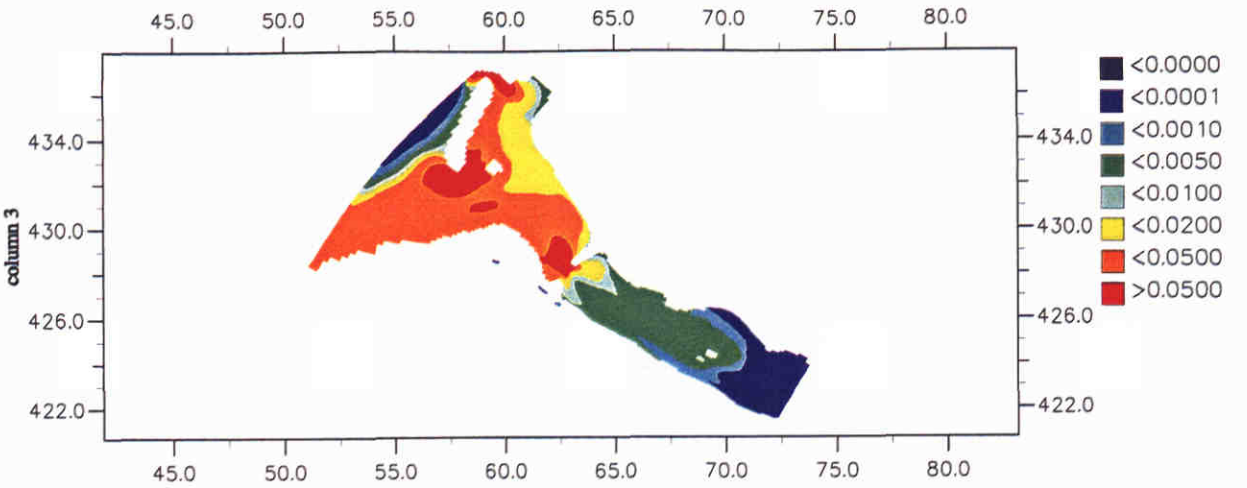


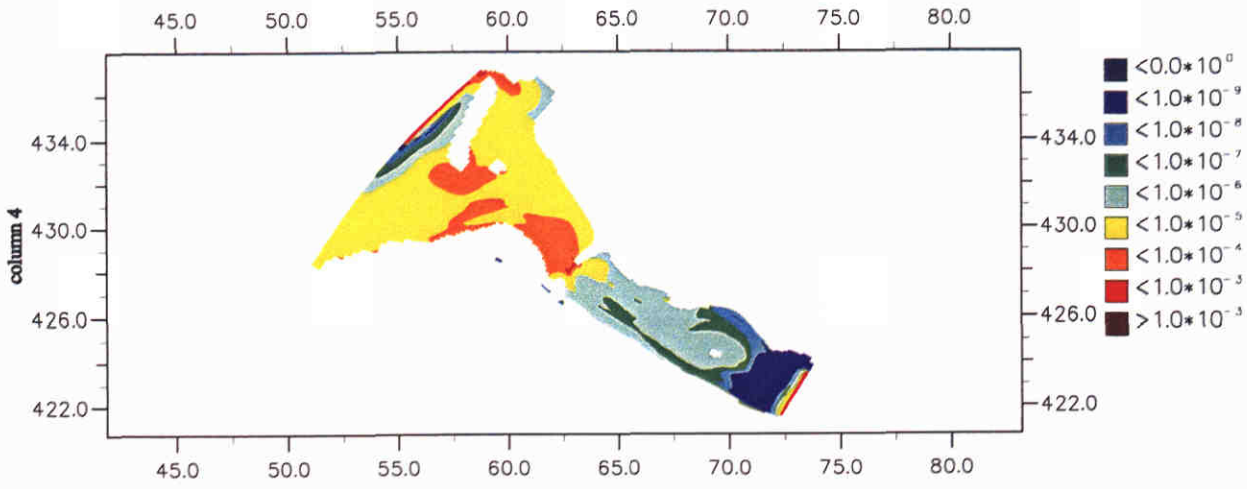


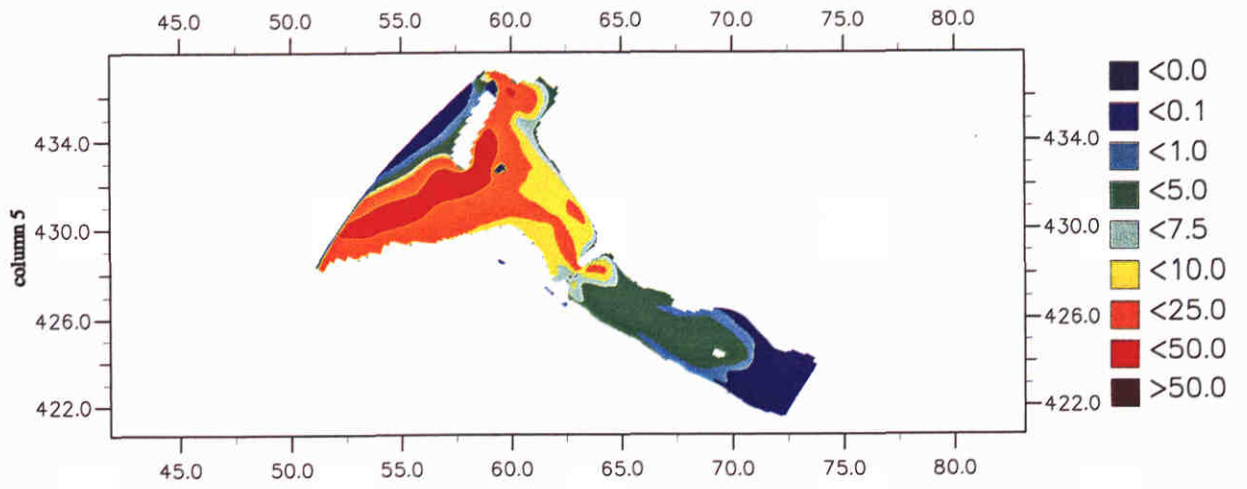


MOHA model (3D)

Horizontal TKE, dissipation and viscosity at 11 March 12:00 hour

Advection: first-order upwind (implicit in time)

Fig. A.3.5

WL | DELFT HYDRAULICS

Z2747.50

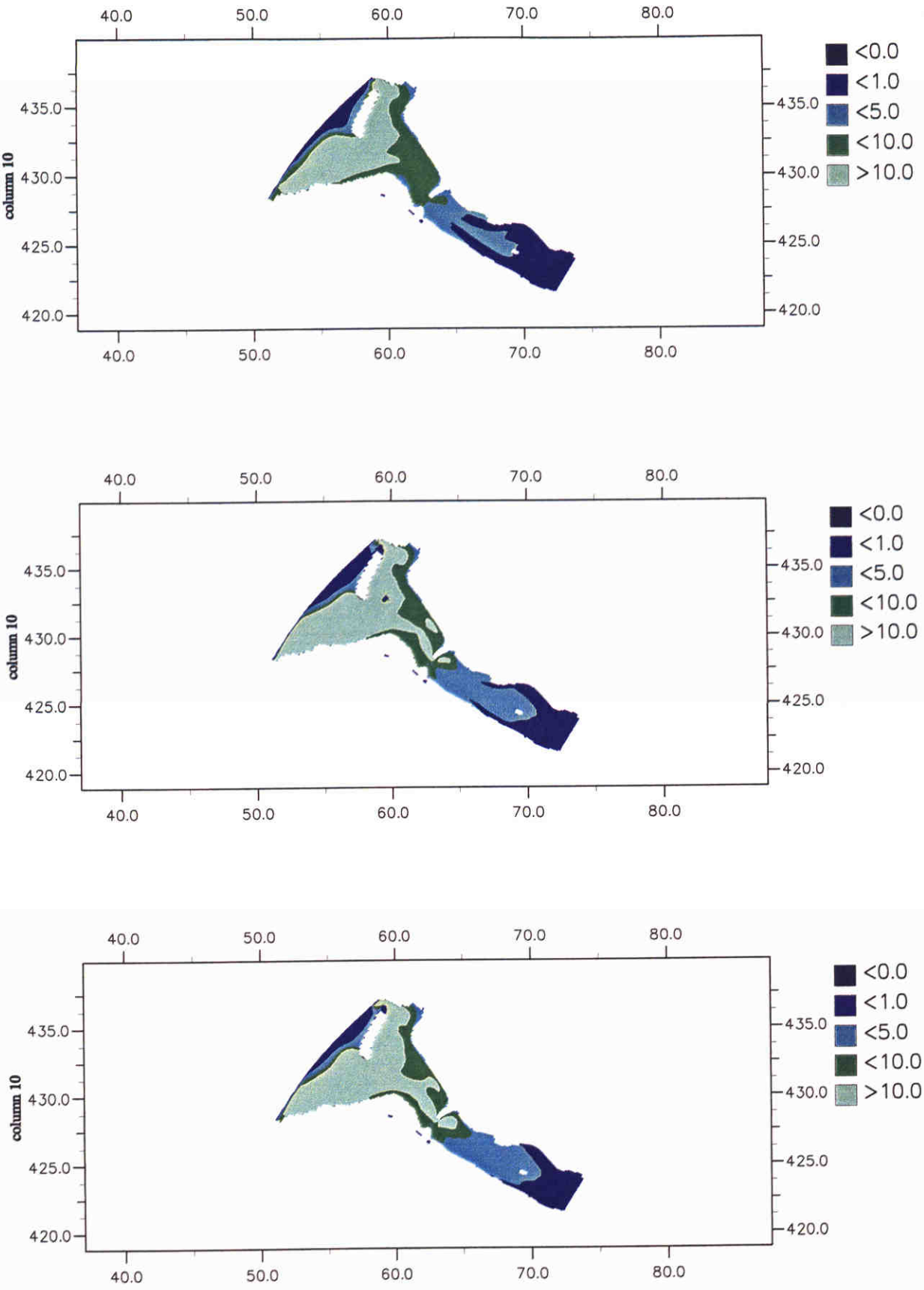


3D MOHA model;
Horizontal viscosity computed by horizontal turbulence model
Upper: 00:00 hr Centre: 12:00 hr Lower: 24:00 hr on 11 March 1997

Fig. A.3.6

WL | DELFT HYDRAULICS

Z2747.50

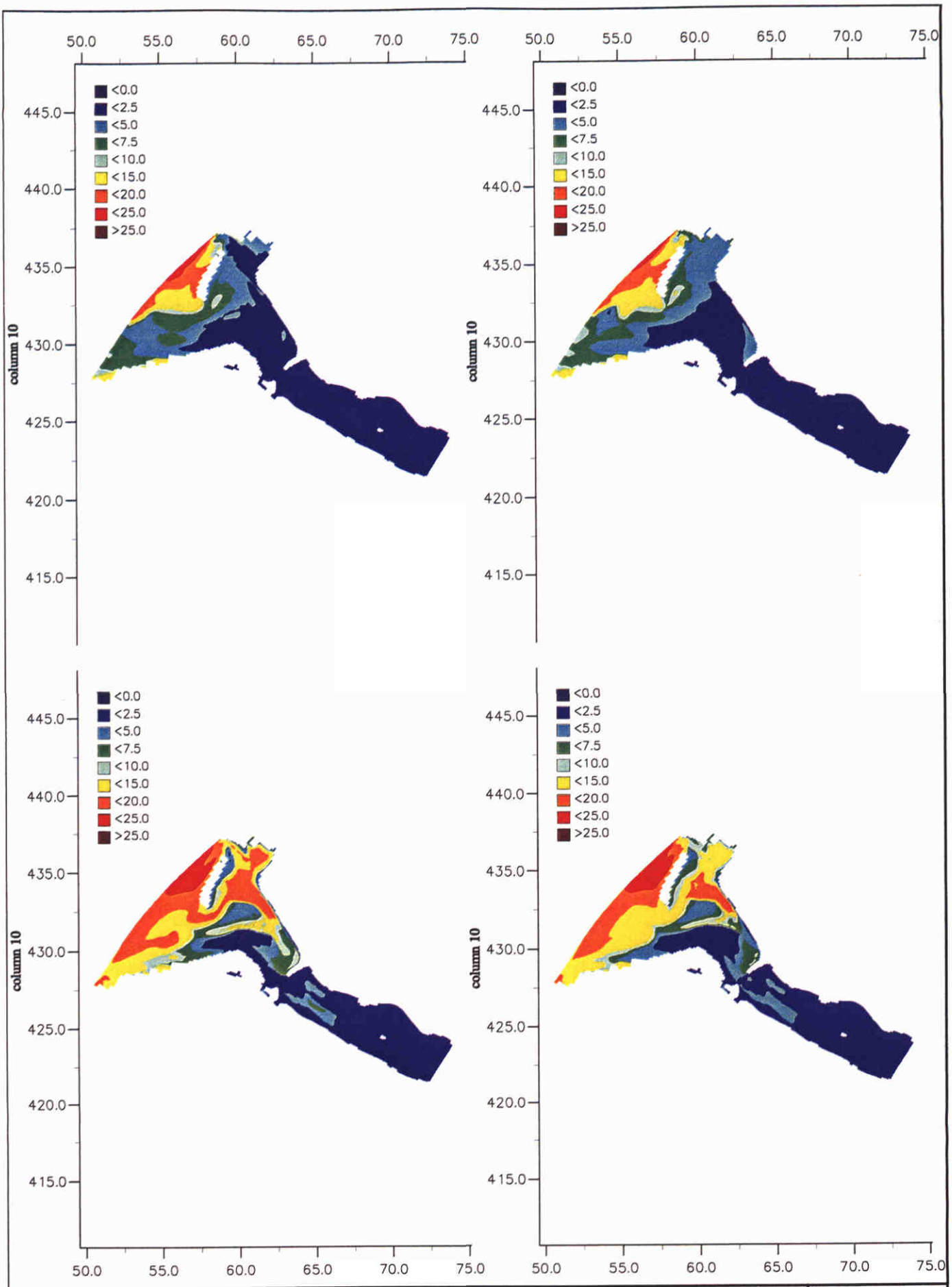


3D MOHA model; Contour plots of salinity at 11 March 00:00 hr.
Upper left: layer 1 (Hor. turbulence); Upper right: layer 1 (Ref.)
Lower left: layer 8 (Hor. turbulence); Lower right: layer 8 (Ref.)

Fig. A.3.7

WL | DELFT HYDRAULICS

Z2747.50

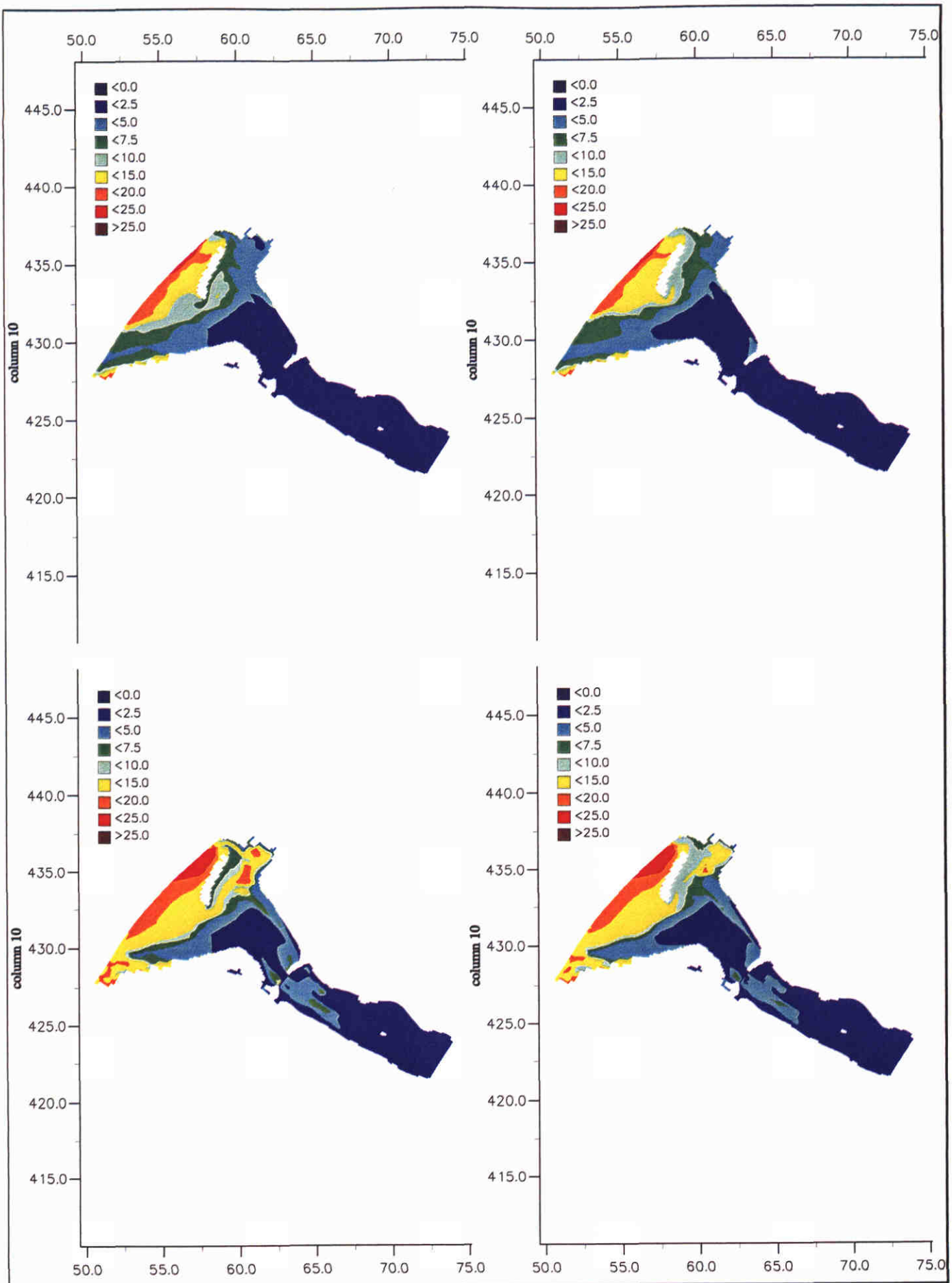


3D MOHA model; Contour plots of salinity at 11 March 12:00 hr.
Upper left: layer 1 (Hor. turbulence); Upper right: layer 1 (Ref.)
Lower left: layer 8 (Hor. turbulence); Lower right: layer 8 (Ref.)

Fig. A.3.8

WL | DELFT HYDRAULICS

Z2747.50

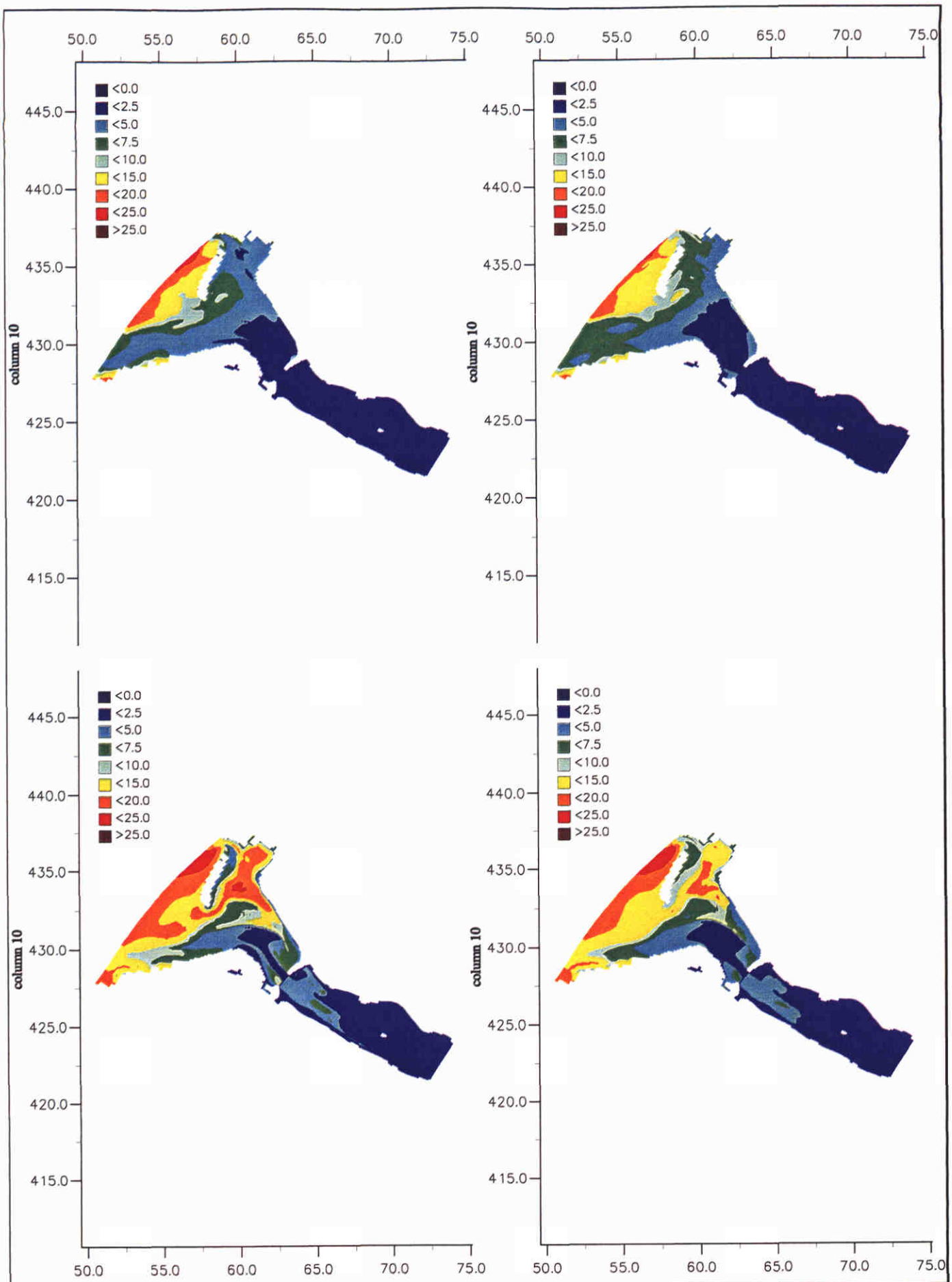


3D MOHA model; Contour plots of salinity at 12 March 00:00 hr.
Upper left: layer 1 (Hor. turbulence); Upper right: layer 1 (Ref.)
Lower left: layer 8 (Hor. turbulence); Lower right: layer 8 (Ref.)

Fig. A.3.9

WL | DELFT HYDRAULICS

Z2747.50


## WL | Delft Hydraulics

Rotterdamseweg 185
postbus 177
2600 MH Delft
telefoon 015 285 85 85
telefax 015 285 85 82
e-mail info@wldelft.nl
internet www.wldelft.nl

Rotterdamseweg 185
p.o. box 177
2600 MH Delft
The Netherlands
telephone +31 15 285 85 85
telefax +31 15 285 85 82
e-mail info@wldelft.nl
internet www.wldelft.nl